Supercontinuum generation in photonic crystal fiber

John M. Dudley*

Département d'Optique P. M. Duffieux, Institut FEMTO-ST, CNRS UMR 6174, Université de Franche-Comté, 25030 Besançon, France

Goëry Genty†

Helsinki University of Technology, Micronova, P.O. Box 3500, FIN-02015 HUT, Finland

Stéphane Coen‡

Department of Physics, University of Auckland, Private Bag 92019, Auckland, New Zealand

(Published 4 October 2006)

A topical review of numerical and experimental studies of supercontinuum generation in photonic crystal fiber is presented over the full range of experimentally reported parameters, from the femtosecond to the continuous-wave regime. Results from numerical simulations are used to discuss the temporal and spectral characteristics of the supercontinuum, and to interpret the physics of the underlying spectral broadening processes. Particular attention is given to the case of supercontinuum generation seeded by femtosecond pulses in the anomalous group velocity dispersion regime of photonic crystal fiber, where the processes of soliton fission, stimulated Raman scattering, and dispersive wave generation are reviewed in detail. The corresponding intensity and phase stability properties of the supercontinuum spectra generated under different conditions are also discussed.

DOI: 10.1103/RevModPhys.78.1135 PACS number(s): 42.65.Re, 42.65.Tg, 42.65.Ky

CONTENTS

*Electronic address: john.dudley@univ-fcomte.fr
†Electronic address: goery.genty@tkk.fi
‡Electronic address: s.coen@auckland.ac.nz

I. INTRODUCTION

Spectral broadening and the generation of new frequency components are inherent features of nonlinear optics, and have been studied intensively since the early 1960s. A fascinating perspective on the history of this subject has been given by Bloembergen (2000). The par-

ticular process known as supercontinuum (SC) generation occurs when narrow-band incident pulses undergo extreme nonlinear spectral broadening to yield a broadband (very often a white light) spectrally continuous output. Supercontinuum generation was first reported by Alfano and Shapiro (1970a, 1970b) in bulk glass, and has since been the subject of numerous investigations in a wide variety of nonlinear media, including solids, organic and inorganic liquids, gases, and various types of waveguide.

Supercontinuum generation has found numerous applications in such diverse fields as spectroscopy, pulse compression, and the design of tunable ultrafast femtosecond laser sources. In a telecommunications context, the spectral slicing of broadband SC spectra has also been proposed as a simple way to create multiwavelength optical sources for dense wavelength division multiplexing applications. An extensive review of the research into SC generation and its applications before 1990 is given in Part I of the monograph by Alfano (2006). An overview of this early work is given in Sec. II.

The advent of a new class of optical waveguides in the form of the photonic crystal fiber (PCF) in the late 1990s attracted widespread interest throughout the scientific community, and has led to a revolution in the generation of ultrabroadband high brightness spectra through SC generation (Ranka *et al.*, 2000a; Knight, 2003; Russell, 2003). The characteristics of PCFs that have led to such interest relate to their guidance properties that yield single-mode propagation over broad wavelength ranges, their enhanced modal confinement and therefore elevated nonlinearity, and the ability to engineer their group velocity dispersion (Reeves *et al.*, 2003).

The design freedom of PCFs has allowed SC generation to be observed over a much wider range of source parameters than has been possible with bulk media or conventional fibers. For example, experiments have reported SC generation using unamplified input pulses of durations ranging from tens of femtoseconds to several nanoseconds, and even using high-power continuous-wave (CW) sources. Supercontinuum generation in PCFs has subsequently been widely applied in interdisciplinary fields such as optical coherence tomography, spectroscopy, and, particularly, in optical frequency metrology. In this field it has led to the development of a new generation of optical clocks, and has opened up new perspectives to study limits on the drift of fundamental physical constants (Jones *et al.*, 2000; Holzwarth *et al.*, 2001; Udem *et al.*, 2002). The award of one-half of the 2005 Nobel Prize in Physics to Hall and Hänsch is of course a measure of the tremendous significance and impact of this work in precision frequency metrology.

Because of the evident significance of PCF-generated supercontinua, a complete understanding of the various underlying physical mechanisms is of prime importance. Somewhat paradoxically, however, the ease with which SC generation in PCF has been observed experimentally has actually made it relatively difficult to understand in clear physical terms. In particular, the wide range of fiber types, pulse durations, and pulse energies that have been used in experiments has led to confusion in isolating the relative contributions of processes such as self- and cross-phase modulation, four-wave mixing, modulation instability, soliton fission, dispersive wave generation, and Raman scattering. As a result, significant misunderstanding has developed in the existing literature, and incorrect identification of the underlying physical processes corresponding to particular experimental conditions is not unusual. This naturally represents a disadvantage for researchers who are not specialists in nonlinear ultrafast optics, because it appears that there is no straightforward way in which to interpret the physics of what is clearly a phenomenon of much interest.

Our objective here is to address this problem, and to present a unified discussion of the various nonlinear SC spectral broadening processes. We structure our review around numerical simulations that illustrate the SC generation characteristics for conditions covering the typical experimental parameter range. We focus on the underlying physics of the nonlinear spectral broadening processes and aim to complement existing, more general, descriptions of PCF nonlinearities that have been given by Knight (2003), Russell (2003), and Zheltikov (2004). In this way, we hope that the reader will be well prepared to study in detail more specific discussions of SC applications such as those by Hansen (2005) and Smirnov *et al.* (2006).

The paper is organized as follows. In Sec. II, we briefly review previous SC generation experiments in bulk media and conventional optical fiber in order to classify the various physical mechanisms involved. We also review a selection of results studying SC generation in PCF, but without attempting to discuss in any depth the underlying physics, which is treated later. In order to allow the advantages of PCFs for SC generation to be appreciated, it is necessary to consider briefly their particular nonlinear and dispersive characteristics, as covered in Sec. III. Our discussion of the SC spectral broadening mechanisms relies heavily on numerical simulations, and the underlying modeling aspects are described in Sec. IV.

A detailed analysis of the SC broadening mechanisms is presented in terms of the injected pulse duration in two broad classes: the femtosecond regime (Secs. V and VI) and the regime using longer picosecond or nanosecond pulses or continuous-wave fields (Sec. VII). Because many important applications of SC generation use femtosecond pulses, we consider this regime in more detail, and attempt to present a "deconstruction" of the SC generation process in terms of a number of key constituent nonlinear and dispersive processes. For both classes of pulse duration, results from numerical simulations are complemented by a review and discussion of experimental results. In many cases, results obtained in PCFs have inspired similar work using optical fiber tapers or highly nonlinear fibers (HNLFs) presenting comparable enhanced nonlinearity, and reference is made to significant results obtained using these technologies where relevant.

In Sec. VIII, we consider other issues related to SC generation and nonlinear pulse propagation in PCFs that might be expected to form the basis of continuing research in this field. Section IX concludes with a summary of criteria to consider when selecting a SC for a specific application, and a brief discussion of possible next steps.

II. INTRODUCTORY LITERATURE REVIEW

In this section, we provide an overview of the nonlinear optics literature as it relates to the SC generation process. We begin by reviewing work studying broadband spectral generation in bulk media and in conventional optical fibers, and then briefly review the results obtained in PCFs. For the latter case, we concentrate on the most influential work in the field, as more detailed technical discussion and review is given in Secs. V–VIII.

A. Results in bulk media

In the first observation of SC generation, Alfano and Shapiro (1970a) reported the generation of a white light spectrum covering the entire visible range from 400 to 700 nm after propagating 5 mJ picosecond pulses at 530 nm in bulk BK7 glass. Shortly afterward, similar results were reported independently by Bondarenko *et al.* (1970). It is important to note that the nonlinear spectral broadening of laser light was not completely new at the time, having been observed earlier by Stoicheff (1963). Indeed, Jones and Stoicheff (1964) had even applied a relatively narrow "continuum" of light in what was the first inverse Raman spectroscopy measurement. Spectral broadening had also been reported in CS_2 (Brewer, 1967) and correctly interpreted in terms of the nonlinear process of self-phase modulation (SPM) (Shimizu, 1967).

What made the experiment of Alfano and Shapiro (1970a) so exciting was the sheer extent of the spectral width of the generated light, more than 10 times wider than anything previously reported. Interestingly, the authors do not particularly emphasize this aspect in their publication. Their work is actually dedicated to the first identification of nonresonant four-photon coupling, i.e., four-wave mixing. The term "supercontinuum" was not even used in Alfano and Shapiro's paper, and was only introduced later (Manassah *et al.*, 1984, 1985). In the meantime, the phenomenon of SC generation was referred to as superbroadening (Bondarenko *et al.*, 1970; Il'ichev *et al.*, 1972), anomalous frequency broadening (Werncke *et al.*, 1972; Bloembergen, 1973), or white-light continuum (Fork *et al.*, 1983).

From the start, it was clear that self-focusing was a key ingredient to SC generation in bulk media, as it was commonly observed that the SC threshold coincided with the critical power for catastrophic collapse, usually associated with the formation of self-trapped filaments (Chiao *et al.*, 1964; Alfano and Shapiro, 1970a; Bondarenko *et al.*, 1970; Il'ichev *et al.*, 1972; Werncke *et al.*, 1972). Beam collapse leads to an explosive increase in the peak intensity, which enhances SPM, but which also gives rise to a range of higher-order nonlinear effects, including self-steepening, space-time focusing (Rothenberg, 1992), multiphoton absorption, avalanche ionization, and the formation of a free-electron plasma (Bloembergen, 1973). In particular, Werncke *et al.* (1972) postulated that SC generation corresponded to "an essential deformation of light pulses within the filaments [which] should lead to a steepening of the backside of the pulse." Self-phase modulation associated with this very steep negative intensity slope then explains the broad extent of bulk SC spectra on the blue side of the pump. Bloembergen (1973) also pointed out that the defocusing effect of the electron plasma could lead to similar behavior.

It was not until the work by Gaeta (2000), however, that a consistent explanation emerged based on full three-dimensional simulations of light propagation. It is now accepted that white-light continuum generation in bulk material is due to the formation of an optical shock at the back of the pump pulses due to space-time focusing and self-steepening, confirming the early ideas of Werncke *et al.* The role of multiphoton absorption and plasma formation is simply to arrest the collapse of the beam and to prevent the optical breakdown of the material. Self-trapped filaments may or may not form in the process depending on the pulse duration and on the relative strength of chromatic dispersion, self-focusing, and plasma defocusing (Aközbek *et al.*, 2001). This scenario is in agreement with all known observations, including the dependence of SC generation on the band gap of the material (Brodeur and Chin, 1998). In material with a small band gap, self-focusing is stopped at lower intensities by free-electron defocusing, preventing the formation of a shock.

From this summary, it is clear that SC generation in bulk material is a highly complex process involving an intricate coupling between spatial and temporal effects. In contrast, SC generation in optical fibers involves purely temporal dynamical processes, with the transverse mode characteristics determined only by linear waveguide properties. In fact, this suggests that a further motivation to study SC generation in PCFs is to clarify the nature of temporal nonlinear propagation effects in order to improve the understanding of the more complex spatiotemporal (bulk) case.

B. Results in conventional fiber

The first SC generation experiments in optical fiber injected high-power pulses in the visible spectral region into standard silica-based optical fiber with zero group velocity dispersion (GVD) wavelength around 1.3 μm. In particular, Lin and Stolen (1976) used visible ~kW peak power pulses from a nanosecond dye laser to generate a SC over a spectral range of ~200 THz on the long-wavelength side of the pump. The observed spectral broadening was attributed to cascaded stimulated Raman scattering and SPM. Subsequent experiments using visible pump pulses in the 10 ps–10 ns range produced similar results. These studies also clarified the im-

portance of the mutual interaction between Raman scattering and SPM, as well as the role of cross-phase modulation (XPM) and various four-wave-mixing processes in providing additional broadening, and in merging discrete generated frequency components to produce a spectrally smooth output (Stolen *et al.*, 1984; Baldeck and Alfano, 1987; Ilev *et al.*, 1996).

The Raman and SPM-dominated broadening in the experiments above was observed for the case of normal GVD pumping. When pumping in the anomalous GVD regime, however, spectral broadening arises from soliton-related dynamics. The possibility of soliton propagation in the anomalous GVD regime of optical fibers was first suggested from theoretical analysis of the nonlinear Schrödinger equation (NLSE) by Hasegawa and Tappert (1973), but the lack of ultrashort pulse sources at wavelengths >1.3 μm delayed experimental observation until the work of Mollenauer *et al.* (1980). In these experiments, ~ 7 ps pulses around 1.55 μm were used to excite not only a nonbroadening stable fundamental soliton, but also higher-order solitons that were observed at increased power levels.

A higher-order soliton[1] is a particular class of solution of the NLSE representing a bound state of N fundamental solitons (Zakharov and Shabat, 1971; Satsuma and Yajima, 1974). Such solutions propagate in a complex manner consisting of both spectral and temporal compression and splitting, followed by subsequent recovery to the original pulse shape after a characteristic propagation distance known as the soliton period. Experiments using picosecond pulses at 1.55 μm have studied different aspects of higher-order soliton propagation, including explicit measurements of pulse restoration over a soliton period (Stolen *et al.*, 1983) and application to pulse compression (Mollenauer *et al.*, 1983). These latter experiments are of particular significance because they show that, although higher-order soliton evolution can be very complex, the initial phase of propagation is always associated with relatively simple SPM-induced spectral broadening and temporal compression due to the fiber-anomalous GVD. This will be of particular importance in interpreting the results presented in Sec. V.

Also of much importance in this context are a number of early studies on the sensitivity of soliton propagation to perturbations such as Raman scattering and higher-order dispersion. For the case of a fundamental soliton, intrapulse stimulated Raman scattering (i.e., Raman scattering within the soliton bandwidth) was found to lead to a continuous downshift of the mean frequency known as the soliton self-frequency shift (Gordon, 1986; Mitschke and Mollenauer, 1986). In a study of solitons propagating close to the fiber zero-dispersion wavelength (ZDW), Wai *et al.* (1986) numerically studied the effect of third-order dispersion on soliton stability and found significantly different consequences for fundamental and higher-order solitons. For fundamental solitons, although the shape of the soliton was only slightly affected, third-order dispersion was found to stimulate the resonant transfer of energy from the soliton to a low-amplitude nonsolitonic narrow-band dispersive wave background with frequency in the normal GVD regime. In contrast, higher-order soliton evolution was found to be more seriously perturbed by higher-order dispersion, with the soliton temporally breaking up and separating into its constituent fundamental soliton components. This process is now generally referred to as soliton fission.

Soliton fission is an important example of symmetry breaking in a nonlinear optical system, and has been studied extensively. Kodama and Hasegawa (1987) derived explicit expressions for the amplitudes and widths of the constituent fundamental soliton components, and showed that the energy of the higher-order soliton was equal to the sum of the energies of its components. In fact, while seemingly a trivial observation, this result highlights the intrinsic instability of higher-order soliton propagation that arises from an absence of any binding energy. Indeed, numerical studies by Golovchenko *et al.* (1985) noted the instability of higher-order soliton propagation in the presence of self-steepening, and other theoretical and experimental studies have shown that it can be induced by Raman effects (Dianov *et al.*, 1985; Tai *et al.*, 1988), two-photon absorption (Silberberg, 1990), and input pulse chirp perturbations (Friberg and DeLong, 1992; Krylov *et al.*, 1999).[2]

Experiments on soliton fission around 1.3 μm were performed by Beaud *et al.* (1987) and Schütz *et al.* (1993) using 1–3 ps pulses, Gouveia-Neto *et al.* (1988b) using 90 ps pulses, and around 1.55 μm by Islam *et al.* (1989a, 1989b) using 14 ps pulses. These results showed that soliton fission leads to an equivalent form of SC generation, allowing broadband spectral generation over the telecommunications wavelength range. Moreover, numerical simulations clarified that the SC generation process occurred broadly in three phases: (i) an initial period of spectral broadening and temporal compression, (ii) fission into a series of distinct fundamental soliton components, and (iii) the continued propagation of these solitons. This last phase was shown to be associated with a continuous shift to longer wavelengths through the Raman soliton self-frequency shift and the generation of corresponding dispersive waves on the short-wavelength side of the ZDW. This detailed physical interpretation was present in the literature by 1989, and the same mechanisms continue to play dominant roles, even in the different parameter regime associated with PCF.

Islam *et al.* (1989a, 1989b) and Nakazawa *et al.* (1989) interpreted the soliton fission process in terms of a modulation instability process on the input pulse envelope. Modulation instability is a phenomenon exhibited

[1]The literature also uses terms such as N-soliton, breather, or multisoliton bound state.

[2]Another "perturbation" that is frequently encountered is insufficient resolution in numerical simulations of the NLSE! Indeed, checking on the numerical stability of ideal higher-order solitons provides an important test of simulation fidelity.

by waves propagating in nonlinear dispersive media, in which weak amplitude perturbations at different frequencies are subject to gain. As we discuss in Sec. VII, the development of a temporal modulation on the input field is associated with the growth of sidebands at characteristic frequencies and can equivalently be interpreted in terms of a four-wave-mixing process.

These studies were significant in highlighting the sensitivity of soliton fission to input pulse noise. Because the nonlinear pulse propagation depends on input power, fluctuations on the input pulse can lead to jitter in both the spectral and temporal characteristics. This has practical consequences in that the actual spectral characteristics observed are an ensemble average of constituent fundamental solitons that have undergone different frequency shifts. The fact that such jitter could introduce an effective smoothing of spectral characteristics had, in fact, been previously noted by Beaud *et al.* (1987) and by Islam *et al.* (1989a, 1989b). This latter work also reported experimental characterization of spectral instabilities using cross-correlation between different SC spectral bands to demonstrate that different output wavelengths were not necessarily simultaneously present in each individual pulse.

The possibility of generating broadband SC spectra around 1.3 and 1.55 μm motivated research aimed at developing multiwavelength sources for wavelength division multiplexing transmission (Morioka *et al.*, 1993, 1994). For such applications, the absolute bandwidth required is relatively low (around 20–40 THz), but it is important that the SC source is generated at GHz repetition rates with low noise and with a flat spectrum.

A number of experiments were therefore carried out to study the instabilities observed during soliton fission in more detail. Nakazawa *et al.* (1998) characterized what they termed coherence degradation by observing the noise level between longitudinal modes of the broadened spectrum (see also Kubota *et al.*, 1999). The timing jitter of SC pulses was analyzed by Nowak *et al.* (1999) using the standard technique of measuring the energy of a high harmonic of the rf spectrum (von der Linde, 1986), and directly using a sampling oscilloscope by Tamura *et al.* (2000). Boyraz *et al.* (2000) used a different approach by checking that pulse trains carved out of the SC exhibited the correct behavior with regard to SPM-induced spectral broadening and mode-beating induced repetition rate multiplication after dispersive propagation.

Although the majority of SC generation studies in conventional fiber focused on the regime where pumping used ultrafast pump pulses, the detailed physics underlying SC generation using longer pump pulses or CW excitation remained a subject of active research. Particularly important work was reported by Golovchenko *et al.* (1990, 1991), where numerical simulations were used to elucidate the relationship between modulation instability, soliton dynamics, and Raman scattering under CW pump conditions. This work highlighted the fact that the SC generation in the anomalous GVD regime using CW pumps also involved soliton dynamics as in the case of pulsed excitation. Although an important physical insight, the lack of suitable high-power CW sources somewhat limited follow-up experimental studies in this field.

C. Results in photonic crystal fiber

Before discussing SC generation in PCF, we consider briefly the historical development of the fiber itself, and explain why its guidance characteristics have had such a pronounced recent influence on nonlinear fiber optics.

Conventional optical fibers consist typically of two concentric glass cylinders of differing refractive indices. If the refractive index of the inner core is higher than that of the outer cladding, then guidance occurs through total internal reflection at the core-cladding boundary. In the majority of conventional fibers, the core-cladding refractive index difference is small ($\sim$0.1 %), and many of the propagation characteristics are amenable to analysis (Snyder and Love, 2000). The possibility to modify the guidance properties by introducing a microstructure in the refractive index profile of optical fibers was suggested in the 1970s (Kaiser and Astle, 1974), but it has been only since the seminal work of Russell and co-workers in 1996 (Knight *et al.*, 1996) that the fabrication of such fibers has become technologically commonplace.

Because an important motivation at this time was the idea to fabricate a fiber in which light was confined and guided through a photonic band-gap effect (Russell, 1991), the term photonic crystal fiber was introduced, and this is the term that we use consistently in this article.[3] However, depending on the particular PCF geometry, light guidance can occur in one of two ways. In the case in which the fiber has a hollow core in the center of the structure, genuine photonic band-gap guidance can occur, and PCFs of this type have attracted much interest because of their potential for lossless and distortion-free transmission, particle trapping, optical sensing, and for novel applications in nonlinear optics (Benabid *et al.*, 2002; Knight, 2003; Ouzounov *et al.*, 2003; Russell, 2003).

This class of hollow core PCF, however, is not that used in SC generation experiments. Rather, SC generation is observed in PCFs having a solid core in the center of the structure, so that the fiber consists of a region of solid glass surrounded by an array of airholes running along its length. In this case, the effective refractive index of the central region of the PCF is higher than that of the surrounding air-hole region (often referred to as the photonic crystal cladding), and guidance occurs through modified total internal reflection (Birks *et al.*, 1997). Although this is conceptually similar to the guidance mechanism in conventional fibers, the additional degrees of freedom offered by modifying the hole size and periodicity in such an index-guiding PCF open up

[3]Other terms are to be found in the literature. The most common are holey fiber, microstructure fiber, or even microstructure optical fiber.

possibilities to engineer the fiber waveguide properties in ways that simply do not exist in standard fiber.

In particular, Mogilevtsev *et al.* (1998) showed that suitable design of the photonic crystal cladding could shift the ZDW of a PCF to wavelengths shorter than the intrinsic ZDW of silica around 1.3 μm. Separately, Broderick *et al.* (1999) noted that the reduced effective area of the propagating mode in this type of fiber enhanced the Kerr nonlinearity relative to standard fiber, leading to significant new opportunities in nonlinear fiber optics. The combination of these two effects was then subsequently (and strikingly) demonstrated in two independent experiments. Using nanojoule energy pulses at 770 nm of 100 fs duration from a self-mode-locked Ti:sapphire laser, Ranka *et al.* (2000a) were able to generate a 550 THz bandwidth SC spanning over an octave from 400 to 1500 nm using only 75 cm of PCF fabricated to have a ZDW in the region 765–775 nm. Shortly after, using comparable pump pulse parameters and a similar PCF fabricated at the University of Bath, Wadsworth *et al.* (2000) exploited the fiber's near-infrared anomalous GVD to study soliton propagation effects around 850 nm. This latter work also included a brief report of SC generation from the ultraviolet to the infrared, although the precise extent of the spectral broadening was not quantitatively reported.

These were dramatic results, because previous work generating comparably broad spectra in bulk materials had required significantly more complex sources with pulse energies at the microjoule level. However, because the development of dispersion-engineered PCFs occurred at the time when femtosecond Ti:sapphire lasers were becoming commonplace in ultrafast laboratories, it was clear that the generation of broadband SC spectra was now a widely accessible technology. Moreover, an additional advantage was that the broadband single-mode guidance properties of the PCF resulted in the generated SC retaining a uniform spatial profile, in contrast to the case often observed in bulk experiments where SC generation was often associated with filamentation effects.

One application that immediately suggested itself was in the field of frequency metrology. It had been known since the pioneering work of Udem *et al.* (1999) that the modes of a femtosecond laser pulse train could be used as a calibrated frequency comb to measure optical frequency intervals between a reference and an unknown frequency. With PCF-generated SC spectra possessing bandwidths exceeding an octave, it was possible to measure and control the absolute position of the frequency comb using an interferometric technique based on the beat note from SC components at frequencies f and $2f$ (Diddams *et al.*, 2000; Jones *et al.*, 2000). As a result, it has been possible to develop stabilized frequency combs that have opened up new directions in optical frequency metrology such as the possibility to perform precision measurements on the stability of fundamental constants (Udem, Reichert, Holzwarth, Niering, *et al.*, 2000; Hollberg *et al.*, 2001; Holzwarth *et al.*, 2001). In addition, because stabilization of the frequency comb is equivalent to stabilizing the relative phase between the peak of the pulse envelope and the underlying electric field carrier wave (Jones *et al.*, 2000), it has also been possible to study ultrafast optical processes that are directly sensitive to the electric field of each pulse, and not just to the intensity envelope. This has allowed significant progress in studying highly nonlinear phenomena such as above-threshold ionization, strong field photoemission, and the generation of soft-x-ray attosecond pulses through high harmonic generation (Udem *et al.*, 2002).

Even though PCF-generated SCs were finding wide application, at this stage there was still no quantitative theory of the physics underlying the spectral broadening. Nonetheless, the importance of the PCF's enhanced nonlinearity and modified dispersion had been stressed by both Knight *et al.* (2000) and Ranka *et al.* (2000b). Simultaneously, a number of experiments were exploring the different conditions under which similarly broad SC could be generated. In one experiment, Birks *et al.* (2000) showed that the use of PCF *per se* was not fundamentally necessary, because essentially identical dispersion and nonlinearity characteristics could be obtained simply by an appropriate tapering of standard optical fiber. By injecting ~200 fs pulses of nJ energy into a 9 cm taper of around 2 μm diameter, comparable octave spanning SCs to those seen with PCF were observed. By emphasizing the central role played by the dispersion and nonlinearity characteristics, this experiment was a crucial step in developing an understanding of the SC generation process in PCF.[4]

Other key experiments reported the generation of broadband SC using nonfemtosecond pulse sources. Using 0.8 ns duration, 300 nJ energy pulses from a Q-switched microchip laser at 532 nm, Provino *et al.* (2001) were able to generate over 250 THz of SC from 460 to 750 nm in 1.8 m of PCF, through excitation of a higher-order mode whose ZDW at 580 nm was reached from the pump wavelength by cascaded Raman scattering. Parametric gain calculations showed that the SC development from this point could be well explained in terms of four-wave mixing about the ZDW. A similar combination of Raman scattering and four-wave mixing was also observed in an experiment by Coen *et al.* (2001), where 60 ps duration, 40 nJ energy pulses at 647 nm generated a 450 THz SC from 400 to 1000 nm in the fundamental mode using 10 m of PCF with ZDW at 675 nm. This work also reported the first use of a generalized NLSE including higher-order dispersion and Raman scattering to model the SC generation process in PCF, and numerical simulations were shown to quantitatively reproduce the spectral characteristics seen in experiments.

[4]In fact, the possibility of enhancing the Kerr nonlinear response in tapers had been proposed much earlier by Dumais *et al.* (1993). However, the vast potential for SC generation was left unexplored in this work because the pump wavelength chosen was far from the taper ZDW.

Numerical modeling of SC generation in PCF using femtosecond pulses was initially reported by Husakou and Herrmann (2001), and the crucial role of soliton fission in the spectral broadening process was highlighted for the first time. However, numerical simulations used in this work were based on a set of reduced Maxwell equations in which the Raman effect was neglected, and much of the detailed structure seen in experimentally measured spectra was not quantitatively reproduced (Herrmann *et al.*, 2002).

In parallel with this work, it was found that the generalized NLSE approach including higher-order dispersion and stimulated Raman scattering was also capable of accurately modeling SC generation in the femtosecond regime. In one study, Liu *et al.* (2001) used an extended NLSE limited to cubic dispersion terms, yet obtained good qualitative agreement between simulations and experiments modeling spectral generation over 43 THz using tapered PCF pumped around 1.3 μm. Focusing on the properties of Raman solitons generated during the SC generation process, Washburn *et al.* (2001) used a model incorporating the global PCF dispersion characteristics, and were able to accurately model experimental results from a Ti:sapphire-pumped PCF around 806 nm over a ~150 THz frequency span from 700 to 1100 nm.

These results were followed by a number of more careful comparisons between experiment and simulation, in both the picosecond (Coen, Chau, *et al.*, 2002) and femtosecond regimes (Dudley, Provino, *et al.*, 2002; Washburn *et al.*, 2002). A further important contribution by Genty *et al.* (2002) quantitatively studied the femtosecond pump case in the context of the soliton fission theory of Kodama and Hasegawa (1987). Other noteworthy results of a purely experimental or theoretical nature were also made by Apolonski *et al.* (2002), Fedotov *et al.* (2002), Husakou and Herrmann (2002), and Wadsworth *et al.* (2002). Further details of the key experimental studies into SC generation are given in Secs. VI and VII for the femtosecond and the picosecond-CW regimes, respectively.

As a result of this extensive research effort, the dominant spectral broadening mechanisms underlying SC generation in PCF were clearly identified by 2002. The physics was interpreted as essentially identical to that previously encountered in standard optical fibers, with soliton fission and the Raman self-frequency shift responsible for the long-wavelength components of the SC, and dispersive wave generation responsible for the short-wavelength components.

Of course, research continued in order to improve the quantitative agreement between experiment and simulation, and to study the detailed SC stability properties. Early studies had reported significant temporal and spectral fluctuations on the generated SC (Udem, Reichert, Holzwarth, Diddams, *et al.*, 2000; Hollberg *et al.*, 2001; Gu *et al.*, 2002) and this was of particular concern because key applications such as precision optical frequency metrology or multiwavelength optical sources require highly coherent SC light with limited pulse-to-pulse variations and reduced timing jitter. The noise and spectral structure appeared to be a very sensitive function of experimental parameters, but there were no clear guidelines as to why this was the case. At this point, studies by Dudley and Coen (2002a) and Gaeta (2002) showed that the spectral and temporal structure of the SC could exhibit extreme sensitivity to input pulse noise. This was shown to lead to shot-to-shot intensity fluctuations that could wash out spectral fine structure when averaged over many shots, and shot-to-shot phase fluctuations that could degrade the SC spectral coherence.[5]

As shown below, research into SC generation remains very active, but we have arrived at a natural point at which to conclude this literature review: the major developments in both generating and modeling SC generation in PCF have been surveyed, and the key connections with the existing nonlinear fiber optics literature have been made. We now proceed to a more technical description.

III. SOLID CORE PHOTONIC CRYSTAL FIBERS

In this section, we review the most important guidance properties of solid core PCF that are relevant to the SC generation process. We begin by showing in Fig. 1 a segment of the PCF used in the SC generation experiments reported by Ranka *et al.* (2000a). Figure 1(a) shows an electron micrograph of the full fiber cross section, clearly illustrating the presence of a central microstructure of air holes (black) embedded within a pure silica fiber strand (gray). Figure 1(b) shows a more detailed view of the central microstructure, and Fig. 1(c) presents a schematic representation of an ideal hexagonal structure with perfect regularity, defining the structural parameters Λ (the pitch) and ϕ (the hole diameter).

Understanding the guidance properties of such a PCF is straightforward. The fiber consists of a uniform refractive index material in which a microstructure lattice of air holes is embedded that runs along the fiber length. The removal of an air hole in the center introduces a defect associated with a locally elevated refractive index, and guided wave propagation within this elevated-index region occurs through an equivalent total internal reflection process (Birks *et al.*, 1997).

The guided mode characteristics for a given PCF structure can be obtained from the numerical solution of the vectorial transverse wave equation, and a number of numerical approaches for this purpose have been developed. The most general of these is based on the complete finite difference time-domain solution of the wave equation, but because this is so computationally expensive it is rarely used in practice. Rather, more efficient techniques such as the multipole method or the imaginary distance beam propagation method are preferred,

[5]Note that when we discuss the SC coherence in this paper, we are referring to the stability of the phase at each wavelength across the SC spectrum. The SC is of course assumed to be perfectly spatially coherent in all cases considered.

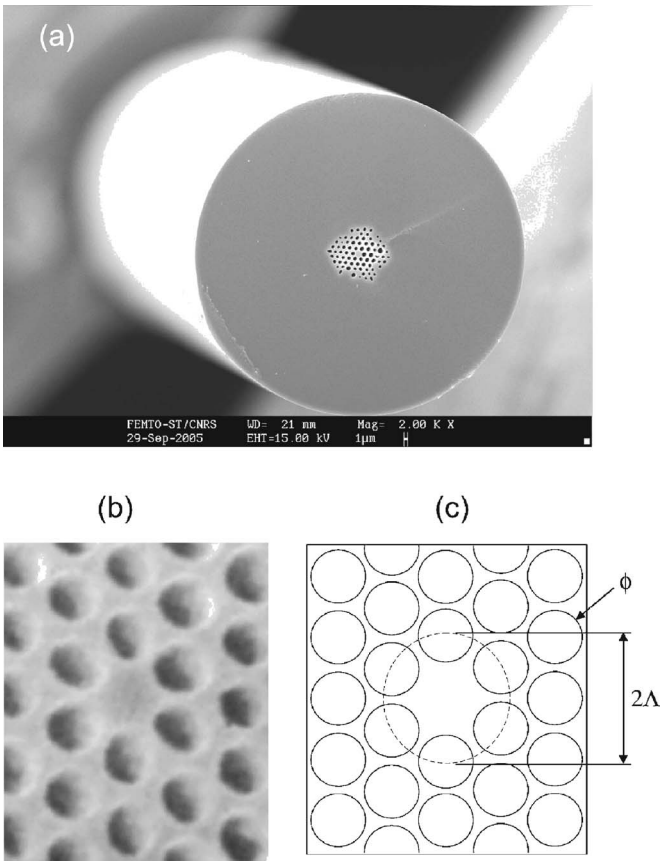

FIG. 1. Photonic crystal fiber structure. (a) Electron micrograph of the PCF used in the original supercontinuum generation experiments of Ranka *et al.* (2000a). (b) Detail of central microstructure and (c) ideal hexagonal structure defining parameters $\Lambda=1.6$ μm (pitch) and $\phi=1.4$ μm (hole diameter).

and a number of open-source and commercial packages exist for this purpose. More detailed discussions of the guidance properties of PCF and references to numerical techniques have been given by Bjarklev *et al.* (2003), Roberts *et al.* (2005), and Zolla *et al.* (2005).[6]

A particularly important property of PCF as identified by Birks *et al.* (1997) is its ability to exhibit endlessly single-mode behavior, in which propagation in higher-order modes is not observed, even at very short wavelengths. This is a specific property of PCF that is not observed in standard circular fibers. However, the class of PCF that is used in SC generation is generally different from this type of endlessly single-mode fiber. Endlessly single-mode PCFs have a relatively small air-fill fraction and large core areas, whereas the highly nonlinear PCFs used for SC generation generally have a high-air-fill fraction, leading to strong confinement and thus high nonlinearity. As a result, such fibers can exhibit multimode behavior, but the fundamental mode is nevertheless robust to excitation of higher-order modes due to the strong wave-vector mismatch between the fundamental and higher-order modes. The majority of SC generation experiments in PCF have been reported in this regime, with the SC output consistently observed in the fundamental mode (Ranka *et al.*, 2000a, 2000b). For this reason, our numerical modeling presented in the following sections assumes propagation in only the fundamental guided mode of the fiber. Nonetheless, some early experiments studying SC generation in the nanosecond regime did report multimode excitation (Provino *et al.*, 2001), and the particular conditions under which multimode excitation arises from high power pumping have recently been considered by Vidne and Rosenbluh (2005).

Another parameter that must be considered in any numerical treatment is possible PCF birefringence. Although Steel *et al.* (2001) have shown that PCF structures with perfect rotational symmetry are nonbirefringent, asymmetries (intentional or otherwise) introduced during fabrication can yield residual birefringence and polarization-maintaining behavior. Strong birefringence would certainly be expected to influence pulse propagation in PCF, but many reported SC generation experiments have been carried out under conditions in which birefringence effects were negligible, or by confining propagation along only one polarization eigenaxis. In these cases, the essential spectral broadening mechanisms can be well explained assuming scalar propagation, and this is therefore the approach we adopt here. For completeness, an overview of polarization-dependent effects is given in Sec. VIII.C.

The chromatic dispersion of the fundamental mode plays a critical role in SC generation because it determines the extent to which different spectral components of an ultrashort pulse propagate at different phase velocities in the fiber. Moreover, when coupled with nonlinear effects, a wide variety of different processes can occur as discussed below. The phase velocity is defined as $v_p=\omega/\beta(\omega)$ and thus the propagation of an ultrashort pulse is governed by its range of wave numbers $\beta(\omega)$. Relative to the pulse central frequency ω_0, the wave number at any frequency ω can be expanded in a Taylor series as $\beta(\omega)=\beta(\omega_0)+\beta_1(\omega_0)\Omega+(1/2)\beta_2(\omega_0)\Omega^2+(1/6)\beta_3(\omega_0)\Omega^3+\cdots$, where $\beta_k(\omega_0)=d^k\beta/d\omega^k|_{\omega_0}$ and $\Omega=\omega-\omega_0$. In this expansion, the first term simply describes the effective refractive index of the propagating mode, the second term is related to the group velocity of the pulse through $v_g=\beta_1^{-1}$, and the third term β_2 is the GVD. In nonlinear fiber optics, it is very common to encounter an alternative GVD parameter $D=-(2\pi c/\lambda^2)\beta_2$. We use both parameters here as convenient.

The total dispersion in a PCF depends on both material and waveguide contributions. The fabrication material of standard and photonic crystal fibers is very often based on fused silica, and thus the material dispersion contributions are essentially identical in the two cases. However, PCFs possess a revolutionary advantage compared to standard fibers in that the high-index contrast between the core material and the air holes leads to a very strong waveguide contribution that is extremely

[6]Without expressing any endorsement, we note that our GVD calculations used the *RSoft Photonics CAD Suite 5.1.4* (RSoft Design Group, Inc., NY), 2003.

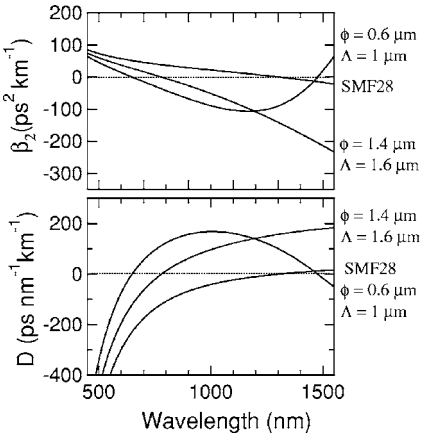

FIG. 2. Calculated GVD parameter β_2 (top) and D (bottom) for PCFs with parameters as shown: $\Lambda=1$ μm, $\phi=0.6$ μm; $\Lambda=1.6$ μm, $\phi=1.4$ μm [that used by Ranka *et al.* (2000a)]; and standard Corning SMF28 single-mode fiber.

sensitive to the geometrical distribution of air holes in the cladding microstructure.

Of particular interest for SC generation are so-called highly nonlinear PCF structures, where the guided mode is tightly confined in the core region through a high air-fill fraction and a pitch that is comparable to the wavelength of the modal field. In such cases, the effective area of the guided mode is typically two orders of magnitude smaller in PCF than in standard fiber, and there is thus a corresponding enhancement of the nonlinear response. In addition, such fibers present dispersion properties that are simply impossible to obtain with standard fiber technology.[7]

Figure 2 shows this explicitly, comparing the GVD (both β_2 and D) of two different PCF structures with that of standard telecommunications fiber SMF28. In particular, we see how the parameters $\Lambda=1.6$ μm and $\phi=1.4$ μm as used by Ranka *et al.* (2000a) shift the zero-dispersion wavelength from around 1.31 μm in SMF28 to approximately 780 nm in the PCF. Increasing the confinement using parameters $\Lambda=1$ μm, $\phi=0.6$ μm modifies the dispersion in an even more significant manner, leading to a local maximum in the GVD curve (plotted in terms of D) and a second ZDW (Knight *et al.*, 2000). In the context of SC generation, it is the first type of PCF structure that has attracted the most attention, and that is used in the numerical analysis presented below. Some interesting properties and applications of PCF with multiple zero-dispersion wavelengths are discussed in Sec. VIII.

IV. NUMERICAL MODELING

A. Nonlinear propagation equation

The starting point of any model for optical propagation is Maxwell's equations, and as discussed above their direct numerical solution was used in some of the first modeling of SC generation in PCF by Husakou and Herrmann (2001). However, because this approach neglected stimulated Raman scattering, most subsequent studies of pulse propagation in PCF have used some form of nonlinear propagation equation for the pulse envelope, in which Raman scattering can be straightforwardly included (Agrawal, 2001).

An added advantage of the envelope-based approach is that it has been extensively used to model nonlinear pulse propagation in fibers since the 1970s, and it facilitates comparison with results obtained in these many previous studies. However, compared to previous modeling in standard fibers, the dispersion and nonlinearity properties of PCF lead to significant quantitative differences in the extent of the nonlinear spectral broadening observed, resulting in particular problems in ensuring accurate simulation results. Moreover, particular physical processes that can be safely neglected when simulating pulse propagation in a standard fiber become significant in PCF and must be specifically included in any numerical model.

A propagation equation describing the evolution of the optical pulse envelope in an optical fiber can be derived from analytic simplification of Maxwell's equations. Under the assumption of unidirectional and single-mode scalar propagation, the work by Kodama and Hasegawa (1987) provided a comprehensive description of the procedure involved, with numerous references to early derivations of the well-known NLSE propagation equation. They also developed an important generalized nonlinear Schrödinger equation (GNLSE) to include effects of higher-order dispersion and stimulated Raman scattering. Blow and Wood (1989) and Mamyshev and Chernikov (1990) derived even more general scalar propagation equations, including a time-derivative contribution to the nonlinear term in order to model the frequency dependence of the medium nonlinear response. Complementary work by François (1991) derived an equivalent propagation equation that, in contrast to those above, was expressed in the frequency and not the time domain.

All of these GNLSE approaches involve only the first derivative with respect to the longitudinal spatial coordinate along the propagation direction, and it is often assumed that this limits their validity when compared to Maxwell's wave equation. A related concern is that the decomposition of the field in terms of an envelope and a carrier necessarily introduces a slowly varying envelope approximation.

An expected consequence of this approximation would be that envelope-based propagation equations lose physical validity as the duration of the pulse envelope approaches the carrier oscillation period, or equivalently when the bandwidth of the propagating field approaches the carrier frequency. A number of studies, however, have shown that the powerful concept of the pulse envelope can be extended down to the single optical cycle regime, and that envelope-based propagation equations can indeed accurately describe single-cycle

[7]Details of how equivalent nonlinear and dispersive properties can be obtained with suitable tapering of standard fibers have been presented by Wadsworth *et al.* (2002).

pulse propagation and extreme spectral broadening processes such as SC generation.

An important study by Brabec and Krausz (1997) derived a generic three-dimensional nonlinear envelope equation, and demonstrated its validity down to the single-cycle regime by direct comparison with the numerical solution of Maxwell's equations. For the particular case of propagation in optical fibers, Karasawa *et al.* (2001) adopted the same approach, deriving a one-dimensional few-cycle nonlinear envelope equation that was essentially identical to that obtained earlier by Blow and Wood (1989). The Blow-Wood equation has since proven to quantitatively describe the characteristics of SC spectra observed in experiments, and is the basis of the numerical modeling described here. We note nonetheless that ongoing theoretical work is still pushing the validity of the nonlinear envelope approach to its limits, and regimes where it needs possible correction are currently being discussed (Biancalana *et al.*, 2003; Kolesik *et al.*, 2004; Tyrrell *et al.*, 2005).

We now review the use of the scalar GNLSE to model ultrabroadband pulse propagation in PCF. We concentrate on the time-domain formulation, although we note that the frequency-domain formulation by François (1991) has also been used in a number of studies (Genty *et al.*, 2002; Chang *et al.*, 2003). The frequency-domain approach does show more directly the frequency dependence of effects such as dispersion, loss, and the effective mode area, but the time-domain approach has been preferred in the nonlinear fiber optics literature because its analytic similarity to the NLSE facilitates the physical interpretation of results. Moreover, the time-domain formulation has been formally extended to include noise effects (Drummond and Corney, 2001; Amans *et al.*, 2005), and this has proven to be indispensable in modeling the coherence and stability properties of SC generation. Of course, we have carefully checked that for the parameter regimes considered in this paper both approaches give identical results.

We define the electric field (linearly polarized along $\boldsymbol{x}$) as $\boldsymbol{E}(\boldsymbol{r},t)=(1/2)\boldsymbol{x}\{E(x,y,z,t)\exp(-i\omega_0 t)+\text{c.c.}\}$. In the frequency domain, the Fourier transform of $E(x,y,z,t)$ is $\tilde{E}(x,y,z,\omega)=F(x,y,\omega)\tilde{A}(z,\omega-\omega_0)\exp(i\beta_0 z)$, where $\tilde{A}(z,\omega)$ is the complex spectral envelope, while ω_0 and β_0 are the usual carrier frequency and wave number at that frequency, respectively. $F(x,y,\omega)$ is the transverse modal distribution with effective area defined as

$$A_{\text{eff}}(\omega)=\frac{\left(\int\int_{-\infty}^{+\infty}|F(x,y,\omega)|^2dxdy\right)^2}{\int\int_{-\infty}^{+\infty}|F(x,y,\omega)|^4dxdy}. \tag{1}$$

The time-domain envelope is obtained from $A(z,t)=(1/2\pi)\int_{-\infty}^{\infty}\tilde{A}(z,\omega-\omega_0)\exp[-i(\omega-\omega_0)t]d\omega$, and note that the amplitude is normalized such that $|A(z,t)|^2$ gives the instantaneous power in watts. With the change of variable $T=t-\beta_1 z$, we transform into a comoving frame at the envelope group velocity β_1^{-1}, and the corresponding GNLSE for the evolution of $A(z,T)$ is

$$\frac{\partial A}{\partial z}+\frac{\alpha}{2}A-\sum_{k\geq 2}\frac{i^{k+1}}{k!}\beta_k\frac{\partial^k A}{\partial T^k}=i\gamma\left(1+i\tau_{\text{shock}}\frac{\partial}{\partial T}\right)\left(A(z,t)\int_{-\infty}^{+\infty}R(T')\times|A(z,T-T')|^2dT'+i\Gamma_R(z,T)\right). \tag{2}$$

The left-hand side of Eq. (2) models linear propagation effects, with α the linear loss and the β_k's the dispersion coefficients associated with the Taylor series expansion of the propagation constant $\beta(\omega)$ about ω_0. In fact, given $\beta(\omega)$ the dispersion operator can be applied directly and in an approximation-free manner in the frequency domain through multiplication of the complex spectral envelope $\tilde{A}(z,\omega)$ by the operator $\beta(\omega)-\omega\beta_1-\beta_0$, and this is the approach to be recommended. Linear loss can also be straightforwardly included, but in the interests of clearly isolating the nonlinear and dispersive interactions this has been neglected in the simulations presented here.

The right-hand side of Eq. (2) models nonlinear effects: $\gamma=\omega_0 n_2(\omega_0)/c\,A_{\text{eff}}(\omega_0)$ is the usual nonlinear coefficient, where $n_2(\omega_0)$ is the nonlinear refractive index and $A_{\text{eff}}(\omega_0)$ is the mode effective area, both evaluated at the carrier frequency ω_0. The response function $R(t)=(1-f_R)\delta(t)+f_R h_R(t)$ includes both instantaneous electronic and delayed Raman contributions, with $f_R=0.18$ representing the Raman contribution. For h_R, it is common to use the experimentally determined Raman cross section (Stolen *et al.*, 1989), although essentially identical results can be obtained using the analytic forms in Blow and Wood (1989) or Hollenbeck and Cantrell (2002). The term Γ_R models the effects of spontaneous Raman noise and is discussed in Sec. IV.D. In simulations where noise is not included, $\Gamma_R=0$.

The time derivative term on the right-hand side of Eq. (2) models the dispersion of the nonlinearity. This is usually associated with effects such as self-steepening and optical shock formation, characterized by a time scale $\tau_{\text{shock}}=\tau_0=1/\omega_0$. As shown by Brabec and Krausz (1997), this term is, in fact, a key factor in allowing the extension of the envelope-based GNLSE to the single-cycle regime.

In the context of fiber propagation, additional dispersion of the nonlinearity arises from the frequency dependence of the modal effective area A_{eff} (Mamyshev and Chernikov, 1990). Although some studies of this effect in PCF have been reported (Iliew and Lederer, 2002; Fang *et al.*, 2003; Kolesik *et al.*, 2004), it has been neglected in much previous modeling of SC generation. However, the frequency dependence of A_{eff} can be included to first order through a simple correction to the value of τ_{shock} in Eq. (2). The corrected shock time scale

has been derived by Blow and Wood (1989) and Karasawa *et al.* (2001),

$$\tau_{\text{shock}} = \tau_0 + \frac{d}{d\omega}\left[\ln\left(\frac{1}{n_{\text{eff}}(\omega)A_{\text{eff}}(\omega)}\right)\right]_{\omega_0}$$
$$= \tau_0 - \left[\frac{1}{n_{\text{eff}}(\omega)}\frac{dn_{\text{eff}}(\omega)}{d\omega}\right]_{\omega_0}$$
$$- \left[\frac{1}{A_{\text{eff}}(\omega)}\frac{dA_{\text{eff}}(\omega)}{d\omega}\right]_{\omega_0}. \quad (3)$$

Calculating the corrected value of τ_{shock} requires only computation of the frequency dependence of A_{eff} and the effective index $n_{\text{eff}}(\omega)$.

Furthermore, the frequency dependence of n_{eff} is typically very small compared to that of the effective area, so the term in Eq. (3) that is dependent on its frequency derivative can be neglected. The qualitative effect of the modified shock term can now be easily seen. Since it is clear that the effective mode area in a single-mode waveguide decreases with increasing frequency (shorter wavelengths), the derivative term $[dA_{\text{eff}}(\omega)/d\omega]_{\omega_0} < 0$. Quantitatively, the effective area correction therefore increases the shock time scale τ_{shock}, which thus leads to a proportional increase in the dispersion of the nonlinear response through the time derivative term in Eq. (2). Further details can be found in Kibler *et al.* (2005). Finally, we note that this approach implicitly assumes that the frequency variation of n_2 is negligible, but this is usually a good approximation far from the ultraviolet resonances in fused silica (Milam, 1998).

B. Numerical issues

The numerical solution of Eq. (2) is carried out using an enhanced version of the well-known split-step Fourier scheme (Agrawal, 2001). In this method, the linear and nonlinear terms of the right-hand side of Eq. (2) are integrated separately and the results are combined to construct the solution to the full problem. The linear part of the equation is solved in the frequency domain, but the evaluation of the nonlinear term is less straightforward. Following Blow and Wood (1989), we treat the time derivative in the nonlinear term as a perturbation and use a second-order Runge-Kutta method to carry out the integration of the nonlinear step.[8] The convolution integral between the field intensity and the delayed Raman response is calculated as a simple product in the frequency domain. Both real and imaginary parts of the Raman susceptibility are included.

Although the practical implementation of the split-step Fourier method is quite straightforward, accurate results require care in the choice of time-frequency discretization and in the choice of longitudinal computation step. For temporal and spectral computation windows spanning T_{span} and F_{span}, respectively, the sampling theorem imposes the condition $T_{\text{span}}F_{\text{span}} = N_p$, where N_p is the number of discretization points. For the femtosecond pumping parameters considered here, the broadest SC typically require $F_{\text{span}} \sim 1000$ THz and $T_{\text{span}} \sim 20$ ps so that a very large number of points $N_p > 2^{15}$ is typically required. Of course, when equivalent bandwidths are generated using even longer pulses in the picosecond or nanosecond regime, the sampling condition implies that even greater computational effort is required. It is also important to ensure that the time window is sufficiently large to avoid cyclic wrapping of the temporal envelope with propagation, and this can be checked through inclusion of an absorbing window together with calculations to check photon-number conservation during propagation.

The longitudinal step size used is also of crucial importance, and must be sufficiently small to accurately model the nonlinear and dispersive interactions as the field propagates (Agrawal, 2001). An additional criterion concerns the need to avoid artifacts arising from numerical periodicity (Matera *et al.*, 1993). In this regard, we note that a recent review of strategies for the appropriate choice of step size in a systems context by Sinkin *et al.* (2003) can also be usefully applied to the case of modeling SC generation. In any case, it is essential always to test the simulation fidelity through a convergence study. This involves methodically changing the computational resolution in order to find an optimal choice that eliminates numerical artifacts while simultaneously minimizing computation time.

C. The spectrogram

Numerical integration of Eq. (2) yields the complex pulse envelope of the SC field, from which we can calculate both the temporal and spectral SC characteristics for comparison with experiment. In the vast majority of early experiments, however, the SC at the fiber output was only partially characterized through measurements of the optical spectrum. Although comparisons of simulated and measured SC spectra were important in establishing the validity of numerical models, it is clear that characterizing the SC field in such an incomplete way was unsatisfactory.

The problem of how to completely characterize an ultrafast optical field in both intensity and phase is a long-standing one, and it was only with the invention of techniques such as frequency-resolved optical gating (FROG) in the 1990s that it was solved in a satisfactory manner (Trebino, 2002). The FROG technique is based on the characterization of an ultrafast field through measurement of an optical spectrogram (or short-time Fourier transform), a function that represents the field in the time and frequency domains simultaneously. With $E(t)$ the field to be characterized, the spectrogram is defined by

[8]The reader is referred to Cristiani *et al.* (2004) where a number of misprints in Blow and Wood (1989) relating to the Runge-Kutta integration have been corrected.

$$\Sigma(\omega,\tau)=\left|\int_{-\infty}^{\infty}E(t)g(t-\tau)e^{-i\omega t}dt\right|^2, \tag{4}$$

with $g(t-\tau)$ a variable-delay gate function with delay value τ. Physically, the spectrogram describes the set of spectra of time-gated portions of $E(t)$, and provides a highly intuitive display of any waveform. In particular, the spectrogram allows direct visual inspection of the nature of the field spectral phase properties, and convenient identification of correlated temporal and spectral features (Treacy, 1971; Cohen, 1989). From an experimental point of view, although directly measuring $E(t)$ on femtosecond time scales is not possible, measuring its spectrogram is relatively straightforward. Moreover, using phase retrieval techniques it is possible to effectively invert the spectrogram to obtain the corresponding $E(t)$, allowing the complete characterization of the incident field (Trebino, 2002).

In the context of SC generation, experimental spectrogram measurements have been made by gating a replica of the input pulse to the PCF $[g(t)]$ with the output SC field $[E(t)]$ through cross correlation in a $\chi^{(2)}$ crystal phase-matched for sum-frequency generation. The spectral resolution of the sum-frequency field as a function of delay yields the spectrogram defined in Eq. (4), which is often referred to as the cross-correlation FROG trace (Linden *et al.*, 1998). It is interesting to remark here that although cross-correlation FROG was initially developed for experimental applications, it has subsequently initiated much interest in the theoretical representation of complex pulse propagation dynamics.[9] It is primarily in this context that we shall be using the spectrogram representation here, in order to more clearly illustrate the femtosecond dynamics of SC generation.

D. Inclusion of noise

Noise effects during SC generation can be rigorously modeled within the GNLSE framework through the inclusion of appropriate stochastic variables to model quantum-limited shot noise on the injected input field and spontaneous Raman fluctuations along the length of the fiber (Drummond and Corney, 2001). The effect of spontaneous Raman scattering during propagation appears explicitly through the multiplicative stochastic variable Γ_R shown in Eq. (2). In particular, this noise term has frequency-domain correlations given by

$$\begin{aligned}\langle\Gamma_R(\Omega,z)\Gamma_R^*(\Omega',z')\rangle &= \frac{2f_R\hbar\omega_0}{\gamma}|\mathrm{Im}[h_R(\Omega)]|[n_{\mathrm{th}}(|\Omega|)+U(-\Omega)]\\ &\times\delta(z-z')\delta(\Omega-\Omega').\end{aligned} \tag{5}$$

Here $\Omega=\omega-\omega_0$, the thermal Bose distribution $n_{\mathrm{th}}(\Omega)=[\exp(\hbar\Omega/k_BT)-1]^{-1}$, and U is the Heaviside step function. All other symbols have their usual meaning. The inclusion of the stochastic Raman term in the simulations was carefully checked against known analytic predictions for the relative spontaneous growth of the Raman-Stokes and anti-Stokes peaks under CW pumping conditions.

In addition to spontaneous Raman scattering, input pulse shot noise is modeled semiclassically through the addition of a noise seed of one photon per mode with random phase on each spectral discretization bin. An equivalent approach in the time domain involves adding a stochastic variation in the input field amplitude in each temporal discretization bin whose standard deviation is equal to the square root of the number of photons in the bin. Although the presence of linear loss during propagation can contribute an additional stochastic noise term to Eq. (2), this term has been neglected here.

Performing numerical simulations in the presence of noise allows us to investigate how fluctuations on the input pulse or during propagation influence the intensity and phase stability characteristics of the output SC. The approach that we use is based on performing multiple simulations in the presence of different random noise seeds to generate an ensemble of output SC fields. Statistical analysis over this ensemble can then conveniently yield different physical quantities for direct comparison with experiment. Specifically, we are able to examine how the presence of noise induces shot-to-shot fluctuations in both the temporal and spectral intensity distributions, and we can calculate mean temporal and spectral profiles for comparison with experiments. This simple calculation allows us to understand why fine structure in the spectral characteristics obtained from simulations is often unobserved in experiments that use optical spectral analyzers with limited spectral resolution and long integration times.

More quantitative insight is obtained by examining the wavelength dependence of the intensity and phase fluctuations across the SC spectrum. To characterize fluctuations in spectral phase across the SC, it is natural to think of an interferometric measure of the relative coherence between successive SC spectra generated in a multishot experiment. In this context, we note that studies of SC generation in bulk media have demonstrated a convenient experimental technique for characterizing SC coherence using a modified Young's two-source experiment (Bellini and Hänsch, 2000). Here, the two spatially separated sources that interfere are independently generated SC that yields a polychromatic interference pattern when combined in the far field. The spectral resolution of this pattern revealed distinct fringes at each wavelength in the spectrum, and the wavelength dependence of the fringe visibility provides a rigorous measure of the local coherence properties, since it is equal to the modulus of the complex degree of (mutual) coherence between the independent SC.

As shown by Dudley and Coen (2002a, 2002b), this measure of SC phase stability can be calculated from

[9] See, e.g., Dudley, Gu, *et al.* (2002), Genty *et al.* (2002), Efimov *et al.* (2004b), Genty, Lehtonen, and Ludvigsen (2004), Hilligsøe *et al.* (2004), Hori *et al.* (2004), Frosz *et al.* (2005), Schreiber *et al.* (2005).

numerical simulations. Quantitatively, the modulus of the complex degree of first-order coherence is defined at each wavelength in the SC by

$$|g_{12}^{(1)}(\lambda,t_1-t_2)| = \left| \frac{\langle E_1^*(\lambda,t_1)E_2(\lambda,t_2)\rangle}{\sqrt{\langle|E_1(\lambda,t_1)|^2\rangle\langle|E_2(\lambda,t_2)|^2\rangle}} \right|. \quad (6)$$

Here the angular brackets denote an ensemble average over independently generated pairs of SC spectra $[E_1(\lambda,t),E_2(\lambda,t)]$ obtained from a large number of simulations, and t is the time measured at the scale of the temporal resolution of the spectrometer used to resolve these spectra. Also, since we are mainly interested in the wavelength dependence of the coherence, we can calculate the modulus $|g_{12}^{(1)}|$ at $t_1-t_2=0$, which corresponds to the fringe visibility at zero path difference in Young's two-source experiment described above.

It is useful to introduce a spectrally averaged coherence $\langle|g_{12}^{(1)}|\rangle=\int|g_{12}^{(1)}(\lambda,0)||E(\lambda)|^2d\lambda/\int|E(\lambda)|^2d\lambda$ in order to quantify the overall coherence across the SC spectrum. $|g_{12}^{(1)}|$ is a positive number that lies in the interval $[0;1]$, with a value of 1 denoting perfect coherence. The value of $|g_{12}^{(1)}|$ is primarily a measure of phase stability, because two fields that have perfect phase coherence but whose intensities are completely uncorrelated still yield a high fringe contrast. For example, $|g_{12}^{(1)}|=0.75$ for field of uniformly distributed random amplitude and perfect phase stability. It is also important to note that $|g_{12}^{(1)}|$ is calculated over a finite bandwidth at each wavelength in the SC, fixed by the resolution of the simulations. When considering typical mode-locked sources with repetition rates around 80 MHz, such a simulation bandwidth is much greater than the longitudinal mode separation, and thus $|g_{12}^{(1)}|$ should be considered an effective average coherence over a large number of longitudinal modes. We must note as well that, in this limit, the average spectral density of the pulse train S_{avg} as measured, e.g., by a typical optical spectrum analyzer that does not resolve the individual modes, is simply given by the average of the spectral densities obtained from each individual simulation, i.e., $S_{\text{avg}}=\langle|E(\lambda)|^2\rangle$.

Wavelength-dependent intensity fluctuations can be quantified through the relative intensity noise (RIN). This is calculated from the rf noise spectrum measured within a particular optical bandwidth at each wavelength across the SC (von der Linde, 1986). The RIN (with units of dBc/Hz) is specified at a particular rf frequency and yields the noise power within a 1 Hz electrical bandwidth relative to the rf carrier. In the optical domain, the RIN is also equal to the variance of the intensity fluctuations at a particular frequency over the square of the average intensity and is directly related to the percentage of pulse-to-pulse amplitude jitter. The RIN is straightforward to calculate from an ensemble of simulations by analyzing the rf noise spectra assuming a given repetition rate of the SC spectra generated. Naturally, it is important that such a numerical analysis reproduces all relevant experimental conditions, but this model has been successfully tested against accurate experiments (Corwin *et al.*, 2003a, 2003b).

Although the modulus of the complex degree of first-order coherence $|g_{12}^{(1)}|$ and the RIN characterize different things, i.e., phase and intensity fluctuations, respectively, SC spectra that exhibit strong phase fluctuations also exhibit strong intensity fluctuations. Hence, the dependence of these two parameters on the pumping conditions follows similar trends. Because the first-order coherence $|g_{12}^{(1)}|$ has a more straightforward interpretation in terms of classical optics, we will mainly use this parameter to discuss noise-related issues in this review. We also point out that our discussion is focused on the fundamental broadband noise component due to shot noise and spontaneous Raman scattering. We therefore do not consider explicitly the large-amplitude noise component at low frequencies that results from technical noise, i.e., fluctuations in the laser input power that are in excess of shot noise (Newbury *et al.*, 2003). This can in principle be reduced by using a highly stabilized laser. In contrast, the broadband noise component discussed here will always be present since it results from intrinsic quantum fluctuations.

V. SUPERCONTINUUM GENERATION IN THE FEMTOSECOND REGIME: SOLITON DYNAMICS DECONSTRUCTED

In this section, we present results from numerical simulations to illustrate the SC generation process when pumping using femtosecond pulses in the anomalous GVD regime of the fiber. We discuss this in particular detail because it corresponds to the case in which the first results were obtained by Ranka *et al.* (2000a), and because it forms the basis of important applications in optical frequency metrology.

Many of the spectral broadening effects in this regime are dominated by soliton-related dynamics, and as will be clear from Sec. II these have been studied in other contexts since the early days of nonlinear fiber optics. Nonetheless, our objective here is to present a useful and synthetic treatment for the nonspecialist, isolating as much as possible distinct signatures of particular physical processes that occur during propagation. More detailed discussion of particular dependences on input pulse wavelength and duration for the femtosecond regime is considered in Sec. VI. SC dynamics for longer pulses are discussed in Sec. VII.

A. Basic numerical results

We first present numerical results obtained using typical experimental parameters with anomalous GVD regime pumping. We use the full GNLSE in Eq. (2), and consider a 15 cm length of a highly nonlinear PCF structure as shown in Fig. 1 with hole diameter $\phi=1.4$ μm, pitch $\Lambda=1.6$ μm, and ZDW around 780 nm. We assume a pump wavelength of 835 nm where the nonlinear parameter $\gamma=0.11$ W^{-1} m^{-1}. Although we use the global

TABLE I. Taylor series expansion coefficients at 835 nm for the GVD of the PCF used in the simulations. The structure has $\phi=1.4$ μm and $\Lambda=1.6$ μm. The full GVD curve is shown in Fig. 2.

$\beta_2=-11.830$ ps^2/km
$\beta_3=8.1038\times10^{-2}$ ps^3/km
$\beta_4=-9.5205\times10^{-5}$ ps^4/km
$\beta_5=2.0737\times10^{-7}$ ps^5/km
$\beta_6=-5.3943\times10^{-10}$ ps^6/km
$\beta_7=1.3486\times10^{-12}$ ps^7/km
$\beta_8=-2.5495\times10^{-15}$ ps^8/km
$\beta_9=3.0524\times10^{-18}$ ps^9/km
$\beta_{10}=-1.7140\times10^{-21}$ ps^{10}/km

PCF dispersion characteristics in our simulations, Table I provides the terms of a corresponding Taylor series expansion truncated at β_{10} that yields near-identical results.

The initial injected pulse used in the simulations has a hyperbolic secant field profile $A(0,T)=\sqrt{P_0}\,\mathrm{sech}(T/T_0)$, where $T_0=28.4$ fs and the peak power is $P_0=10$ kW. Note that hyperbolic secant input pulses are assumed for all other simulation results presented. The corresponding intensity full width at half maximum (FWHM) is $\Delta\tau=2\ln(1+\sqrt{2})T_0=1.763T_0=50$ fs. The parameter $\tau_{\mathrm{shock}}=0.56$ fs, which was calculated including the frequency dependence of the guided mode in the fiber using Eq. (3), as described above.

This choice of fiber and input pulse parameters allows us to investigate the SC generation process under conditions typical of many experiments in the literature. Noise sources as described in Sec. IV have been included so that initial evolution dynamics are accurately modeled, but results from only single simulations are presented; the statistical effects of noise are treated in detail in Sec. VI.D.

The first results we present illustrate the dynamics of the spectral and temporal evolution that can be examined through the numerical solution of Eq. (2). Figure 3 presents results for propagation over the 15 cm length of PCF. In Figs. 3(a) and 3(b), we plot spectral and temporal slices at representative propagation distances as shown. The SC spectra are shown on a logarithmic scale to illustrate the fine structure of the spectrum generated, and to show its continuity over an octave at the −20 dB level over 550–1100 nm at the fiber output.

The output spectral structure seen in the simulations qualitatively reproduces the SC characteristics seen in a number of experimental studies (Ranka *et al.*, 2000a; Dudley, Provino, *et al.*, 2002; Genty *et al.*, 2002; Herrmann *et al.*, 2002; Washburn *et al.*, 2002). Understanding the underlying physics, however, requires consideration of the dynamical evolution of the initial pulse toward the output SC, and it can be seen clearly that this is very complex. In fact, the use of discrete slices as in Fig. 3 only partially captures the richness of these dynamics, and significant additional insight is provided using a density plot representation as shown in the bottom subfigures. Here we represent both the spectral and temporal intensity using a logarithmic density scale truncated at −40 dB relative to the maximum value. This representation is particularly useful in showing the generation and evolution of low-amplitude temporal and spectral components.

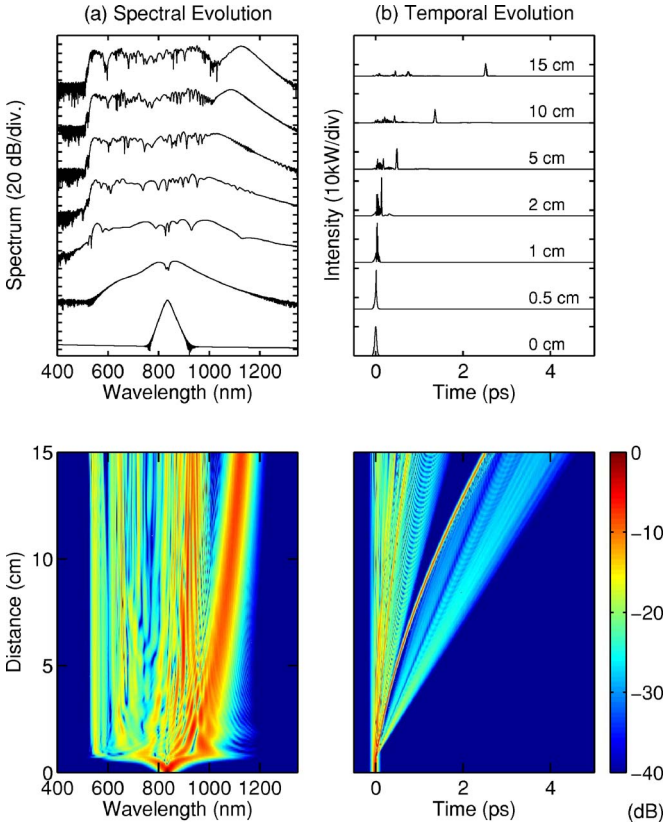

FIG. 3. (Color online) Results from numerical simulations showing (a) spectral and (b) temporal evolution for selected propagation distances. The input sech^2 input pulse at 835 nm has 10 kW peak power and 50 fs FWHM. Fiber parameters are given in the text. Bottom curves show the advantage of representing these results as (logarithmic) density plots. Unless otherwise stated, the 40 dB dynamic range density scale shown applies to all density plots.

We are now in a position to begin the development of an accurate description of the SC generation process. We first note that the initial stage of propagation is dominated by approximately symmetrical spectral broadening, most of which occurs within the first 0.5 cm. Strong temporal compression also occurs over this range but, after around 1 cm, the spectral broadening becomes strongly asymmetric with the development of distinct spectral peaks on both the short- and long-wavelength sides of the injected pump. This is associated with the development of distinct temporal peaks that sit upon a broader low-amplitude background. This temporal background is particularly apparent on the logarithmic density plot.

Although the majority of spectral broadening occurs within the initial stages of propagation, further propaga-

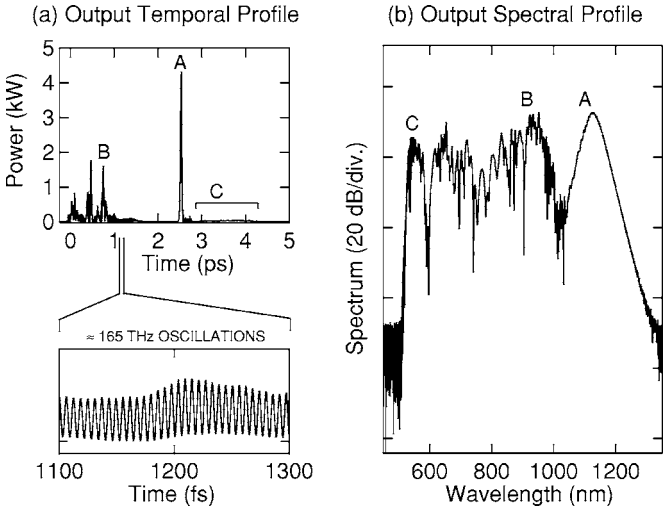

FIG. 4. Detailed view of output (a) temporal and (b) spectral characteristics. The labels *A*, *B*, and *C* show correlated temporal and spectral features.

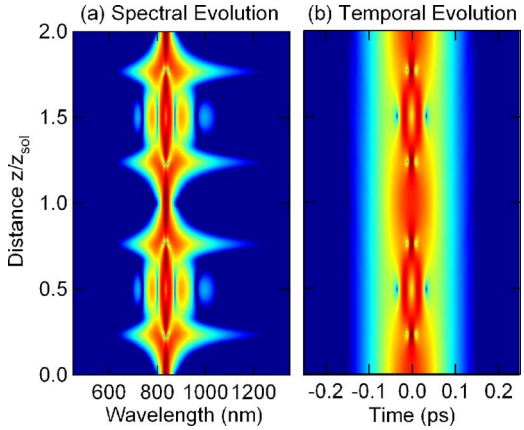

FIG. 5. (Color online) Periodic evolution of the spectral and temporal characteristics of the higher-order $N=3$ soliton as described in the text. The propagation distance is in units of the soliton period, which for these parameters is $z_{\mathrm{sol}}=10.6$ cm.

tion is associated with a clear continuous redshift of the long-wavelength components and the temporal separation of distinct peaks in the time domain. In contrast to this continuous shift to longer wavelengths, however, the short-wavelength edge of the SC does not undergo further extension with propagation.

Additional insight is obtained by plotting the output pulse characteristics in more detail as shown in Fig. 4. In particular, using numerical filtering we can readily correlate prominent features in the temporal intensity profile and the spectrum. For example, we can relate the distinct temporal peaks labeled *A* and *B* with the corresponding peaks on the long-wavelength side of the output spectrum, and we can correlate the strong normal GVD regime peak *C* around 550 nm with the broad low-amplitude pedestal on the trailing edge of the highest-amplitude temporal peak. The figure also shows other complex structure such as ultrafast oscillations on the temporal intensity profile that are shown on an expanded timebase.

A complete physical description of the SC generation process must be capable of explaining all of these characteristics. Of course, it is equally clear that a straightforward and intuitive explanation for such complex dynamics is not immediately apparent. Nonetheless, as we shall see, the essential features of the SC evolution seen in the preceding figures can be readily appreciated in terms of well-known aspects of soliton propagation dynamics. To do this, however, it is necessary to simplify the propagation problem and consider the major nonlinear processes individually.

B. Deconstructing the dynamics

1. Soliton fission

Supercontinuum generation with anomalous GVD regime pumping is dominated by soliton-related propagation effects. The most important of these in the initial stages is the soliton fission process alluded to in Sec. II.B, whereby a pulse with sufficient peak power to constitute a higher-order soliton is perturbed and breaks up into a series of lower-amplitude subpulses.

The soliton order of the input pulse N is determined by both pulse and fiber parameters through $N^2=L_D/L_{\mathrm{NL}}$. Here $L_D=T_0^2/|\beta_2|$ and $L_{\mathrm{NL}}=1/\gamma P_0$ are the characteristic dispersive and nonlinear length scales, respectively. For the pulse and fiber parameters given in the preceding section, $N\simeq 8.5$. Although the signatures of pulse break up and decay are certainly apparent with such a high value of N, the underlying physics can be illustrated more clearly using a lower soliton order. We choose $N=3$, which corresponds to a peak power of $P_0=1.25$ kW with the other parameters as above.

To discuss the soliton fission process in detail, we begin by considering the propagation characteristics of an ideal higher-order soliton where propagation is described by the standard NLSE. This corresponds to neglecting all higher-order nonlinear and dispersive effects (and all noise sources) in Eq. (2).[10] In this case, an injected higher-order soliton shows periodic spectral and temporal evolution over a soliton period $z_{\mathrm{sol}}=(\pi/2)L_D$. For our parameters, $L_D=6.8$ cm and $z_{\mathrm{sol}}=10.6$ cm. These ideal periodic propagation characteristics are shown in Fig. 5, which plots the higher-order soliton evolution over two soliton periods.

In the femtosecond regime, higher-order dispersion and Raman scattering are the two most significant effects that can perturb such ideal periodic evolution and induce pulse breakup through soliton fission. Which of the two effects dominates depends primarily on the input pulse duration. For input pulses of durations exceeding 200 fs, the input pulse bandwidth is sufficiently low that the Raman perturbation generally dominates, whereas for pulses of duration less than 20 fs, it is the

[10]Specifically, we consider only β_2 in Table I; we take $f_R=0$, $\tau_{\mathrm{shock}}=0$, and turn off all noise sources in Eq. (2).

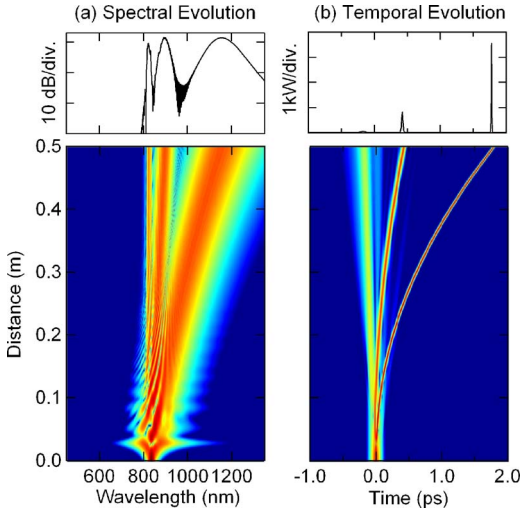

FIG. 6. (Color online) Results from numerical simulations showing (a) spectral and (b) temporal evolution for Raman-induced fission of an incident $N=3$ soliton as described in the text. Top curves show the output profiles after 0.5 m propagation.

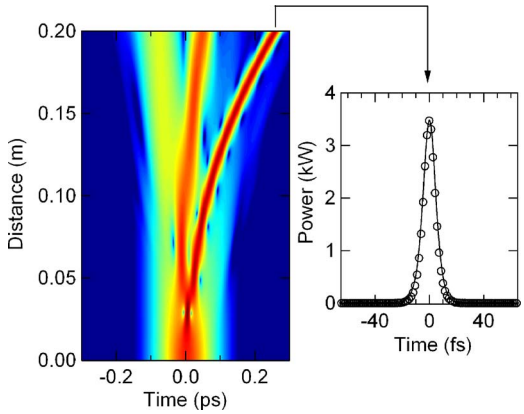

FIG. 7. (Color online) Soliton fission detail. Left: The initial soliton fission process in the presence of only Raman scattering for $N=3$. In particular, we note the onset of soliton fission around $L_D/N \simeq 2.3$ cm. Right: The intensity profile of the first ejected soliton (solid line) compared with that predicted from Kodama and Hasegawa (1987) (circles).

dispersive perturbation that induces the pulse breakup. For pulses of intermediate duration such as those that we consider here (recall that $\Delta\tau=50$ fs), Raman and higher-order dispersion introduce comparable perturbation. However, to isolate the fission process from other dispersion-related effects discussed in the next section, it is convenient to consider only Raman-induced perturbations.[11]

The Raman perturbation of periodic higher-order soliton evolution is shown in the numerical results of Fig. 6. In particular, we see how the injected pulse undergoes an initial phase of temporal compression and spectral broadening but, instead of periodically recovering to its initial state after $z_{\mathrm{sol}}=10.6$ cm, the pulse breaks up into a train of individual pulses. Each of these pulses is, in fact, a constituent fundamental soliton and the number of pulses is equal to the incident pulse soliton order N.

The individual solitons are ejected from the input pulse in an ordered fashion one by one. The ejected solitons are arranged by peak power with the highest peak power (shortest) solitons exhibiting the largest group velocity difference relative to the pump wavelength. Explicit expressions for the constituent fundamental soliton amplitude and width in terms of the parameters of the injected N soliton have been obtained theoretically by Kodama and Hasegawa (1987). These are $A_j(z,T)=\sqrt{P_j}\mathrm{sech}(T/T_j)$ for $j=1,\ldots,N$, where $P_j=P_0(2N-2j+1)^2/N^2$ and $T_j=T_0/(2N-2j+1)$. Solitons that are ejected earlier have higher amplitudes, shorter durations, and propagate with faster group velocities. For the first (highest amplitude) ejected soliton, good agreement between theory and simulation can be obtained even after a relatively short propagation distance. Figure 7 presents an exploded view of the soliton fission process onset, comparing the intensity profile of the $j=1$ ejected soliton (FWHM 10 fs) from simulations (solid line) with that expected from the soliton fission theory (open circles).

The distance at which fission occurs generally corresponds to the point at which the injected higher-order soliton attains its maximum bandwidth. A number of empirical expressions for this characteristic distance have been obtained in the context of soliton-effect compression (Dianov *et al.*, 1986; Chen and Kelley, 2002), but for our purposes we have found that this fission distance can be usefully (and simply) defined as $L_{\mathrm{fiss}} \sim L_D/N$. For our parameters we have $L_D/N \simeq 2.3$ cm, which agrees well with the numerical results shown in Fig. 7. After the initial fission, each constituent soliton experiences a continuous shift to longer wavelengths from the soliton self-frequency shift because the individual soliton bandwidths overlap the Raman gain. As shown by Gordon (1986a), the dynamics of the frequency shift ν_R can be expressed as $d\nu_R/dz \propto |\beta_2|/T_0^4$. A consequence of this is that the shorter-duration solitons that are ejected earlier in the fission process experience greater self-frequency downshifts and walkoff proportionally faster from the input pump wavelength. This can, in fact, be clearly seen in Fig. 6.

The pulses eventually separate so that the individual fundamental solitons are seen distinctly at the fiber output. We have found that soliton separation begins to become apparent in the temporal and spectral characteristics after a propagation distance of typically $\sim 5L_D$. However, observing distinct signatures of all N solitons in both time and frequency domains can require significantly further propagation. For our parameters $5L_D \simeq 34$ cm, and indeed we see from Fig. 6 that soliton separation is apparent at this stage. At intermediate

[11]Specifically, we consider only β_2 in Table I; we take $f_R=0.18$, $\tau_{\mathrm{shock}}=0$, and turn off all noise sources in Eq. (2).

propagation distances, the figure also shows that the spectral and temporal characteristics are more complex. The spectrum in particular shows a strong modulation behavior for distances less than 20 cm, but this is simply understood as due to the linear spectral interference of the different solitons whose bandwidths still overlap at this stage.

2. Dispersive wave generation

The results in Figs. 6 and 7 clearly facilitate the physical interpretation of the full SC evolution shown in Fig. 3. In particular, the initial evolution is qualitatively similar in the two cases, highlighting the fundamental importance of higher-order soliton dynamics that leads to an initial stage of spectral broadening and temporal compression. After this initial propagation, the temporal pulse break up and the generation of distinct spectral peaks in the anomalous GVD regime can be clearly identified as due to soliton fission and the Raman self-frequency shift of ejected constituent fundamental solitons.

On the other hand, the soliton-fission dynamics alone does not reproduce the normal GVD regime spectral structure or the low-amplitude temporal background that are clearly seen in the full SC generation case. Indeed, the simulations in Fig. 6 for ideal soliton fission show that ejected solitons propagate unperturbed even in the presence of the continuous shift to longer wavelengths. This ideal case, however, has neglected the effect of higher-order dispersion on the propagating solitons, and we now discuss this in detail.

The presence of higher-order dispersion modifies soliton fission in two main ways. First, as an ejected fundamental soliton shifts to longer wavelengths through the Raman effect, it encounters a varying local value of β_2, and its temporal width and peak power adjust themselves to conserve a unit soliton number during propagation.[12] Second, the presence of higher-order dispersion can also lead to the transfer of energy from the soliton to a narrow-band resonance in the normal GVD regime, and the associated development of a low-amplitude temporal pedestal (Wai *et al.*, 1986). The position of this resonance can be readily obtained from a phase-matching argument involving the soliton linear and nonlinear phase and the linear phase of a continuous wave at a different frequency (Akhmediev and Karlsson, 1995). In particular, for a soliton of peak power P_s at frequency ω_s, a dispersive wave is generated at a frequency ω_{DW} where $\beta(\omega_s)-\omega_s/v_{g,s}+(1-f_R)\gamma P_s=\beta(\omega_{\mathrm{DW}})-\omega_{\mathrm{DW}}/v_{g,s}$, with $v_{g,s}$ the soliton group velocity at ω_s. Later work has also examined the structure of the perturbed soliton and pedestal in more detail (Elgin *et al.*, 1995). The study by Akhmediev and Karlsson (1995) is also noteworthy for establishing that the emission of the dispersive wave is equivalent to a Cherenkov radiation process in the frame of reference defined by comoving time T and the propagation direction z.

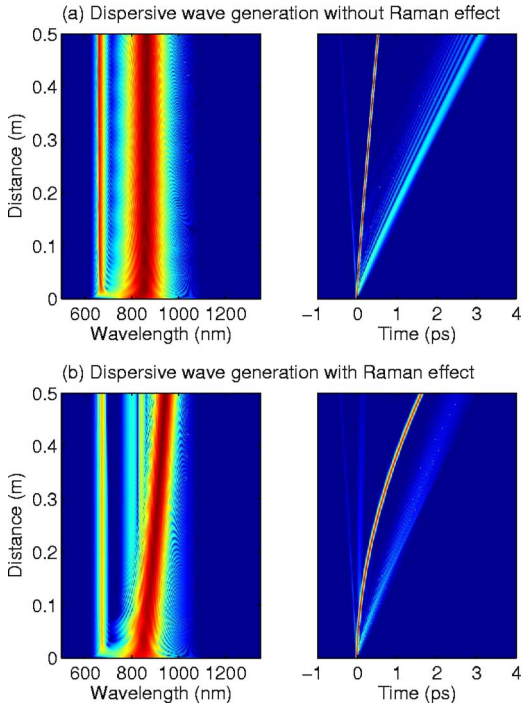

FIG. 8. (Color online) Results from numerical simulations showing the spectral (left) and temporal (right) signatures of dispersive-wave generation from a fundamental soliton (a) in the absence of and (b) in the presence of Raman scattering. The fundamental soliton parameters correspond to the first ejected soliton from the fission process shown in Fig. 7. Here $P_0=3.48$ kW and FWHM 10 fs at 835 nm.

In SC generation, the particular fundamental solitons that stimulate the dispersive wave radiation are those that are successively ejected from the input pulse during its fission. Moreover, the initial emission of dispersive radiation is primarily from the first ejected soliton that possesses the broadest bandwidth and thus has maximum overlap with the dispersive wave resonance. To consider this process in more detail, the results in Fig. 8 isolate the dispersive wave generation process for the first ejected soliton from the fission process described above and seen in Figs. 6 and 7. Specifically, we consider the propagation of the $j=1$ ejected fundamental soliton above, with peak power $P_0=3.48$ kW and FWHM 10 fs ($T_0=5.67$ fs) at 835 nm, and we examine how its characteristics are modified in the presence of the full PCF dispersion curve. We recall that the ZDW of this fiber is at 780 nm.

To isolate the process even further, the first simulation in Fig. 8(a) shows propagation in the absence of Raman scattering. We note both the perturbation of the expected stable solitonic propagation and the clear spectral and temporal signatures of the dispersive wave generation. However, under these conditions the soliton frequency variation with propagation is negligible. These dynamics are of course significantly modified un-

[12]In fact, this is equivalent to conserving the soliton pulse area $\Theta=\sqrt{P_0}T_0$ since the soliton order can be expressed as $N=\Theta(\gamma/|\beta_2|)^{1/2}$.

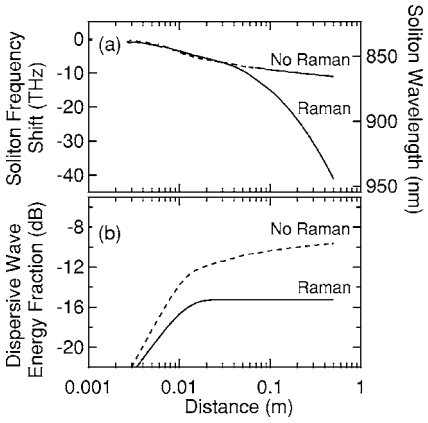

FIG. 9. Simulation results illustrating the influence of Raman scattering on dispersive-wave dynamics showing the evolution with distance of (a) the mean soliton frequency (left axis) and wavelength (right axis) and (b) the relative energy radiated to the dispersive wave.

der the realistic conditions where the Raman effect is present. This is shown in Fig. 8(b), where the continuous shift to longer wavelength due to the self-frequency shift is apparent.

The particular influence on the dispersive wave generation is shown more clearly in Fig. 9, where we show (a) the evolution of the mean soliton frequency for the two cases and (b) the corresponding integrated energy under the dispersive wave frequency component. We see that the continuous shift to longer wavelengths due to the self-frequency shift means that the resonant energy transfer occurs efficiently only during the initial propagation phase. Thus, although the visual dynamics in Figs. 8(a) and 8(b) are similar, the results in Fig. 9 show that the energy transferred to the dispersive wave is significantly reduced in the presence of Raman scattering.

We can now interpret the short-wavelength features in the SC spectra shown in Fig. 3 as due to dispersive wave generation seeded from the initial soliton fission process. The abrupt short-wavelength edge seen on the SC can be understood as arising from the intrinsically narrowband nature of the dispersive wave resonance. Although the resonance position can be determined using a phase-matching condition as discussed above, describing the growth dynamics and spectral structure of the dispersive wave component in detail is significantly more complex, depending on factors such as the particular dispersion properties of the PCF used and the wavelength of the pump radiation relative to the fiber ZDW. Indeed, a quantitative description generally requires a numerical approach, and detailed studies based on the full PCF dispersion profile have been reported by Herrmann *et al.* (2002), Hilligsøe *et al.* (2003), and Cristiani *et al.* (2004). Some additional insight can also be obtained from earlier theoretical studies of perturbed soliton propagation (Elgin *et al.*, 1995; Gölles *et al.*, 1997; Horikis and Elgin, 2001).

These results also illustrate the significance of the mutual interaction between stimulated Raman scattering and dispersive wave generation. The presence of higher-order dispersion modifies the evolution of the propagating Raman soliton and reduces the magnitude of the soliton self-frequency shift [compare Figs. 6 and 8(b)], and the Raman scattering itself imposes a fundamental restriction on the propagation distance over which soliton-induced dispersive wave generation occurs. From a practical point of view, although these interactions are unavoidable, they could be considered deleterious because they reduce the SC bandwidth from that expected if it were possible to excite these processes in isolation. However, as shown by Genty, Lehtonen, and Ludvigsen (2004), the generated Raman soliton and dispersive waves can couple through XPM to generate additional frequency components that increase the overall bandwidth.

At this point, recall that the soliton-related dynamics discussed above have been considered in PCF structures with only one ZDW, typical of most reported SC generation experiments. However, as seen in Fig. 2, an appropriate choice of the PCF structural parameters can lead to a fiber with two ZDWs—a large region of anomalous GVD centrally located between two regions of normal GVD. In this case, soliton injection in the central anomalous GVD region can lead to dispersive wave generation and energy transfer across both ZDWs, but with qualitatively different dynamics because of the dispersion curve with different slopes at each point of zero dispersion. Detailed theoretical and experimental studies of these processes have been carried out by Skryabin *et al.* (2003), Efimov *et al.* (2004b), Genty *et al.* (2004), and Hilligsøe *et al.* (2004). This is revisited in Sec. VIII.A.

C. Interpretation using the spectrogram

We are now in a position to reinterpret the temporal and spectral evolution plots shown in Fig. 3 for the case of SC generation when all relevant physical processes are included in the modeling. It is apparent that the full SC generation process is significantly more complex than the two isolated physical processes considered above. Nonetheless, a comparison of Fig. 3 with Figs. 6 and 8 reveals the clear signatures of both (i) soliton fission followed by the Raman shifting of constituent ejected solitons and (ii) the associated generation of dispersive waves from each ejected fundamental soliton due to the effect of higher-order dispersion. When examined in this way, the physical origin of the complex structure of the SC spectrum takes on a more straightforward physical interpretation in terms of effects well known from previous studies of nonlinear pulse propagation in optical fibers.

Even more insight into the SC generation process can be obtained by considering the spectrogram of the SC output. To this end, Fig. 10 plots the calculated spectrogram [from Eq. (4)] where $E(t)$ is the SC field and the gate function $g(t)$ is the 50 fs input pulse, and we project the time-frequency structure of the spectrogram onto

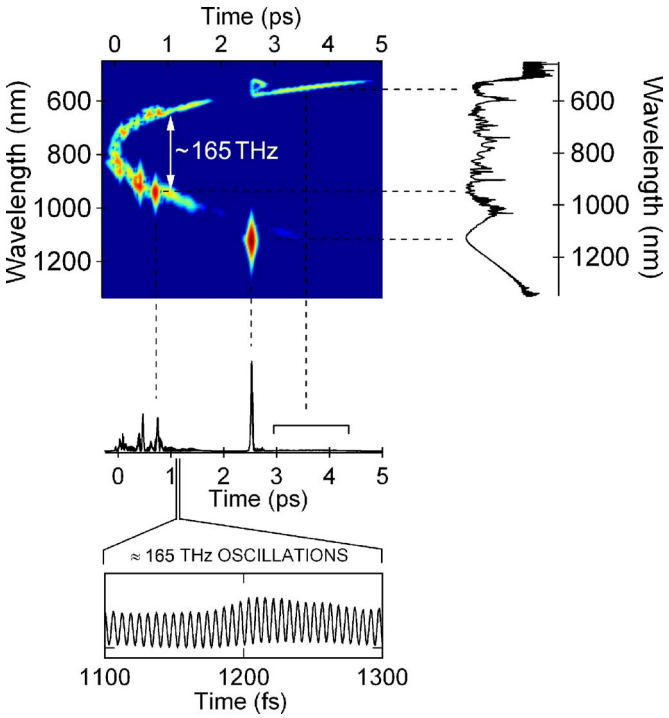

FIG. 10. (Color online) Simulated supercontinuum spectrogram projected onto the temporal intensity and spectrum for input pulses at 835 nm of 10 kW peak power and 50 fs FWHM propagating in 15 cm of PCF. The gate function used is the 50 fs input pulse. An animation of the evolution over the 15 cm propagation length is available as an EPAPS Document cited in the Reference section.

the output temporal intensity (bottom axis) and spectrum (right axis).

The advantages of the spectrogram for interpreting the different SC features can be clearly seen from this figure. For example, simple visual inspection of the spectrogram allows the particular time and frequency domain signatures of the dispersive wave and Raman soliton components to be immediately identified and correlated. In addition, the parabolic group delay variation with wavelength (related to the dispersive characteristics of the fiber) is immediately apparent. Even more significantly, since the portion of the temporal intensity profile that has developed ultrafast oscillations is seen to be associated with two distinct spectrogram wavelength components separated by 165 THz, the origin of the ultrafast modulation can be physically interpreted as a result of the beating between these components. Significantly, the spectrogram allows the origin of this modulation to be readily identified in a way not possible from examining the separate intensity and spectral measurements.

For the purposes of developing an intuitive appreciation of the dynamics of SC generation, we have found it instructive to animate the evolution of the temporal intensity, spectrum, and spectrogram as a function of propagation distance in the fiber (Dudley, Gu, *et al.*, 2002; Genty *et al.*, 2002). For such an animation corresponding to Fig. 10, refer to the EPAPS Document cited

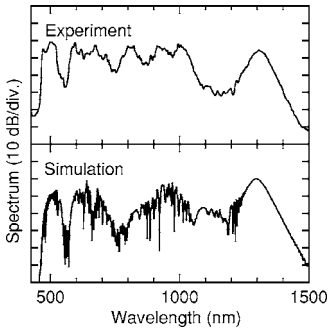

FIG. 11. Comparison between experimental and simulations corresponding to the output SC spectra obtained using ~22 fs (FWHM) pulses of energy 0.9 nJ injected into 15 cm of PCF. Adapted from Corwin *et al.*, 2003b.

in the Reference section. The animation clearly shows how the onset of pulse breakup and the formation of Raman solitons are associated with the development of distinct peaks in the spectrum and, in addition, how the generation of energy in the dispersive wave occurs within the initial stages of propagation. From a theoretical viewpoint, the spectrogram provides a natural way to interpret and correlate complex features in the temporal and spectral domains, and we suggest that its use becomes standard practice in nonlinear fiber optics for analyzing complex pulse propagation dynamics.

D. Comparison with experimental results

In this section, we present some key experimental results that highlight the success of the numerical modeling in reproducing experimentally observed features. A more complete survey of the experimental literature for the femtosecond regime is given in Sec. VI.E.

We begin by showing results of a study reported by Corwin *et al.* (2003a, 2003b) where careful experimental measurements were made of the SC spectral characteristics. In these experiments, an argon-ion laser-pumped femtosecond Ti:sapphire laser was used as a source of pulses with a typical bandwidth of ~45 nm FWHM centered at 810 nm, and at a 100 MHz repetition rate. A double-pass fused-silica prism pair could control the chirp on the laser pulses, and interferometric autocorrelation measurements were used to infer both the input-pulse duration and pulse chirp. With the system configured to produce near Fourier transform limited pulses of 22 fs FWHM, pulses of energy 0.9 nJ were injected into a 15 cm long microstructure fiber having characteristics similar to those described above, but with a ZDW around 770 nm. In this case, Fig. 11 compares the experimentally measured spectrum (top) with that obtained from numerical simulations using the GNLSE model above (bottom). Simulations reproduce the overall spectral width (more than 400 THz at the −20 dB level), as well as the position of the Raman soliton and dispersive wave peaks. Simulations do exhibit fine spectral structure that is not observed in experiments be-

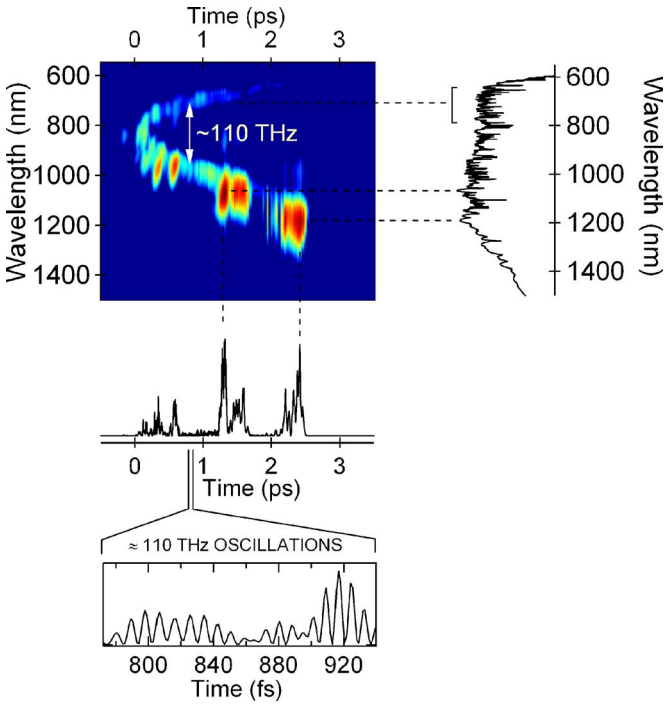

FIG. 12. (Color online) Experimentally measured spectrogram of a SC generated in a 16 cm length of PCF using 25 fs pulses at 800 nm with energy around 1 nJ. Adapted from Dudley, Gu, *et al.*, 2002.

cause of the finite spectrometer resolution (≃2.5 nm), but it is clear that there is extremely good correspondence nonetheless.

Simulations of the SC generation process have also proven extremely valuable to assist in the physical interpretation of the complex structure of SC spectrogram measurements made using cross-correlation FROG. Spectrogram measurements of SC generation had been reported as early as 2001 by Xu *et al.* (2001), and clearly showed that the generated SC possessed very complex spectrotemporal structure. Numerical simulations were then used to interpret these experimental data by projecting the time-frequency structure of the spectrogram onto the experimentally measured temporal and spectral intensity distribution.

Specifically, Fig. 12 shows the experimental results reported by Dudley, Gu, *et al.* (2002) for a SC generated in a 16 cm length of PCF using 25 fs pulses at 800 nm with energy around 1 nJ. Because of uncertainties in the fiber parameters in these experiments, it was not possible to perform a meaningful quantitative comparison with numerical simulations, but it is nonetheless clear that the experimental spectrogram shows many of the features seen in the simulation results in Fig. 10. As with simulations, the spectrogram representation clearly facilitates the physical interpretation of the temporal and spectral characteristics of the SC in a way that is not possible with separate time-domain and frequency-domain measurements.

VI. SUPERCONTINUUM GENERATION IN THE FEMTOSECOND REGIME: GENERAL FEATURES

The preceding section considered the dynamical features of femtosecond SC generation for the particular case in which signatures of soliton-related spectral broadening processes are clear and unambiguous. Although this regime corresponds to that studied in the initial SC generation experiments in PCF (Ranka *et al.*, 2000a), subsequent studies by many different groups have shown that the SC characteristics can vary significantly with the particular combination of pulse and fiber parameters that are used, especially the position of the input pulse wavelength relative to the fiber ZDW.

Because there is little physical insight to be gained by considering every possible pump and fiber parameter combination, our aim is to emphasize the major SC dynamical regimes that depend particularly on the input pulse wavelength and duration. Although many experiments have reported SC generation using pulses of different peak power, we do not explicitly consider this dependence, as it is evident that increased input power impacts directly on the magnitude of the observed spectral broadening. We consider a fixed 15 cm length of the same fiber type as in the preceding section, but our focus on discussing the dynamics readily allows the SC dependence on propagation distance (thus fiber length) to be seen. We also stress that the simulation parameters chosen are intermediate between the extremes that have been reported in the literature, and allow us to discuss all important features that have been experimentally observed.

A. Dependence on input pulse wavelength

Our objective in this section is to examine the dependence of the SC characteristics on pump wavelength, and to discuss the particular dynamical differences observed as the input wavelength is tuned across the ZDW. An important motivation here is to address a common misconception that the dramatic SC generation results in PCF have been obtained primarily because of the enhanced nonlinearity of the fiber. In fact, the position of the input pulse relative to the fiber ZDW is as critical to the SC generation process as is the enhanced nonlinearity. This is because the dispersion characteristics influence the fundamental nature (nonsolitonic or solitonic) of the propagation dynamics, as well as phase-matching criteria associated with processes such as dispersive wave generation. It is therefore more correct to say that the dramatic SC results in PCF have been obtained because of the combination of enhanced nonlinearity with the ability to engineer the dispersion properties of PCF relative to the emission wavelengths of available mode-locked lasers.

In our simulations, we consider an identical 15 cm fiber segment to that in the preceding section, and use the same input pulse peak power (10 kW) and duration (T_0=28.4 fs, $\Delta\tau$=50 fs). Maintaining constant peak power and duration in these simulations illustrates the

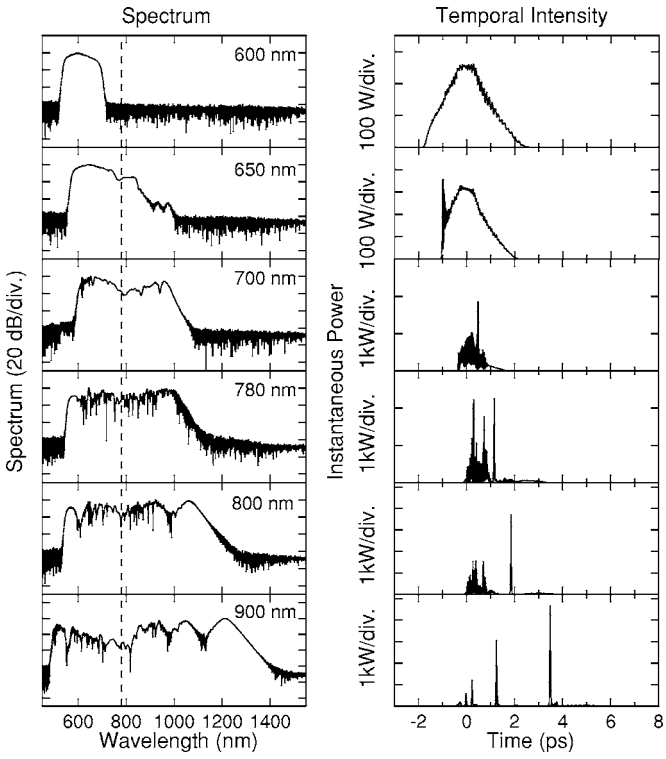

FIG. 13. Results from numerical simulations showing the spectral and temporal SC characteristics observed for selected pump wavelengths as indicated. The input pulse peak power is 10 kW and duration (FWHM) is 50 fs. The dashed line shows the fiber ZDW. Spectrogram animations for the 650, 700, and 780 nm cases are available as an EPAPS Document cited in the Reference section.

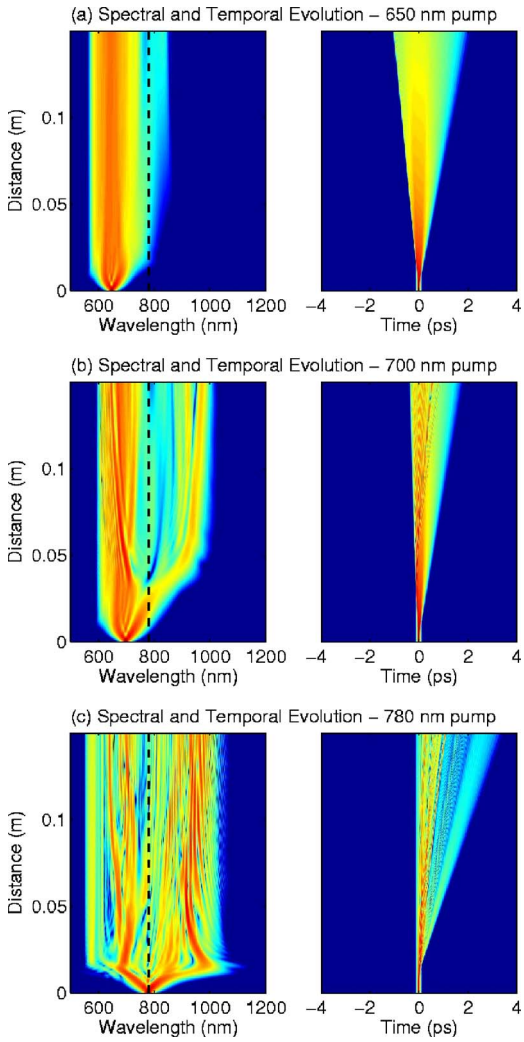

FIG. 14. (Color online) Results from numerical simulations showing density plots of the spectral and temporal evolution of supercontinua generated by pulses with wavelengths of (a) 650, (b) 700, and (c) 780 nm. The input pulse peak power is 10 kW and duration (FWHM) is 50 fs. The dashed line shows the fiber ZDW.

importance of dispersion (rather than nonlinearity) in influencing the dynamics.

Figure 13 summarizes the results obtained, showing the fiber output characteristics for selected pump wavelengths as indicated. The dashed line in the spectral plots shows the PCF ZDW. From the figure it is possible to broadly identify three different regimes of spectral broadening. For a normal GVD pump wavelength of 600 nm far from the ZDW, SPM is the dominant nonlinear process, and the approximately symmetric temporal and spectral properties are typical of those expected from the interaction of SPM and the normal GVD of the fiber (Agrawal, 2001). As the pump wavelength approaches the ZDW but still lies within the normal GVD regime, the initial spectral broadening due to SPM transfers spectral content into the vicinity of the ZDW and across into the anomalous GVD regime. This can be seen to some extent for a 650 nm pump, but is more apparent for a 700 nm pump. For pump wavelengths exceeding 780 nm, the energy transferred into the anomalous GVD regime increases, and soliton dynamics play an increasingly important role. Specifically, the spectral and temporal SC characteristics exhibit clear signatures of soliton fission and dispersive wave generation as seen above.

Although normal GVD propagation characteristics are well known, and the soliton propagation dynamics have been considered above, certain aspects of the wavelength-dependent behavior seen in Fig. 13 merit further discussion. We first consider the transition from nonsoliton to soliton dynamics over the range 650–780 nm. To this end, Fig. 14 shows the detailed spectral and temporal evolution of the input pulses along the fiber at selected wavelengths of (a) 650, (b) 700, and (c) 780 nm. For corresponding spectrogram animations, refer to the EPAPS Document cited in the Reference section. The gate pulse used in the spectrogram calculations had FWHM 50 fs.

For the 650 nm case in Fig. 14(a), the initial dynamics are dominated by the interaction of SPM and normal GVD. Because this leads to significant temporal broadening and rapid decrease of peak power over the first few centimeters of propagation, the extent of nonlinear spectral broadening is necessarily limited. Nonetheless, the spectral broadening that does occur is sufficient to

transfer energy in the vicinity of the ZDW (Yanovsky and Wise, 1994), leading to characteristic temporal oscillations on the pulse envelope (Dudley *et al.*, 1997). These ultrafast oscillations are, in fact, seen in Fig. 13 on the leading edge of the pulse temporal intensity profile for the 650 nm case. Dispersion of the nonlinearity and Raman effects also plays a role in modifying the spectral structure, and both phase and group velocity matching criteria can be significant (Boyer, 1999).

As the pump wavelength further approaches the ZDW, the energy transferred into the anomalous GVD regime increases, and we observe mixed normal GVD and soliton dynamics. This is illustrated in Fig. 14(b) for a 700 nm pump, and is particularly clear in the spectral evolution, where we see that the SPM-dominated broadening in the normal GVD regime is accompanied by the development of Raman soliton components in the anomalous GVD regime. We also see corresponding perturbations of the short-wavelength spectral structure. Processes such as dispersive wave generation and XPM between the soliton and nonsoliton field components are expected to contribute to the detailed structure observed, but their effects are difficult to isolate directly in the spectrum. The reader is encouraged to examine the spectrogram animations referred to above in order to obtain a clearer view of these dynamical processes. With further wavelength tuning such that excitation occurs directly at the ZDW as shown in Fig. 14(c), it is clear that the soliton dynamics become significantly more dominant.

We now consider the variation in the SC characteristics as the pump wavelength increases from 800 to 900 nm in the anomalous GVD regime. Spectrogram animations are not explicitly shown for these wavelengths as they are qualitatively very similar to the 835 nm case referred to above.

From the results in Fig. 13, we note that an increase in pump wavelength clearly leads to an increased spectral width and more distinct soliton peaks appearing in both the spectral and the temporal intensity. At first glance this is perhaps surprising because the strong wavelength dependence of the GVD reduces the input soliton order $N=(\gamma P_0 T_0^2/|\beta_2|)^{1/2}$ for longer wavelengths (see Fig. 2), and thus might be expected similarly to reduce the extent of soliton-related spectral broadening. This behavior, however, illustrates a number of subtleties in the SC generation process that require more careful consideration.

First, when interpreting these results we must consider not only the value of N at any particular wavelength, but also the corresponding characteristic propagation distance ($\sim 5L_D$) over which constituent ejected solitons begin to separate. Specifically, considering the pump wavelength of 800 nm, $\beta_2=-4.259$ ps^2/km, which yields $N\simeq 14.4$ and $5L_D\simeq 94$ cm. Although the input soliton order is high in this case, the relatively short propagation distance of 15 cm compared to $5L_D$ results in only one clearly separated soliton peak in the temporal intensity. A related consequence is that a large fraction of the input pump energy remains concentrated in the vicinity of the pump wavelength, resulting in a relatively uniform SC spectrum. On the other hand, at a longer pump wavelength of 900 nm, $\beta_2=-26.48$ ps^2/km, $N\simeq 5.5$, and $5L_D\simeq 15$ cm. In this case, the characteristic soliton separation distance is comparable to the fiber length. A greater number of ejected solitons, therefore, appear distinctly in both the time and frequency domains, and we see a significant depletion of spectral energy in the vicinity of the pump.

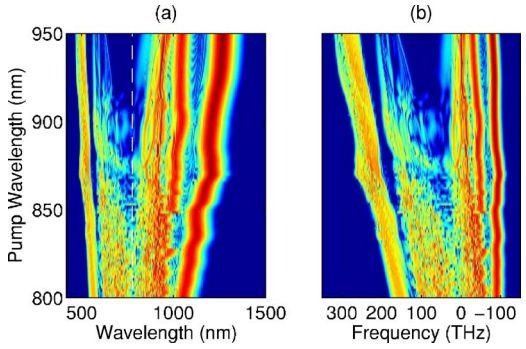

FIG. 15. (Color online) The variation in SC spectral density with pump wavelength (left axis) shown in density plot representation. The input pulse peak power is 10 kW and duration (FWHM) is 50 fs for all cases. The SC spectra are plotted as a function of (a) wavelength and (b) relative frequency. To facilitate comparison between these curves, the frequency axis in (b) is reversed. The dashed line in (a) shows the ZDW.

Second, although plotting the SC output spectra in Figs. 13 and 14 in terms of wavelength is convenient for comparison with experimental, interpreting the exact magnitude of the spectral broadening relative to the pump is difficult. To this end, Fig. 15 presents additional numerical results showing the output spectra in a density plot representation plotted (a) against wavelength and (b) against the frequency offset from the pump. The spectra are obtained for different input pump wavelengths in the range 800–950 nm, which defines the vertical axis.

Figure 15 is very useful in highlighting the physical origin of the observed spectral broadening for different pump wavelengths. For example, because we see from Fig. 15(b) that the Raman frequency downshift remains approximately constant (in fact it slightly decreases) around −90 THz over this range of pump wavelengths, we can interpret the observed increase in the long-wavelength edge of the SC spectra as due to the increase in the pump wavelength used. In contrast, however, the shift in the dispersive wave position is manifested in terms of both wavelength and frequency, which arises because longer pump wavelengths are increasingly detuned from the ZDW, leading to a corresponding increase in the position of the phase-matched dispersive wave. We also note that the increased detuning from the ZDW at pump wavelengths greater than 900 nm results in a gap in the SC spectra between the dispersive wave and distinct Raman soliton components.

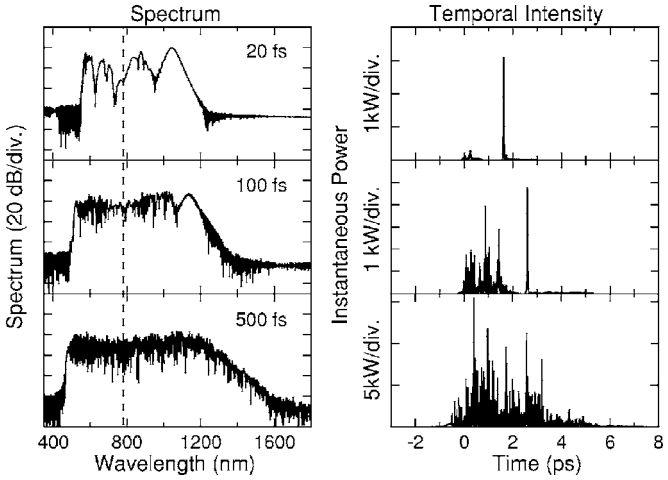

FIG. 16. Spectral and temporal characteristics for SC generated with pulse durations in the 20–500 fs range as indicated. The input pulse peak power is 10 kW and the wavelength is 835 nm. For spectrogram animations, see the EPAPS Document cited in the Reference section.

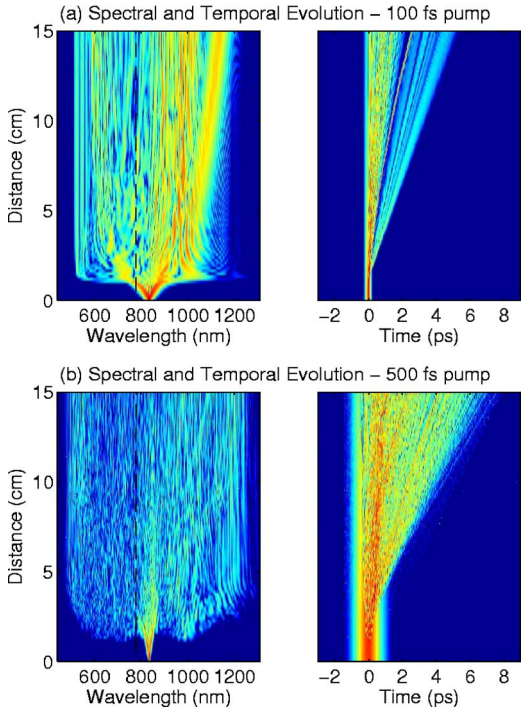

FIG. 17. (Color online) Results from numerical simulations showing density plots of the SC spectral and temporal evolution generated by pulses with duration (FWHM) of (a) 100 and (b) 500 fs. The input pulse peak power is 10 kW and wavelength is 835 nm. The dashed line shows the fiber ZDW.

B. Dependence on input pulse duration

In this section, we consider impact of input pulse duration on SC evolution in the range 20–500 fs (FWHM). We restrict our discussion to the anomalous GVD pumping regime where dynamical differences are more significant. We consider the same fiber parameters as above, and identical input pump wavelength and peak power of 835 nm and 10 kW, respectively, for all simulations. Maintaining the peak power constant in these simulations means that the input pulse energy and input soliton number N both increase directly proportional to the input pulse duration.

Typical simulation results are shown in Fig. 16 for pulse durations (FWHM) of 20, 100, and 500 fs. For corresponding spectrogram animations, refer to the EPAPS Document cited in the Reference section.[13] For the 20 and 100 fs input pulses, we see clear spectral and temporal signatures of soliton and dispersive wave dynamics as discussed above. To interpret these results we note that shorter input pulses are associated with a lower soliton order N and input energy, which leads to a smaller overall spectral width at the fiber output. On the other hand, shorter pulses are associated with a reduced value for the characteristic separation distance $5L_D$, so that a more distinct soliton structure is apparent at the fiber output. More quantitatively, an input 20 fs pulse is associated with $N \simeq 3.4$ and $5L_D \simeq 5.4$ cm, whereas for a 100 fs pulse we have $N \simeq 17$ and $5L_D \simeq 1.4$ m.

For the 500 fs case, signatures of soliton dynamics are less clear, and the SC spectral and temporal characteristics appear even more complex. To illustrate this further, Fig. 17 compares density plots of the spectral and temporal evolution along the fiber length for (a) 100 fs and (b) 500 fs input pulses. The key difference between the evolution in these two cases is the initial spectral broadening phase. First, we note that the extent of initial broadening is reduced for the 500 fs pulse case. Of more significance, however, is that the initial spectral content in this case actually develops spontaneously from noise at frequencies that do not overlap with the broadened bandwidth of the propagating pulse. This is apparent from Fig. 17(a) after $\simeq 1$ cm of propagation. In fact, the earliest stage of broadening is associated with the development of sideband structure around the pump (at ~ 700 and ~ 1000 nm), and this is shown particularly in the spectrogram animation. This evolution for the 500 fs pulse is in contrast to the dynamics with the 100 fs pulse, where generation of both long- and short-wavelength components in the SC spectrum is seeded by the spectral broadening phase of soliton fission evolution. In this context, the reader is also referred to the density plot shown in Fig. 3 for a 50 fs input pulse.

These results are important because they illustrate the onset of a different dynamical regime where initial spectral broadening is more usefully described in terms of four-wave mixing or modulation instability processes. In this case, the breakup of the pulse temporal envelope into subpulses arises from modulation instability effects, and the fact that this is seeded from noise has dramatic consequences for SC coherence. Soliton and dispersive wave dynamics do play a role in modifying the subse-

[13]The gate function used in the spectrogram calculations was identical to the input pulse for the 20 and 100 fs cases. To better illustrate the temporal fine structure in the spectrogram for the 500 fs case, a gate of 50 fs FWHM was used.

quent evolution of the subpulses, however, and this is also seen in the spectrogram animation. These aspects are discussed further in the noise section below, and in Sec. VII in the context of picosecond pulse SC generation.

C. Dependence on input pulse chirp

A related question that it is appropriate to consider concerns the dependence of the SC characteristics on input pulse chirp, as this would be expected to influence the soliton fission dynamics in a significant way (Krylov *et al.*, 1999).

Specific numerical studies for PCF have been carried out for two different cases, both considering anomalous GVD regime pumping under typical femtosecond pumping conditions. In the first, Corwin *et al.* (2003b) examined the effect of a linear chirp obtained by imposing a quadratic spectral phase on the input pulses while maintaining constant pulse bandwidth. In this case, the pulse energy remains fixed, but increased chirp is associated with an increased pulse duration and reduced peak power. Simulations showed that the maximum generated SC bandwidth was obtained near zero pulse chirp corresponding to the case of maximum input peak power. In the second case, Zhu and Brown (2004a) examined the effects of a linear chirp imposed by a phase modulation of the input pulse while maintaining constant pulse duration. Here, the pulse peak power and energy remain fixed but the pulse bandwidth increases with added chirp. The effect of both positive and negative chirp on the pulse evolution was considered. The key result obtained was that a positive chirp increases the output bandwidth because of a modified initial compression phase prior to the soliton fission point. The possibility that the results obtained were simply due to the modified bandwidth was eliminated by showing that significantly different SCs were obtained with pulses having identical spectra yet differing signs of input chirp. Related numerical studies were also reported by Fu *et al.* (2004) and Tianprateep *et al.* (2005).

D. Effects of input pulse noise

As discussed in Sec. II, the sensitivity to noise of SC generation in both conventional fiber and PCF has been reported by a number of authors. Our objective in this section is to discuss the physics that underlies the development of unstable SC spectra, and to identify regimes in which these instabilities can be minimized. We concentrate here on the case of SC generation in the femtosecond regime. Noise-related issues for longer pump pulses will be discussed in Sec. VII.D.

1. Introduction

So far, all results presented have been obtained by performing single-shot simulations, i.e., by performing a single simulation for each set of numerical parameters. However, because our model includes stochastic contributions from Raman scattering and input pulse shot noise, simulations with identical input pulse and fiber parameters yet different noise seeds can lead to different results. As we shall see, depending on the parameter regime considered these differences may be barely detectable or, in the extreme cases, can lead to strong shot-to-shot variations in the output SC. We stress that this phenomenon is not a numerical artifact. It is the expression of the sensitivity of the spectral broadening mechanisms (and of the soliton fission process in particular) to precise input pulse conditions.

We begin by considering SC generation seeded by sech^2 pulses of duration (FWHM) $\Delta\tau$=150 fs and 10 kW peak power at a pump wavelength of 835 nm. We model propagation in an identical PCF to that used in simulations above, but examine results over a shorter propagation distance of 10 cm. Figures 18(a) and 18(b) present the spectral and temporal output characteristics obtained for five numerical simulations performed with different random noise seeds. These figures clearly show shot-to-shot variations in both the spectral and temporal intensity of the output SC. The significant jitter in the temporal position of generated Raman solitons is particularly apparent, associated with shifts in the wavelengths of the corresponding peaks in the spectrum.

The bottom curve of Fig. 18(a) shows the mean spectrum calculated over an ensemble of 20 simulations. It is clear that there is significant averaging of the fine structure that is apparent in single-shot simulations. These

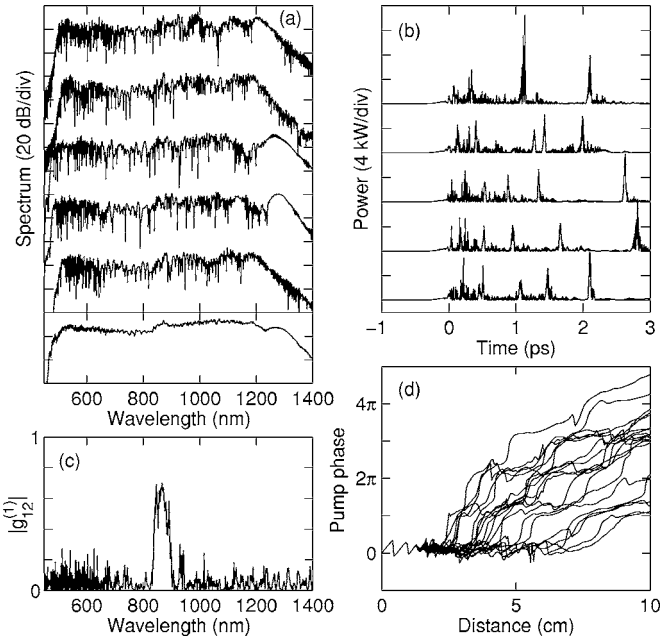

FIG. 18. Simulation results illustrating noise sensitivity. (a) Spectral and (b) temporal intensities for five simulations using 10 kW peak power 150 fs pulses at a wavelength of 835 nm injected into 10 cm of PCF. Bottom curve in (a) shows the averaged spectrum. (d) The spectral phase at the pump wavelength evolving along the fiber length for 20 simulations. (c) The degree of coherence $|g_{12}^{(1)}|$ calculated over that ensemble of simulations.

results are consistent with previous results obtained in conventional fibers by Islam *et al.* (1989a, 1989b). In addition to intensity fluctuations, the spectral and temporal phase of the propagating pulses also suffers from these shot-to-shot variations. This is illustrated in Fig. 18(d), where we show the evolution with distance of the phase of the SC spectrum at the central pump wavelength of 835 nm, plotting results from 20 different simulations. Following an initial common evolution (related to the well-behaved initial higher-order soliton evolution of the injected pump pulse), the phase at 835 nm in different simulations branches off and follows individual random trajectories. At the fiber output, the phase is spread on an interval larger than 4π. As discussed below, the point where different trajectories branch off can be associated with the occurrence of soliton fission.

As discussed in Sec. IV.D, these fluctuations can be characterized in several different ways. Here we have chosen to use the spectrally resolved modulus of the complex degree of first-order coherence at zero path difference, $|g_{12}^{(1)}(\lambda, t_1 - t_2 = 0)|$ [see Eq. (6)]. This parameter has been calculated from an ensemble average on the results of 20 simulations which yielded 200 pairs of SC obtained from input pulses with different random quantum noise. The results are plotted in Fig. 18(c). We see that the output spectrum exhibits only any significant degree of coherence around the pump wavelength, while the main part of the spectral bandwidth of the generated SC is almost completely incoherent. This is consistent with Figs. 18(a), 18(b), and 18(d). Significantly setting the Raman gain to zero and repeating these simulations yielded similar coherence properties, implying that it is the sensitivity to input shot noise and not spontaneous Raman scattering that is the primary cause of coherence degradation in our conditions.

2. Mechanism of decoherence

Insight into the mechanism of this decoherence is obtained from previous telecommunication-related studies discussed in Sec. II.B. Of particular relevance is the work by Nakazawa *et al.* (1998), who showed that amplified spontaneous emission present on higher-order solitons injected into conventional fibers could strongly perturb the soliton fission process through modulation instability (see Sec. VII.A). Specifically it was shown that modulation instability can amplify low level noise at the input, resulting in large fluctuations in the amplitude (and duration) of subsequently generated fundamental solitons. These fluctuations are then converted into wavelength fluctuations through the soliton self-frequency shift, which in turn leads to significant temporal jitter through the effect of chromatic dispersion.

Kubota *et al.* (1999) gave direct numerical proof of this mechanism by showing that an optical filter at the fiber input that suppressed amplified spontaneous emission in the vicinity of the modulation instability gain maxima led to a strong improvement in the SC coherence. This work, as well as that by Nakazawa *et al.* (1998), also suggested various other ways to maintain the

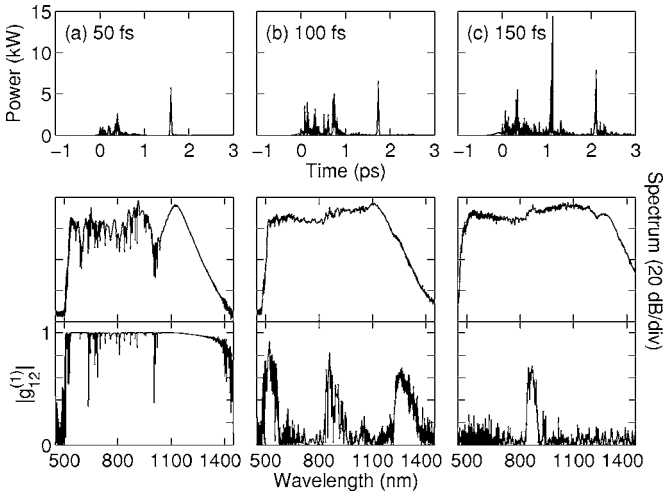

FIG. 19. Output temporal intensity profile from one simulation, mean spectrum, and degree of coherence (from top to bottom) obtained with 10 kW pulses at 835 nm for the different input pulse durations (FWHM) shown. Results correspond to propagation in 10 cm of PCF.

coherence of the pump beam during the SC generation process by using a dispersion-decreasing fiber and the adiabatic soliton compression of $N=1$ fundamental solitons rather than high-order soliton pump pulses, or by pumping the fiber in the normal GVD regime where modulation instability does not occur. Both cases avoid the soliton fission process altogether. Similarly, Nowak *et al.* (1999) proposed a scheme based on a very short fiber length in which pump pulses only propagate over a fraction of a soliton period in such a way that the spectral broadening process is interrupted when the soliton has maximum bandwidth but before fission can occur. In fact, this distance corresponds to the fission distance ($L_{\text{fiss}} \sim L_D/N$) as discussed in Sec. V.B.

These ideas directly apply to the case of SC generation in PCFs. The only differences are that pump laser shot noise replaces amplified spontaneous emission as the input noise seed, and that the very high nonlinearity of PCFs makes coherence degradation effects more dramatic. Of course recall that the presence of any significant technical noise would only degrade the SC coherence even further, but we restrict our discussion to shot-noise limited input pulses.

An important consequence of this model of coherence degradation is that it suggests that superior coherence properties would be expected for SC generated with shorter input pulses, where self-phase modulation plays a more significant role in spectral broadening, and the effects of modulation instability are reduced. This is confirmed in Fig. 19, which compares simulation results for 150 fs input pulses with those obtained for shorter input pulse durations (FWHM) of 100 and 50 fs. The wavelength and peak power were maintained at 835 nm and 10 kW, respectively. It is clear that, although the spectral broadening in all cases is comparable, the coherence properties improve significantly as the input pulse duration is decreased, and indeed $|g_{12}^{(1)}| \approx 1$ over more than an

octave for the shortest input pulses of 50 fs.

Further insight into the decoherence mechanism can be obtained by studying how decoherence is correlated with the spectral evolution of injected pump pulses. To this end, Fig. 20 presents density plots showing the evolution along the fiber length of the spectral intensity for one particular simulation (left, logarithmic scale) in parallel with the associated degree of coherence calculated over an ensemble of 20 simulations (right). The figure compares results for (a) 100 fs and (b) 150 fs pump pulses.[14]

Although we observe the generation of comparable spectral bandwidths in the two cases, the coherence evolution is significantly different. In particular, we note that the initial spectral broadening (over the 1–2 cm range) in the 100 fs case is coherent, with near unity coherence ($|g_{12}^{(1)}| \approx 1$) over the major part of the SC from 500 to 1200 nm. For the 150 fs case, however, even though a comparable bandwidth is generated after 2 cm of propagation, a high degree of coherence is only maintained in the immediate vicinity of the broadened pump around 750–900 nm. The spectral components generated far from the pump wavelength in this case are incoherent. For both pulse durations, subsequent propagation is associated with continued coherence degradation such that $|g_{12}^{(1)}| \ll 1$ over most of the SC spectrum at the fiber output.

The differences in the coherence evolution seen in Fig. 20 can be understood by noting that, at constant peak power, high-order solitons of shorter duration evolve more rapidly and reach their maximal spectral extent over a shorter distance (recall that $L_{\text{fiss}} \sim L_D/N \propto T_0$). As a result, the spectral extent of shorter pulses can overlap with the frequencies of maximum modulation instability gain before significant amplification of the noise background has taken place, resulting in a coherent seeding of the modulation instability gain bandwidth. In this case, subsequent soliton fission (induced by higher-order dispersion, for example) will occur in a more deterministic manner, and will result in improved overall coherence. In contrast, the reduced initial spectral broadening associated with longer pulses means that the modulation instability amplified noise background becomes a dominant feature of the propagation dynamics. Note that we have already discussed aspects of this process when considering the spectral and temporal characteristics of longer input pulses shown in Fig. 17.

The key point in understanding the coherence properties for longer pulses is that the amplified noise is random or, equivalently, that the modulation instability frequency components are not coherent with the pump. As a result, the noise itself on the pulse envelope can break the symmetry of higher-order soliton propagation and induce soliton fission before other perturbations such as higher-order dispersion or Raman scattering become significant. In this case, fission occurs randomly, and fission products are completely incoherent. Indeed, it is perhaps more meaningful to describe the process as a modulation instability-induced breakup of the pump pulse envelope, as this better emphasizes the role of modulation instability in the propagation dynamics (Nakazawa *et al.*, 1989; Kutz *et al.*, 2005).

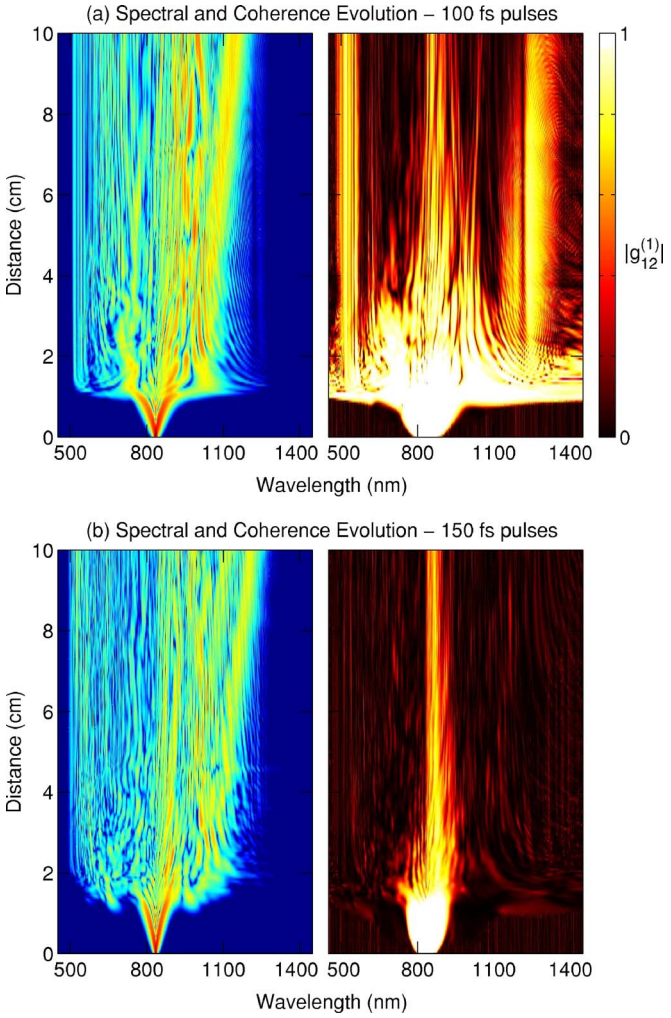

FIG. 20. (Color online) Evolution along the fiber length of the spectrum of one particular simulation (left) and of the corresponding degree of coherence (right) for supercontinuum generation obtained with 10 kW peak power pulses of (a) 100 and (b) 150 fs duration at a 835 nm pump wavelength.

3. Wavelength dependence of the coherence

The dependence of the SC coherence on the pump wavelength can be similarly interpreted in terms of a competition between soliton fission and modulation instability. In Fig. 21(a), we have plotted the average coherence $\langle |g_{12}^{(1)}| \rangle$ integrated over the SC spectrum (see Sec. IV.D) as a function of pump wavelength for the case of 150 fs pulses of 4 kW peak power. For completeness,

[14]Results for the 50 fs pulse are not shown because the initial spectral and coherence evolution is essentially identical to the 100 fs case. In contrast, however, the SC generated with the 50 fs pulse maintains its initial near-perfect coherence with subsequent propagation.

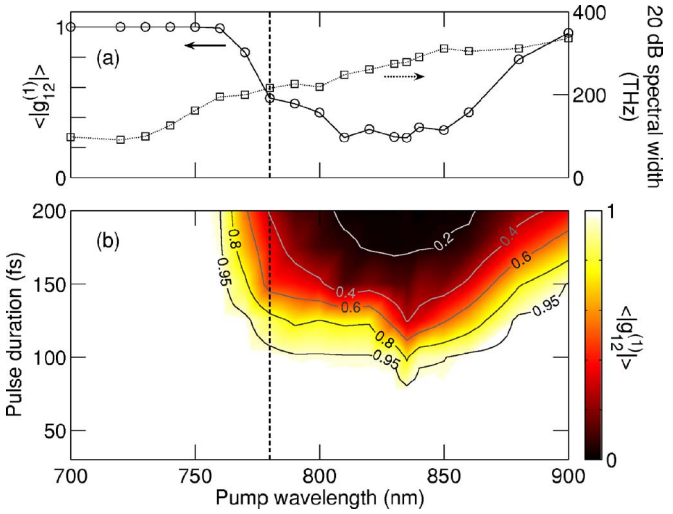

FIG. 21. (Color online) Wavelength dependence of coherence characteristics. (a) Dependence of the average coherence $\langle|g_{12}^{(1)}|\rangle$ on pump wavelength (left axis) for SC obtained with 150 fs pulses of 4 kW peak power for 10 cm of PCF. Right axis shows the corresponding −20 dB SC spectral width. (b) Average coherence shown in a density plot representation as a function of both pump wavelength and pump pulse duration for a fixed peak power of 4 kW. The dashed line indicates the position of the ZDW.

the graph also shows the 20 dB spectral width of the generated SC (right axis).

As can be seen, the generated SC is essentially perfectly coherent when the fiber is pumped in the normal GVD regime at wavelengths <760 nm. This is not surprising since modulation instability and soliton-related effects are completely inhibited in this case (in a scalar approximation). Pumping a PCF in the normal GVD regime is thus a simple method to ensure coherent SC generation. However, as was pointed out by Nakazawa *et al.* (1998), the drawback is that the SC spectral width is comparatively much smaller due to the rapid initial temporal spreading of the pump pulses; see also Fig. 14(a).

When approaching the ZDW and moving to the anomalous GVD regime, the SC spectral width increases at the expense of the degree of coherence, which drops dramatically due to the increased influence of modulation instability. On the other hand, when pumping deep in the anomalous GVD regime above 880 nm, coherence is restored. This effect is perhaps surprising, but it has been reported experimentally by Lu and Knox (2004).

This effect can be understood in a straightforward way by considering the relative distance scales associated with the processes of modulation instability and soliton fission. Specifically the characteristic gain length for modulation instability is proportional to the nonlinear length only (Agrawal, 2001), and thus varies only negligibly over the wavelength range considered. On the other hand, the increased value of the dispersion ($|\beta_2|$) at longer wavelengths results in a decrease in the characteristic fission length, so that soliton fission can occur

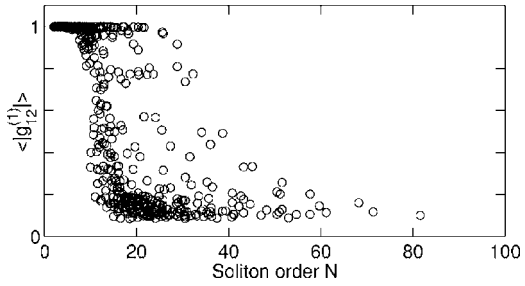

FIG. 22. Average coherence of the SC versus soliton order N calculated for pump wavelengths in the range 790–900 nm, pulse durations in the range 30–200 fs, and peak powers in the range 3–30 kW. Propagation in 10 cm of PCF is considered.

before the input pulse noise is significantly amplified by modulation instability.

Additional results are provided in Fig. 21(b), which uses a density plot to show how the average coherence varies as a function of both pump wavelength and pump pulse duration. From this graph, we see that the behavior discussed for the specific 150 fs case is actually quite general for pulse durations in the 50–200 fs range. In addition, we note that similar curves are obtained irrespective of the particular peak power used. Significantly, these results show that it is only for pulses $\lesssim$50 fs that coherence is maintained in all cases independent of the particular wavelength range considered, explaining why it was found necessary to use such short pulses in frequency metrology experiments that required such high coherence.

A general conclusion from this section is that SC coherence depends in a complex way on the relative importance of soliton fission and modulation instability processes. It is therefore natural to suppose that the generation of a coherent SC would require that the characteristic soliton fission distance ($L_{\rm fiss} \sim L_D/N$) be significantly less than the distance over which modulation instability has amplified any input noise to a level where it can significantly impact on the evolution dynamics. By adapting criteria discussed by Smith (1972) [see also Agrawal (2001)], we can estimate such a characteristic distance for modulation instability as $L_{\rm MI} \sim 16 L_{\rm NL}$. This suggests, in fact, that the condition $N \ll 16$ might represent a general condition on the soliton number that ensures a high level of SC coherence.

We have carried out extensive simulations to test this for pulses of different wavelengths in the range 790–900 nm, different pulse durations in the range 30–200 fs, and different peak powers in the range 3–30 kW. For each set of input pulse parameters, the average SC coherence is calculated and plotted against the input pulse soliton order, and Fig. 22 is a scatter plot of all results obtained. Although from this graph it is not possible to identify one unique scaling law in terms of N that universally applies to any arbitrary combination of initial conditions, it appears that input pulses where $N<10$ possess high coherence, and input pulses where $N>30$ possess low coherence.

We propose that these criteria are useful guidelines when considering the design of particular SC generation experiments, but stress that a precise evaluation of the expected coherence for any particular set of experimental conditions needs to be carefully checked using specific numerical simulations. Specifically, it is important to verify that the high coherence is obtained while generating a bandwidth sufficient for the particular application in question.

E. Review of experimental results

The literature review in Sec. II has discussed some early experimental studies of SC generation that immediately followed the initial demonstration by Ranka *et al.* (2000a). Some specific comparisons between numerical modeling and experiments have also been presented in Sec. V.D. The objective of this section is to provide a more complete review of the experimental literature, and focus in particular on experimental observations of the various dynamical aspects of SC generation that have been discussed above.

The first attempt to quantitatively analyze SC generation in PCF in terms of soliton fission was reported by Herrmann *et al.* (2002), and a comparison was presented between experiment and simulation using nanojoule pulses at 807 and 850 nm. At both pump wavelengths, pulses with durations of 29 and 100 fs were injected into 40 cm of PCF. Two different PCFs with ZDWs of 670 and 790 nm were used. These experiments allowed studying the SC generation process over a wide parameter regime, and spectral measurements clearly showed soliton and dispersive wave signatures. Nonetheless, the detailed spectral structure seen in experiments was not reproduced in numerical simulations because the underlying theoretical model neglected stimulated Raman scattering.

The importance of Raman scattering on the long-wavelength structure of SC generation in PCF had, however, been previously discussed by Washburn *et al.* (2001). Using an extended GNLSE equation model including the Raman response of fused silica, excellent agreement between simulation and experiment was reported. However, the results were not interpreted in terms of soliton fission. Later research by Washburn *et al.* (2002) reported SC generation experiments in 1.7 m of PCF with ZDW at 767 nm. Using 110 fs pulses of 76 W peak power, experiments studied the SC spectral characteristics as the input wavelength varied from 770 to 820 nm in the anomalous GVD regime. Numerical simulations using the same GNLSE-based model were shown to yield results in excellent agreement with experiment, and a brief discussion of the results in terms of soliton fission was also given.

A further detailed comparison between experiments and GNLSE simulations was provided by Genty *et al.* (2002). Pulses of 100 fs duration at 804 nm were injected into 5 m of PCF with ZDW at 650 nm at peak powers up to ~7 kW. A detailed analysis of the experimental soliton and dispersive wave structure was given both using numerical simulations and through a comparison with the theoretical model of Kodama and Hasegawa (1987). Particular studies on the dependence of the Raman soliton self-frequency shift with varying peak power were also presented. Additional experiments using 14 m of PCF with ZDW at 950 nm studied spectral broadening with normal GVD dynamics. At a pump wavelength of 746 nm, the results showed primarily the effects of spectral broadening due to SPM, but with a pump at 807 nm closer to the ZDW, energy transfer into the anomalous GVD regime resulted in soliton fission dynamics. These results were also interpreted using numerical simulations. The results by Genty *et al.* (2002) can be well understood in terms of the processes shown in Figs. 13 and 14.

Similar studies were reported by Ortigosa-Blanch *et al.* (2002) using 200 fs kW peak power pulses injected into 16 m of PCF with ZDW at 806 nm. Experiments at pump wavelengths over the range 817–870 nm, and at 753 nm, allowed both anomalous and normal GVD dynamics to be observed. The same group subsequently reported a similar study using a wider range of different PCFs and, significantly, several fiber tapers (Wadsworth *et al.*, 2002). Only spectral data were reported, but using ~20 kW peak power 200 fs pulses at 850 nm, comparable spectral bandwidths and structure were reported when pumping relatively short 9 cm lengths of PCF and tapered fiber with comparable dispersion characteristics (specifically a ZDW around 750 nm). Related experimental studies of the anomalous GVD regime and soliton fission dynamics include the reports by Akimov *et al.* (2001), Apolonski *et al.* (2002), Fedotov *et al.* (2002), Price *et al.* (2002a), and Sakamaki *et al.* (2004). Reeves *et al.* (2003) also highlighted the key role of the PCF dispersion characteristics by injecting nanojoule energy 100 fs pulses at 1550 nm into 1 m lengths of different PCFs with relatively uniform tailored normal and anomalous GVD in this wavelength range. The expected signatures of anomalous and normal GVD propagation were reported in the pulse spectra.

Extending the short-wavelength edge of the SC spectrum is of interest for many applications, and a number of experiments have therefore focused on the dispersive wave dynamics observed during SC generation. Using 100 fs pulses with ~10 pJ energy at pump wavelengths over the range 710–941 nm, Hilligsøe *et al.* (2003) studied the initial appearance of dispersive wave components around 400 nm after propagation in 75 cm of PCF with ZDW at 660 nm. Similar results were reported by Tartara *et al.* (2003). Cristiani *et al.* (2004) using autocorrelation measurements after ~33 cm of propagation in PCF demonstrated that the dispersive wave components were of picosecond duration. The mutual interaction between the generated dispersive waves and Raman solitons present in a SC were investigated experimentally and numerically by Genty, Lehtonen, and Ludvigsen (2004). Cross phase modulation was shown to play a crucial role in extending the SC toward shorter wave-

lengths, and experimental observations using sub-30-fs pump pulses were confirmed through numerical simulations.

An interesting approach to achieve precise control over the soliton fission and dispersive wave generation process has been reported by Lu and Knox (2005) and Lu *et al.* (2005). Here, a short (~cm) length segment of PCF is tapered so that its core diameter (and thus its GVD properties) continuously changes along the fiber length. In this way, it is possible to micromanage the propagation dynamics to enhance particular nonlinear processes. This was used to improve the efficiency of dispersive wave generation, and a detailed comparison with results obtained using untapered PCF or tapered standard fiber also showed advantage in the micromanagement technique in yielding SC with improved coherence.

As discussed in Sec. V.D, the FROG experiments and analysis reported by Xu *et al.* (2001), Dudley, Gu, *et al.* (2002), and Gu *et al.* (2002) allowed direct measurement of the temporal structure of soliton and dispersive wave signatures in SC generation. Follow-up experiments by Cao *et al.* (2003) characterized the onset of the soliton fission process after only 8 mm of propagation in a PCF with zero dispersion at 780 nm. These experiments used 40 fs input pulses with 2 nJ energy at 816 nm, and the results clearly showed the expected temporal breakup into subpulses with temporal structure on the 10 fs scale. Numerical simulations were also shown to be in good qualitative agreement. Kano and Hamaguchi (2003) used FROG measurements in a polarization-gating geometry to analyze selected visible spectral components of the SC, and also reported evidence for pulse splitting and rapid spectral broadening during the initial propagation phase. Subsequent uses of FROG to study SC generation over a wider range of experimental parameters includes work by Efimov *et al.* (2004b) and Konorov *et al.* (2004).

A small number of experiments have also studied the influence of the input pulse chirp on the SC generation dynamics. Cormack *et al.* (2002) used a dispersive prism delay line to manipulate the chirp of ~nJ energy pulses at 810 nm with the aim of generating tunable Raman solitons in PCF. The minimum pulse duration launched was 69 fs and the maximum pulse duration for positive (negative) chirp was 136 (176) fs. Chirp control was observed to lead to tunable Raman soliton generation over a 60–100 THz frequency range.

Corwin *et al.* (2003a, 2003b) used a comparable experimental setup to carry out a detailed analysis on the chirp dependence of both the SC bandwidth and noise properties. (More details of these particular experiments are also given in the following paragraphs.) A detailed study reported by Xu *et al.* (2004) used a spatial light modulator to modify the spectral phase of 800 nm ~nJ energy pulses with a transform-limited pulse duration (FWHM) of 30 fs. Using 70 cm of PCF with ZDW at 760 nm, the output SC characteristics were shown to be strongly dependent on both the duration and temporal symmetry of input pulses. In addition, a genetic algorithm was used to adaptively modify the imposed spectral phase to optimize the overall SC spectral bandwidth and wavelengths of particular generated Raman solitons. Related work (but using standard optical fibers) was also reported by Efimov *et al.* (2004a). Finally, we note that studies of SC generation in optical fiber tapers by Türke *et al.* (2006) have shown that linear and nonlinear chirp accumulated in the input untapered pigtail segment can also modify the SC dynamics and reduce the observed spectral broadening. However, the use of a spatial light modulator pulse shaper before injection in the fiber taper was shown to be an effective solution to precompensate for any deleterious effects.

The SC intensity and phase stability properties in Sec. VI.D have been the subject of significant interest. The presence of intensity fluctuations on PCF-generated SC was first noticed in the context of frequency metrology experiments, where broadband (white) amplitude noise at rf frequencies was observed to interfere with the precision of optical clockworks (Udem, Reichert, Holzwarth, Diddams, *et al.*, 2000; Hollberg *et al.*, 2001). Noise was observed to extend well beyond the frequency rolloff of any laser technical noise (Ivanov *et al.*, 2001) and, although empirical techniques were developed to reduce the noise to acceptable levels for metrology, it appeared nonetheless to represent a fundamental limit to applying PCF-generated SC to optical frequency metrology. Important insight into the origin of this noise was then provided by Gu *et al.* (2002), who demonstrated the presence of large shot-to-shot fluctuations in the SC spectrum on the basis of both integrated multishot and single-shot measurements.

A detailed experimental and numerical study into the SC intensity noise characteristics was carried out by Corwin *et al.* (2003a, 2003b). These experiments used pulses at 810 nm of 45 nm bandwidth, and a dispersive delay line modified their spectral phase so that positively and negatively linearly chirped pulses in the range 20–90 fs could be used to excite the SC generation process. In 15 cm of PCF with a ZDW at 780 nm, the RIN was measured at different wavelengths across the SC as a function of input pulse chirp. The measured RIN exhibited a complex wavelength-dependent structure, but a useful figure of merit for the overall SC stability was found to be the median RIN calculated across the extreme −20 dB points of the SC spectrum. The median RIN was observed to increase with input pulse chirp and duration, and attained its minimum value when the input pulses were transform-limited around 22 fs duration. Significantly, the median RIN of −130 dBc/Hz and the spectral width of ~450 THz under these conditions would allow such SC to be used for frequency metrology. Experimental results obtained were compared with the results of stochastic numerical simulations in Sec. VI.D, and shown to be in very good quantitative agreement. A parallel experimental study of the rf noise properties was reported by Ames *et al.* (2003), and a similar dependence of the SC stability on pulse duration was observed. Quantitative characterization of the SC stability dependence on laser technical noise was reported by

Haverkamp and Telle (2004), where 30 fs pulses from a mode-locked Ti:sapphire laser were intensity modulated using an acousto-optic modulator before being coupled into a PCF for SC generation. The intensity and phase modulation in the spectrally broadened SC output were characterized as a function of wavelength, allowing an effective complex intensity modulation transfer function of the SC to be extracted. A related (although numerical) study of the noise scaling properties of SC generation was also given by Washburn and Newbury (2004).

As well as measurements of the intensity noise characteristics, experiments have also studied the SC phase stability through interferometric measurements of the wavelength-dependent mutual coherence function in Sec. VI.D. The first results in PCF were reported by Gu *et al.* (2003). In these experiments, 60 fs pulses at 800 nm were injected into two 18 cm segments of PCF with ZDW at 760 nm, and the wavelength-dependent interference pattern between the two SCs was used to extract the mutual degree of coherence. The average coherence integrated over the SC spectrum was relatively low at $\langle|g_{12}^{(1)}|\rangle \sim 0.5$, attributed to both technical noise and different pulse energies (0.25 and 0.57 nJ) injected into each segment. A careful study by Lu and Knox (2004) used a 6 cm tapered fiber with ZDW at 820 nm, and a delayed pulse (Mach-Zehnder) technique to measure the mutual coherence between SC generated from successive incident pulses. Using ~0.4 nJ energy 100 fs pulses, coherence properties were studied over an input wavelength range of 780–920 nm. Clear degradation in SC coherence was measured as the pump wavelength was tuned from the normal to the anomalous GVD regime. However, experiments recorded that coherence passed through a minimum value of $\langle|g_{12}^{(1)}|\rangle \sim 0.15$ at 860 nm, recovering as the input wavelength was tuned further into the anomalous GVD regime and reaching a value of $\langle|g_{12}^{(1)}|\rangle \sim 0.7$ at 900 nm. The experimental behavior observed in this study is in good qualitative agreement with the wavelength-dependent behavior expected from the numerical results presented in Fig. 21.

A similar experimental configuration based on an asymmetric Michelson interferometer was used by Kobtsev *et al.* (2005) to study the coherence properties of SC generated in PCF, with a major result being the observation of particularly high coherence across the Raman soliton components of the generated SC. Finally, we note that a novel dual pulse pumping spectral interferometry technique developed by Zeylikovich *et al.* (2005) has also been used to characterize SC coherence, with results in good qualitative agreement with the behavior expected based on the discussions above.

Complementary studies on SC stability were also carried in the context of pulse compression, since it had been suggested by Husakou and Herrmann (2001) that the SC with bandwidths spanning 100's of THz bandwidth could, in principle, be used to generate sub-10-fs ultrashort pulses with appropriate flattening of the SC spectral phase. Although the SC compression properties were studied in a number of experiments, the reported minimum achievable pulse durations appeared to be limited to the range 20–25 fs (Lakó *et al.*, 2003, Druon and Georges, 2004; McConnell and Riis, 2004). In parallel, numerical studies by Chang *et al.* (2003) pointed out a number of difficulties with the practical implementation of a SC compression scheme due to shot-to-shot fluctuations in the spectral amplitude and phase. In related numerical work, Dudley and Coen (2004) discussed how the generation of a SC that was compressible was equivalent to the generation of one that was coherent. In a sense this is an obvious connection to make, because experimental spectral phase compensation techniques would only work effectively if the spectral phase remained constant from shot to shot. An additional factor identified in this work as being crucial to the success of compression was the need to use spectral phase compensation at the scale of the smallest spectral structure present on the SC.

With appropriate consideration of these stability criteria, successful compression to the 5 fs regime has now been reported. The experimental technique used involves adaptive phase compensation through a spatial light modulator-based pulse shaper technology. In one experiment, Schenkel *et al.* (2005) reported compressed pulses of 5.5 fs, using relatively short initial pulses of 15 fs duration, a 5 mm length of PCF, and pumping with normal GVD, where improved spectral coherence is expected. A study by Adachi *et al.* (2005) reported similar results for normal GVD pumping using a 2 mm length of PCF. In addition, these latter authors also reported compression to 4.8 fs with anomalous GVD regime pumping, but by carrying out filtering and selective compression only over the fraction of the SC spectral bandwidth with the highest coherence.

For completeness, we also mention here some experimental work that has been performed with new glasses and other special fiber types, including HNLFs, as this opens a wide range of unexplored possibilities. In particular, Kumar *et al.* (2002) and Hundertmark *et al.* (2003) have fabricated PCFs made of SF6 glass. This glass exhibits a tenfold increase in nonlinearity in comparison with silica, and this has readily led to the demonstration of an ultra-broadband continuum from 350 to 2200 nm in 75 cm of fiber with 100 fs pulses at 1.55 μm. In parallel, Nicholson *et al.* (2004a, 2004b) have attempted to modify the properties of silica-based PCFs by irradiating the fiber with UV light, resulting in an enhancement of the blue side of SC. Non-PCF structures such as HNLFs have also been studied. HNLFs are usually pumped in the 1.3–1.5 μm region, and SC generation in those fibers has been shown to be particularly attractive for wavelength division multiplexing applications (Hori *et al.*, 2004) as well as for generating long-wavelength continua. In this context, Thomann *et al.* (2003) have demonstrated a SC source extending from 1000 to 2200 nm using 30 fs pulses from a Cr:forsterite laser, while Shirakawa *et al.* (2005) have further pushed the red edge of the continuum into the infrared, generating a spectrum spanning the 1000–2500 nm range from 100 fs pulses at 1560 nm. Other ultrahigh

numerical-aperture fibers with a pure GeO_2 core have also been explored (Marks *et al.*, 2002).

VII. SUPERCONTINUUM GENERATION FOR LONGER PULSES: FROM THE PICOSECOND TO THE CW REGIME

The preceding section has considered the processes underlying SC generation for femtosecond pump pulses at both normal and anomalous GVD wavelengths. In the normal GVD regime, spectral broadening is dominated by SPM, whereas in the anomalous GVD regime the SC characteristics are well explained as a result of soliton fission and related processes.

Although the use of kW peak power femtosecond pulses permits efficient SC generation in centimeter lengths of fiber, other studies have demonstrated broadband SC spectra using what we refer to as longer pulses, in the picosecond, nanosecond, and even the continuous-wave regimes (Coen *et al.*, 2001; Provino *et al.*, 2001; Avdokhin *et al.*, 2003; Schreiber *et al.*, 2003; Wadsworth *et al.*, 2004). These results, however, cannot be explained simply in terms of SPM or soliton fission. First, SPM-induced spectral broadening is inversely proportional to the pulse duration and, for picosecond or longer pulses, is orders of magnitude below experimentally observed SC bandwidths (Coen, Chau, *et al.*, 2002). On the other hand, even though long pulses in the anomalous GVD regime could be interpreted as solitons of high order ($N \propto T_0$), the characteristic fission length also increases with the input pulse duration ($L_{\text{fiss}} \sim L_D/N \propto T_0$), typically far exceeding the fiber lengths used in experiments. Moreover, some of these experiments have also been carried out with normal-GVD pumping (Coen *et al.*, 2001; Provino *et al.*, 2001). Clearly, other mechanisms must be involved.

The objective in this section is to identify and discuss those mechanisms in detail, and to show how they relate to the femtosecond dynamics described above. As with femtosecond pulses, our aim is to emphasize the major dynamical regimes that depend on the input pulse wavelength and duration. The obvious dependence on peak power is not explicitly treated, while the dependence on fiber length is considered implicitly by considering the evolution dynamics. We also examine the SC noise properties, and conclude this section with a detailed review of the experimental literature.

A. Spectral broadening mechanisms for longer pulses

1. Introduction

We begin by considering the spectral broadening mechanisms for anomalous GVD regime pumping. When considering femtosecond SC generation in this regime, we briefly discussed how modulation instability and four-wave-mixing processes play an increasingly important role in the initial dynamics as the pulse duration increases into the 150–500 fs range (refer to Sec. VI.B and VI.D). In the time domain, these processes induce a fast modulation of the pump envelope which can subsequently break up and evolve into a train of femtosecond solitonlike pulses with sufficient distance. Although this process is similar to (femtosecond) soliton fission in the end result, the fact that the initial dynamics are seeded from noise led us to refer to the process as modulation instability-induced breakup.

Recent numerical studies by Mussot *et al.* (2004), Kobtsev and Smirnov (2005), Kutz *et al.* (2005), and Vanholsbeeck *et al.* (2005), have provided further insight into this dynamics, explicitly demonstrating that the effects of the Raman soliton self-frequency shift and dispersive wave generation are also present for such instability-generated solitons. Several of these authors have also provided experimental evidence of these mechanisms. It is therefore correct to say that SC generation with long pulses in the anomalous GVD regime involves similar soliton-related dynamics as in the femtosecond regime. However, in contrast to the femtosecond case, solitons play a relatively minor role during the first step of propagation.

Of course, as this femtosecond soliton structure is generated from noise, the generated SC suffers from significant shot-to-shot fluctuations as discussed in Sec. VII.D. The reason why four-wave mixing and/or Raman scattering dominate the initial steps of SC generation with long pulses simply arises because the characteristic length scale of these processes is shorter than the fission length of the incident pump pulse. This condition implies, in fact, that the temporal scale of any structure that appears on the pulse envelope as a result of four-wave mixing and Raman interactions will be significantly shorter than the envelope duration itself. Indeed, this criterion is itself a useful working definition of what we mean by long pulses, and as discussed in Sec. VI.D also defines the boundary between the generation of coherent and incoherent SC. Moreover, under this condition, the dynamics can be well described using a CW theoretical treatment, where pulse broadening and temporal walkoff effects are neglected. A summary of the CW theory of four-wave mixing and modulation instability is presented in the next section.

2. Four-wave mixing and modulation instability

Four-wave mixing between CW waves is one of the most fundamental processes in nonlinear optics, and has been the subject of extensive study (Stolen and Bjorkholm, 1982; Agrawal, 2001). Many of the key features of four-wave mixing are seen in the degenerate case in which two pump waves are at the same frequency, and the nonlinear interaction involves the conversion of the pump into a pair of parametric sidebands that are frequency downshifted (Stokes) and upshifted (anti-Stokes) relative to the pump. In the undepleted pump approximation (and for pump power P_0), the sidebands grow exponentially with a parametric (amplitude) gain g (units of m^{-1}) given by $g=[(\gamma P_0)^2-(\kappa/2)^2]^{1/2}$. For single-mode fibers, the phase mismatch term κ is given by $\kappa=2\gamma P_0+2\Sigma_{m=1}^{\infty}[\beta_{2m}/(2m)!]\Omega^{2m}$, where Ω is the an-

gular frequency shift from the pump and the β_{2m} terms represent the different even-order dispersion coefficients of the propagation mode considered at the pump wavelength.

In the absence of any initial seeding, four-wave mixing corresponds to an instability of the propagating CW pump and the growth from noise of sidebands symmetric in frequency about the pump. The maximum growth rate occurs at frequencies satisfying the phase-matching condition $\kappa=0$, and the maximum amplitude gain is $g_{\max}=\gamma P_0=1/L_{\mathrm{NL}}$. In the time domain, this leads to the development of an associated ultrafast temporal modulation with a period equal to the reciprocal of the sideband spacing, and the process is referred to as a modulation instability. Of course, four-wave mixing and modulation instability are simply frequency-domain and time-domain descriptions of the same physics and, as pointed out by Stolen *et al.* (1989), one can argue that any stimulated parametric process in the frequency domain is a modulation instability in the time domain, and vice versa. While this may be true in the initial stages of evolution, a disadvantage of the classic four-wave-mixing formalism is that it does not (by definition) describe the generation of additional higher-order sidebands that develop as the modulation develops [see, e.g., Hart *et al.* (1998) and Van Simaeys *et al.* (2002)]. Nonetheless, the respective frequency-domain and time-domain pictures are useful for explaining different aspects of field evolution, and both terms are often encountered in the literature.

In most conventional optical fibers, summation over the Taylor series in the expression for κ can be truncated at the group velocity dispersion term β_2. In this case, satisfying the phase-matching condition requires that $\beta_2<0$, giving rise to the widespread belief that such four-wave mixing and modulation instabilities are only possible with a pump in the anomalous GVD regime. Although this is certainly true in the majority of cases, calculation of the phase-matching condition in fibers with significant higher-order dispersive terms requires using all dispersion orders, opening up new windows for four-wave mixing and modulation instability gain. This has, in fact, been known from theoretical and numerical studies for some time (Cavalcanti *et al.*, 1991; Abdullaev *et al.*, 1994). Experimental observation of parametric sidebands pumping in the normal GVD regime has been reported using both standard dispersion shifted fiber (Pitois and Millot, 2003) and PCF (Harvey *et al.*, 2003). Additional discussion of the characteristics of the novel gain windows that can arise due to the higher-order dispersion of PCF has also considered by Reeves *et al.* (2003), while some numerical simulations have been presented by Demircan and Bandelow (2005).

To illustrate these phase-matching conditions explicitly for PCF, it is convenient to plot the calculated parametric gain in a density representation as shown in Fig. 23(a). Considering the same PCF structure as in the preceding sections, the gain is plotted against the frequency offset from the pump (horizontal axis) for a range of pump wavelengths (vertical axis). We assume a CW pump peak power of 500 W, chosen for consistency with the numerical simulation parameters below. The horizontal dashed line indicates the zero-dispersion wavelength. Although parametric gain bands exist when pumping in both the anomalous and normal GVD regimes, there are clear qualitative differences in the gain spectra. These are illustrated by plotting details of the gain curves at 800 and 750 nm in Fig. 23(b), and note that the vertical axis actually shows the power gain $2g$. We see that the gain spectrum for anomalous GVD regime pumping at 800 nm consists of gain bands that develop immediately from the pump frequency, and have a relatively broad (~20 THz) gain bandwidth. This contrasts with the gain spectrum observed with a 750 nm pump in the normal GVD regime, where gain bands consist of narrow-band peaks significantly displaced from the pump frequency. Both of these features will be shown in our numerical simulations. We also point out that a large frequency separation between the four-wave-mixing sidebands usually corresponds to a large group-velocity mismatch, resulting in the rapid walkoff of amplified waves. This in turn reduces the efficiency of the four-wave-mixing process as temporal overlap between various frequency components is needed for energy transfer to occur (Stolen and Bjorkholm, 1982; Agrawal, 2001; Chen *et al.*, 2005). This effect is particularly important for SC generation in the normal GVD regime [see also Coen, Chau, *et al.* (2002)].

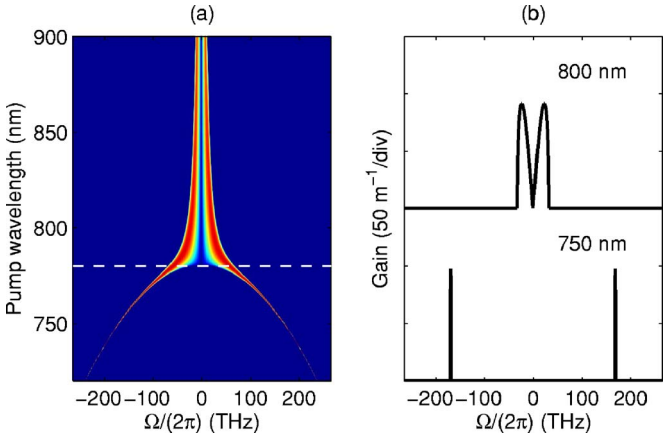

FIG. 23. (Color online) Parametric gain as a function of frequency offset from the pump $\Omega/2\pi$ (in THz). (a) Linear density plot representation for different pump wavelengths (vertical axis). (b) Specific gain curves at two particular wavelengths as indicated. The dashed line in (a) is the ZDW, and calculations assume a CW pump power of 500 W.

3. Raman effects

In addition to four-wave mixing, Raman scattering also plays a central role in SC generation with long pulses or CW radiation (Shen and Bloembergen, 1965; Stolen *et al.*, 1984; Agrawal, 2001). However, since the spectral bandwidth of pulses with duration exceeding several picoseconds is much smaller than the −13.2 THz Raman frequency shift in fused silica, pump pulses do

not suffer significantly from intrapulse Raman scattering as in the femtosecond case. Neither is Raman-induced fission significant since, as we have discussed, fission does not occur with the pulse durations considered here. Rather, the effect of Raman scattering is manifested by amplification from noise of a −13.2 THz frequency downshifted (Stokes) sideband from the pump. This Stokes wave is exponentially amplified by copropagating with the pump, and can seed the generation of additional downshifted Raman orders through a cascading process (Stolen *et al.*, 1984).

The maximum Raman gain is significantly smaller than the gain for phase-matched four-wave mixing (typically about one-quarter of it), and so the signature of a discrete Raman cascade is only observed when the efficiency of four-wave mixing is reduced because of large phase mismatches or large walkoff effects. Because this generally occurs in the normal GVD regime, it allows us to identify Raman scattering as the dominant spectral broadening process for longer pulses with normal GVD pumping. In the time domain, temporal modulation and breakup into ultrashort pulses can also be observed as shown numerically by Golovchenko *et al.* (1990, 1991). At high pump power, the spectrum of the Raman cascade may extend across the ZDW, and the discrete Raman orders will then typically fuse in a continuum spectrum (Stolen *et al.*, 1984). This occurs because the powerful Stokes bands generated from noise in the anomalous GVD region get converted into a random sequence of ultrashort solitons that suffer from various amounts of self-frequency shift, as discussed above for the case of femtosecond dynamics (Golovchenko *et al.*, 1991).

In contrast to four-wave mixing, the Raman gain is antisymmetric so that frequency components on the anti-Stokes side of the pump are in principle absorbed. However, coupling between Raman and parametric gain can nonetheless lead to the emergence of strong Raman anti-Stokes peaks, even under non-phase-matched conditions (Bloembergen and Shen, 1964; Coen, Wardle, and Harvey, 2002). Additionally, under conditions where four-wave-mixing sidebands are phase matched within the Raman bandwidth, the Raman gain can be either suppressed or enhanced up to a level close to that of the parametric gain (Golovchenko *et al.*, 1990; Vanholsbeeck *et al.*, 2003).

B. Dependence on input pulse wavelength

The manner in which Raman and parametric effects combine to generate a broadband continuum can be seen through the use of simulations to examine the dependence of the output SC characteristics on input pulse wavelength. Here, we consider 500 W peak power sech^2 input pulses of 20 ps duration (FWHM) injected into 2 m of PCF with the same fiber parameters as previously considered. These pumping parameters are intermediate between those reported in experimental studies [see, e.g., Coen *et al.* (2001) and Rulkov *et al.* (2005)], and illustrate all important underlying physics. Note that, because of the greater temporal window required in the simulations, typically $N_p > 2^{17}$ time- and frequency-domain grid points were used. The results below correspond to single-shot simulations, although noise at the quantum level is, of course, included so that the broadening dynamics are correctly reproduced. Figure 24 shows the results obtained. The dashed line in the spectral plots shows the ZDW. It is instructive to compare these with results for the femtosecond regime in Fig. 13.

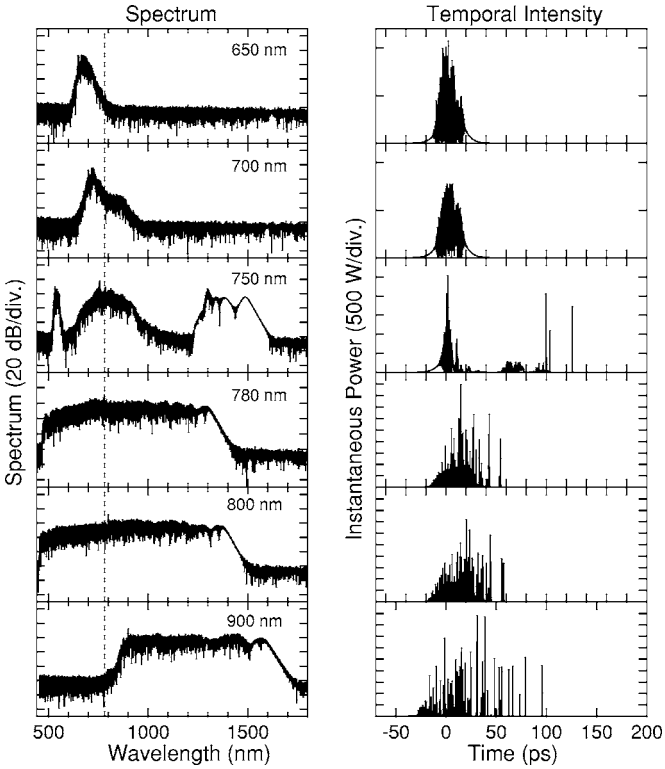

FIG. 24. Results from numerical simulations showing the spectral and temporal characteristics of picosecond supercontinua generated by selected pump wavelengths as indicated in 2 m of PCF. The input pulse peak power is 500 W and duration (FWHM) is 20 ps. Dashed line shows the fiber ZDW.

We first consider the results at 650 and 700 nm which illustrate pumping far from the ZDW in the normal GVD regime. For these cases, four-wave mixing does not play any significant role in the early stages of propagation because the phase-matched parametric sidebands are shifted by more than 200 THz from the pump and suffer from a large group-velocity mismatch. Rather, spectral broadening is dominated by the development of a stimulated Raman cascade on the long-wavelength side of the pump. During the initial evolution phase, the various Raman orders appear distinctly in the pulse spectrum separated by 13.2 THz, but they merge to form a continuous spectrum with sufficient propagation distance due to the combined effects of SPM and XPM. A corresponding temporal modulation is also seen on the output 20 ps pulse envelope.

For the case of the 700 nm pump, the evolution from discrete to cascaded Raman structure in the spectrum can be seen in more detail from Fig. 25(a), where we plot

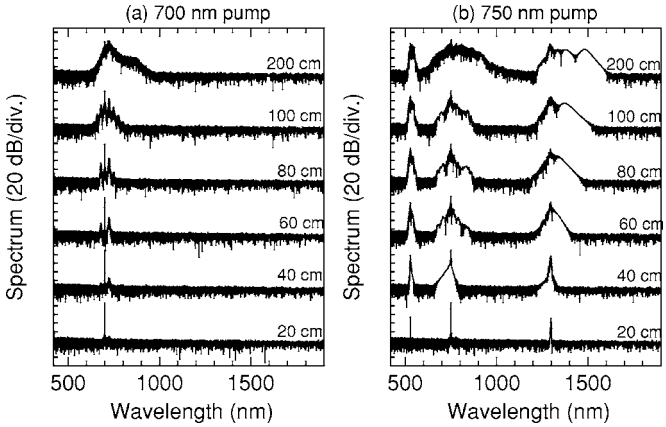

FIG. 25. Results from numerical simulations showing the spectral evolution at propagation distances as indicated for pump wavelengths of (a) 700 and (b) 750 nm. The input pulse peak power is 500 W and duration (FWHM) is 20 ps.

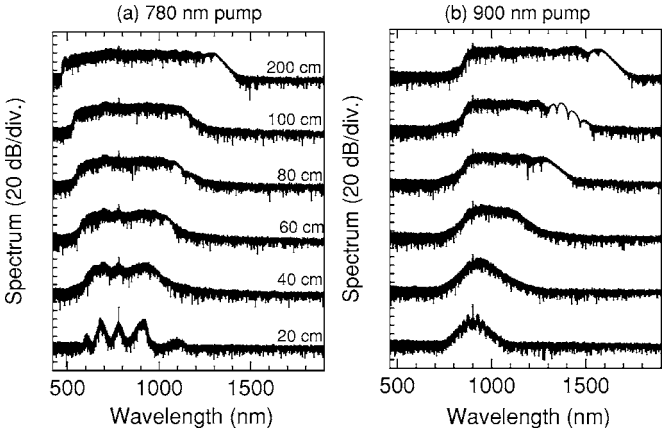

FIG. 26. Results from numerical simulations showing the spectral evolution at propagation distances as indicated for pump wavelengths of (a) 780 and (b) 900 nm.

the spectral characteristics at selected propagation distances. Note that the fine spectral structure observed when longer pump pulses are used makes it more convenient to examine this evolution using line plots rather than a density plot representation. For propagation distances less than 1 m, clear Raman orders can be seen, and the effect of non-phase-matched parametric amplification also leads to strong distinct Raman anti-Stokes peaks (Coen, Wardle, and Harvey, 2002). However, after a distance of 2 m, these sidebands have broadened and merged, and indeed some energy transfer into the anomalous GVD regime is also observed. However, no particular signatures of solitonlike effects are observed, thus spectral broadening for this range of pump wavelengths remains dominated by normal GVD propagation dynamics.

At a pump wavelength of 750 nm, the output spectrum in Fig. 24 shows significantly different spectral structure. Here we see not only distinct broadening around the pump wavelength, but also the appearance of far-detuned spectral structure at wavelengths in both the normal and anomalous GVD regimes. The physical origin of this structure becomes apparent upon examining the corresponding evolution in Fig. 25(b). The far-detuned spectral peaks appear distinctly after only 20 cm of propagation at 527 and 1298 nm, wavelengths that are symmetrically shifted by ±169 THz relative to the pump. These are precisely the phase-matched frequencies shown in Fig. 23(b) for this pump wavelength, allowing us to interpret these peaks as arising from higher-order dispersion phase-matched four-wave mixing. The fact that they appear in the spectrum before any significant Raman structure closer to the pump field is because of the greater relative gain of the parametric process relative to Raman scattering.

With further propagation, a broadband structure does appear around the pump (due to Raman and XPM) but significant spectral broadening also appears around the four-wave-mixing sideband in the anomalous GVD regime. This structure arises from soliton-fission-like dynamics, and Fig. 24 clearly shows the distinct temporal soliton signatures that appear at about 100 ps delay. In some cases, the four-wave-mixing sidebands may be sufficiently close to the pump wavelength or broaden sufficiently to merge with the central broadband Raman structure, and this provides an alternative route to SC generation which has been investigated in detail by Nikolov *et al.* (2003). We point out, however, that phase-matched parametric amplification of narrow-band sidebands far detuned from the pump can be highly sensitive to structural irregularities of the fiber along its length (Stolen, 1975; Karlsson, 1998; Kibler *et al.*, 2004; Wong *et al.*, 2005). This most likely explains why this scenario has not been widely reported experimentally so far [see, e.g., Coen, Chau, *et al.* (2002)].

From Fig. 24, we see that pumping at the ZDW or in the anomalous GVD regime over the range 780–900 nm results in broadband SC with increased uniformity. The evolution dynamics for 780 and 900 nm pumps are shown in Figs. 26(a) and 26(b), and we can see how the initial spectral broadening arises from phase-matched four-wave mixing and leads to symmetric appearance of sideband structure about the pump after 20 cm of propagation in both cases.

Although parametric four-wave mixing plays a critical role during the initial propagation phase, additional effects are responsible for increased spectral broadening during subsequent propagation. In fact, this is evident by examining the spectral and temporal characteristics at the fiber output shown in Fig. 24. In particular, for pumping at both 780 and 900 nm, we see distinct solitonlike structure in both the time and frequency domains arising from the generation of significant spectral content in the anomalous GVD regime.

The subsequent propagation of these solitons results in an increase in the overall spectral width due to contributions from dispersive wave generation, XPM, and the Raman self-frequency shift. Figure 24 shows that maximum spectral broadening for these parameters is observed when pumping slightly in the anomalous GVD regime at 800 nm. In contrast to the femtosecond regime

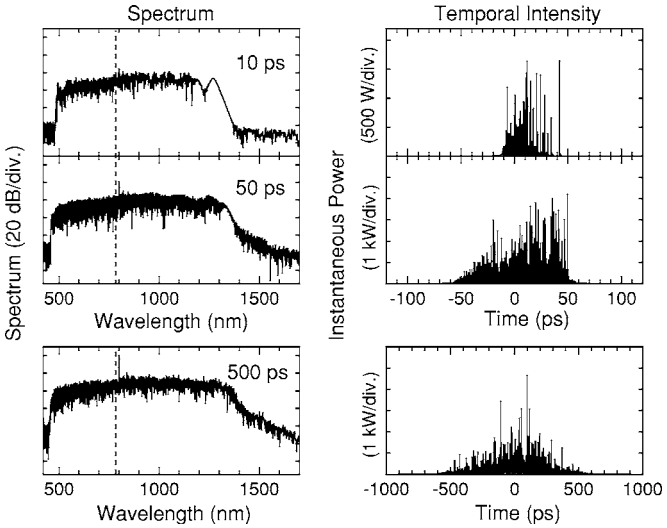

FIG. 27. Spectral and temporal characteristics for SC generated in 2 m of PCF with pump pulse durations in the 10–500 ps range as indicated. Simulations were carried out for pulses at 800 nm with peak power of 500 W. Note the different time scale that has been used to display the temporal results for the 500 ps case.

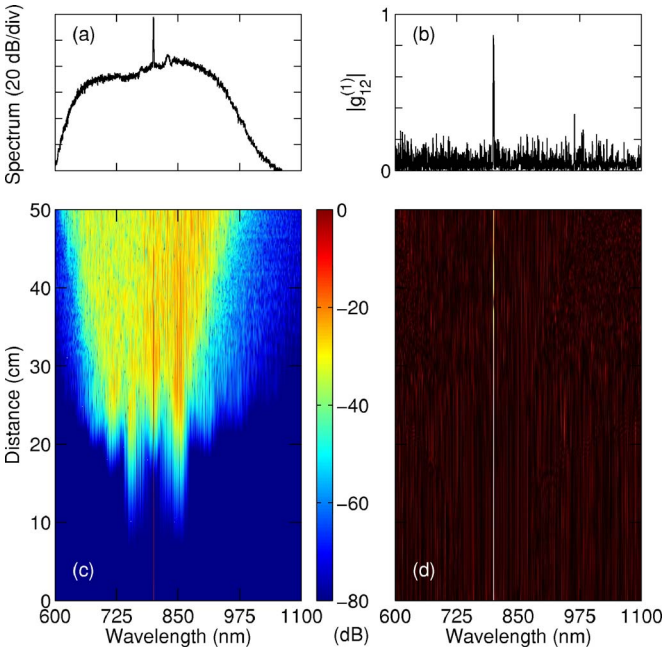

FIG. 28. (Color online) Evolution of spectrum and coherence. (a) Average spectrum and (b) degree of first-order coherence $|g_{12}^{(1)}|$ of a SC obtained with 20 ps pulses of 500 W peak power at a 800 nm pump wavelength in a 50-cm-long fiber. (c) Evolution of the spectrum along the fiber (logarithmic scale, clipped here at −80 dB for clarity) and (d) corresponding evolution of the coherence.

results in Fig. 13, however, pumping further in the anomalous GVD regime results in reduced spectral broadening because the initial spectral broadening does not generate sufficient bandwidth to efficiently seed dispersive wave transfer into the normal GVD regime.

C. Dependence on input pulse duration

Some dependence on the output SC characteristics with pulse duration can also be observed in the long pulse regime. Figure 27 shows simulation results for spectral and temporal characteristics for pulses in the range 10–500 ps. As above, the pulse peak power is 500 W and the fiber length is 2 m. The pump wavelength used here is 800 nm corresponding to where maximum spectral broadening was observed in the results above.

Although the physical mechanisms underlying the spectral broadening do not differ over this range, some differences in the spectral and temporal characteristics can nonetheless be observed. In particular, for shorter input pulses, separated solitons are more distinctly observed both in the temporal trace and in the spectrum. It is easy to see from Fig. 27 how noise and smoothing effects would be expected to become more prominent for longer pulses. Moreover, the transition from the picosecond to the ideal CW excitation case would be expected to exhibit a number of interesting aspects of soliton-related dynamics (Kutz *et al.*, 2005), but it is beyond the scope of this review to consider these in detail.

D. Effects of input pulse noise

The discussion above should have made clear that SC generation with long pulses begins with a fast modulation of the pump pulse envelope due to stimulated Raman scattering and/or four-wave mixing. It is also clear that this modulation arises spontaneously from noise at frequencies that do not overlap with the bandwidth of the pump. Following our discussion on the noise characteristics of femtosecond continua where modulation instability is the principal cause of coherence degradation (Sec. VI.D), this suggests that SCs generated with long pump pulses or in the CW regime are, generally, incoherent.

This is illustrated explicitly in Fig. 28. Here we have evaluated the noise properties of a picosecond SC by performing 20 identical simulations (apart for the random noise components) at an 800 nm pump wavelength and with all other parameters identical to those of Figs. 24–26, i.e., 20 ps pulses of 500 W peak power. For clarity of presentation, the fiber length has been limited to 50 cm. However, no additional information about the coherence properties is obtained for longer propagation distances.

Clearly, the degree of coherence $|g_{12}^{(1)}|$ [Fig. 28(b)] is nearly zero at all wavelengths across the output spectrum except in the immediate vicinity of the pump wavelength (i.e., within a few nanometers). By looking at the evolution of the spectrally resolved degree of coherence along the fiber length [Fig. 28(d)], we observe that this does not result from a progressive coherence degradation during propagation. As a matter of fact, no generated spectral components are at any stage coherent with the pump wave. The spectral broadening is seeded incoherently from noise to start with, and different parts of

the spectrum stay uncorrelated with the pump all along the fiber. In this regard, we have also checked that a similar trend is observed with normal GVD pumping where cascaded Raman generation is responsible for the SC spectra observed. Also, by comparing Figs. 28(a) and 28(b) with Fig. 20 obtained with 100 and 150 fs pulses, we see that what we observe here in the picosecond regime constitutes a natural extension of the way the coherence properties of femtosecond SC varies with pump pulse duration. Accordingly, even though we have not performed specific coherence calculations in the nanosecond and CW regimes, there are strong reasons to believe that continua generated with these pumps are incoherent as well.

As done at several points in this article, we stress that these results are by no means restricted to PCF. Indeed, the early coherence degradation experiments by Islam *et al.* (1989a, 1989b) and Nakazawa *et al.* (1998) in conventional fibers were actually performed in the picosecond regime, and constitute an excellent illustration of what we discuss here. Additionally, we note that the above conclusions do not imply that a coherent picosecond SC source is unattainable. Under the right conditions, e.g., by taking advantage of adiabatic soliton compression of fundamental solitons in dispersion decreasing fibers, coherent picosecond SC sources have been demonstrated (Nakazawa *et al.*, 1998; Nowak *et al.*, 1999; Boyraz *et al.*, 2000; Tamura *et al.*, 2000). It is clear, however, that the necessity to avoid modulation instability and stimulated Raman scattering limits the maximum spectral width that can be achieved. Also, we do not expect these techniques to be applicable to pump pulses much longer than 10–20 ps as this would require unrealistic fiber lengths.

Another important feature which can be observed from Fig. 28(a) is that the averaged output spectrum of our 20 ps SC appears continuous and smooth. Specifically, the highly contrasted spectral structure seen in the single-shot simulations of Figs. 24–26 as well as in the evolution plot shown in Fig. 28(b) is completely smoothed out over many pulses. This is similar to what occurs in the femtosecond regime [see, e.g., Fig. 18 as well as Gaeta (2002) and Gu *et al.* (2002)], and is not particularly surprising. It simply results from the fact that the fine details of the SC spectrum depend critically on the input pulse noise, as discussed before.

More importantly, we point out that on a larger scale the overall structure of the generated spectrum is rather uniform, smooth, and largely featureless, with no visible signatures of underlying femtosecond solitons and associated dispersive waves. This is in sharp contrast with what is typically observed in the femtosecond regime, as presented, e.g, in Fig. 13. Such smooth spectra have been observed for all reported long pulse SC experiments (Coen *et al.*, 2001; Coen, Chau, *et al.*, 2002; Wadsworth *et al.*, 2004) and are particularly striking in CW experiments (including some in HNLF) (Avdokhin *et al.*, 2003; González-Herráez *et al.*, 2003; Nicholson *et al.*, 2003; Abeeluck and Headley, 2004, 2005).

To understand this aspect, we recall that in the long pulse regime the initial step of the SC generation process is the modulation-instability induced breakup of the broad pump into solitonlike pulses and, of course, the number of subpulses generated increases with the pump pulse duration. In the anomalous GVD regime, we can actually use the soliton order of the pump pulse N as an estimate of the number of subpulses generated as it can be interpreted as the number of modulation instability periods that fit within the pump pulse envelope. For the parameters considered in our simulations above $N > 1000$, which is typically several orders of magnitude larger than in the femtosecond regime. Accordingly, each SC pulse is actually made up of hundreds of solitons, all with different random durations, powers, and wavelengths, interacting randomly, and coupled to a whole set of dispersive waves. Moreover, since they originate from noise, each of these components is mostly incoherent with each other and they do not interfere. Rather, the overall spectrum of the SC is a simple superposition of the spectral densities of each of these components. The absence of any signature of soliton-related dynamics and the smoothness of the overall SC spectrum, therefore, simply results from a massive averaging of these components. Under these conditions, the observed overall spectral structure of the generated SC can be interpreted as the envelope of the statistical distribution of all underlying solitonlike pulses (Kobtsev and Smirnov, 2005; Vanholsbeeck *et al.*, 2005).

Early observations by Islam *et al.* (1989a, 1989b) showing that different spectral parts of their picosecond SC were not present simultaneously in every single output pulse support this interpretation. It is in the CW regime, however, that it reaches its full complexity. Here, the partial coherence of the pump starts to play a dominant role as it can be associated with an initial random modulation of the phase and/or intensity of the pump beam, which can seed efficiently modulation instability and Raman scattering (Vanholsbeeck *et al.*, 2005). This ultimately increases the randomness of the SC structure, and hence its spectral smoothness, to the detriment of its coherence properties. As an example, we consider experiments performed in the CW regime which are mainly based on relatively poorly coherent pump lasers such as cascaded Raman fiber lasers. Such lasers typically exhibit a spectral bandwidth larger than 100 GHz, i.e., their output essentially corresponds to a continuous random sequence of about 10 ps pulses or shorter with varying amplitude and durations. During the SC generation process, each of these pulses or parts of the CW pump beam will eventually break up under the influence of random local noise into their own complex superposition of subpulses and they will then all interact with each other in various ways due to group-velocity walkoff. Clearly, it is hard to imagine a more complex light beam, but that is the price to pay for a smooth SC spectra. Of course, as long as they are not critically sensitive to the fine temporal structure of the SC, many applications will still find tremendous advan-

tages in those light sources given their high bandwidths and power densities.

E. Review of experimental results

The literature review in Sec. II has described how the initial demonstration of SC generation by Ranka *et al.* (2000a) was followed by experiments using much longer 60 ps (Coen *et al.*, 2001) and 0.8 ns pulses (Provino *et al.*, 2001). Both of these experiments used normal GVD regime pumping, and the dynamics were dominated by the initial growth of cascaded Raman components and the subsequent contribution of four-wave mixing once the pump energy had been shifted in the vicinity of the ZDW. Numerical simulations and/or calculations of the gain curves for the contributing four-wave-mixing processes reinforced these observations [see also Coen, Chau, *et al.* (2002) and Dudley, Provino, *et al.* (2002)].

These studies were complemented by experiments in which a selection of 2–3 m length PCFs was pumped using different nanosecond sources with kW peak powers operating at ~770 and ~1060 nm (Champert *et al.*, 2002a, 2002b). The PCFs were pumped in the anomalous GVD regime far from the fiber ZDW, so that the generated SC mostly extended on the red side of the pump because of cascaded Raman effects in this regime. A particular significance of this work was that the pump sources operated at MHz repetition rates so that the generated SC possessed multiwatt average power.

Further experiments considered pump wavelengths closer to the ZDW. This was first investigated in the picosecond regime by Seefeldt *et al.* (2003) when injecting 10 ps pulses of a few kW peak power at 1064 nm into 1–5 m long PCFs with ZDWs in the range 975–1065 nm. The resulting SC extended from 500 to 1600 nm, and the importance of modulation instability in the initial spectral broadening was emphasized. Shortly afterward, Schreiber *et al.* (2003) reported detailed experimental and numerical results under similar conditions, and provided important evidence (for the first time in the long pulse regime) of the important role of solitons and associated dispersive waves. Following this, Rulkov *et al.* (2005) used ~3 ps pulses with 10's of kW peak power at 1060 nm to study SCs in 5–65 m lengths of PCF with ZDW at 1040 nm. Under optimal conditions, SCs spanning the 500–1800 nm range were obtained at watt-level average power. A significant characteristic of these high average power SC sources is that their spectral power densities are typically ~mW/nm, compared to ~100 μW/nm obtained using femtosecond pulse sources. Using an identical pumping scheme, Travers, Popov, and Taylor (2005) managed to extend further the blue edge of the continuum down to 350 nm by combining multiple PCFs with sequentially decreasing ZDWs. In this way, advantageous phase matching is obtained over a larger region of the visible spectrum while simultaneously allowing for the efficient generation of long-wavelength Raman solitons.

The pump wavelength dependence of SC generated in the nanosecond regime was investigated by Wadsworth *et al.* (2004). The study was performed with 0.8 ns pulses with a microchip laser at 1064 nm and PCFs with ZDWs in the range 1040–1100 nm. Fiber lengths in the 1–100 m range were used in the experiments. For large normal GVD, cascaded Raman generation was observed to lead to a one-sided SC extending solely toward infrared wavelengths while the spectrum was dominated by four-wave-mixing sidebands as the pump was moved closer to the ZDW. Pumping into the anomalous GVD regime revealed cascaded four-wave mixing with the multiple sidebands eventually merging into a broad and extremely flat SC with further propagation. These observations are consistent with the analysis developed in Sec. VII.B. This study also identifies optimal parameters for the design of a low-cost, compact, nanosecond SC source extending from 500 to beyond 1750 nm. The use of frequency-doubled microchip lasers running at 532 nm and fiber tapers or PCFs with submicron diameter core allows the extension of this scheme for optimal generation of visible light (Leon-Saval *et al.*, 2004). Further discussion of the nanosecond normal GVD dynamics was also provided by Genty *et al.* (2005) when they injected 3 ns pulses into 90–100 m long large-mode area PCFs. In particular, the study showed how the blue edge of the continuum evolves as a function of the pump wavelength and pointed out the role of XPM in this evolution.

Other experiments of interest include those by Town *et al.* (2003), who used a PCF with a random distribution of air holes pumped by 42 ns pulses and by Travers, Kennedy, *et al.* (2005) in low-water-loss PCFs in the CW regime. Also, Yamamoto *et al.* (2003) generated a continuum with 2.2 ps pulses at a 40 GHz repetition rate in a dispersion-flattened polarization maintaining PCF in the 1.55 μm region. The spectrum had a relatively narrow 40 nm width, but might be suitable for wavelength-division multiplexing applications.

Genuine CW SC generation has also been reported using both PCFs and HNLFs. In one experiment, Avdokhin *et al.* (2003) used a 100 m long PCF pumped at 1065 nm. With a CW pump power as low as 8.7 W (to be compared to the 0.1–10 kW power levels typical of long pulse experiments), a 3.8 W single-mode SC spanning the 1065–1375 nm wavelength range was generated with a power density as high as 12 mW/nm. The redshifted continuum mainly resulted from cascaded Raman scattering, but later experiments performed closer to the ZDW (González-Herráez *et al.*, 2003; Nicholson *et al.*, 2003; Abeeluck *et al.*, 2004) using cascaded Raman fiber lasers and km lengths of HLNF identified the importance of modulation instability and four-wave-mixing processes. The case of normal GVD CW pumping was also investigated by Nicholson *et al.* (2003) and Abeeluck and Headley (2005) in HNLF, and revealed the usual combined Raman and four-wave-mixing scenario.

The physical processes underlying SC generation in the CW pumping regime are similar to those involved in

the nanosecond-femtosecond regimes. Of particular significance when using a CW pump, however, is the partially coherent nature of the CW pump beam, which can have a significant influence on the initial spectral broadening dynamics [Mussot *et al.* (2004)]. This was further stressed by Abeeluck and Headley (2004), who used a 5 W low-coherence laser diode as a pump source and interpreted the broad bandwidth of the generated continuum (1.2–1.8 μm) as due to the efficient seeding of modulation instability by the large level of phase and amplitude noise present in the incoherent pump beam. Subsequent numerical results partly support these ideas (Kobtsev and Smirnov, 2005; Vanholsbeeck *et al.*, 2005).

From the discussion in the preceding section, the generated SC spectra in the CW and longer pulse regimes would be expected to be highly unstable from shot to shot, and possess very low spectral coherence. This has been confirmed in the picosecond pump regime using delayed pulse measurements of the mutual coherence function by Nicholson and Yan (2004) using SC generated in HNLF and by Türke *et al.* (2005) using SC generated in tapered fibers.

VIII. OTHER ISSUES

Although we have concentrated on the properties of SC generation under the most commonly encountered experimental conditions, a number of closely related research areas deserve additional discussion.

A. Fibers with multiple zero-dispersion wavelengths

Although most studies of SC generation have used fibers with only one ZDW, we have seen in Fig. 2 that it is possible to design PCFs with a second ZDW further in the infrared. In fact, this is also possible with an equivalent small-diameter taper and, indeed, has also been demonstrated earlier in specialty dispersion-shifted standard fiber (Mamyshev *et al.*, 1993). In the vicinity of the second ZDW, the slope of the GVD parameter D when plotted in terms of wavelength is negative, i.e., $dD/d\lambda < 0$, and such a fiber is often described as having a negative dispersion slope in this region. Interestingly, this condition also corresponds to $\beta_3 < 0$ so that the same terminology applies irrespective of the definition of the dispersion parameter used.

A number of novel SC and pulse propagation effects have been studied in such fibers. For example, Gaeta (2002) pointed out that such a negative dispersion slope coupled with anomalous GVD would significantly modify the SC generation process through the generation of *redshifted* dispersive waves, allowing SC generation to be extended further into the infrared.

Surprisingly (perhaps due to limited fiber availability), there have been relatively few experimental studies. However, the potential for extended infrared SC generation was demonstrated by Harbold *et al.* (2002) using 80 fs pulses launched into a 1 μm diameter tapered fiber designed to have the second ZDW at the center laser wavelength of 1260 nm. For pulse energies of 1 nJ, a SC from 1000 to 1700 nm was generated. Subsequently, Hilligsøe *et al.* (2004) studied spectral broadening in a fiber with two closely lying ZDWs at 780 and 945 nm when it was pumped at 790 nm in the anomalous GVD regime between the two points of zero dispersion. In this case, using 0.7 nJ energy pulses with 40 fs FWHM, the output SC consisted of two peaks in the two normal GVD regions, while there was almost complete depletion in the central anomalous GVD region. Although these features are consistent with four-wave-mixing effects (Andersen *et al.*, 2004), the mechanism responsible for the double-peaked SC structure was later clarified as arising from pump energy transfer to both redshifted and blueshifted dispersive waves (Falk *et al.*, 2005; Frosz *et al.*, 2005).

A further important feature of the SC dynamics in such PCFs pointed out by Genty, Lehtonen, Ludvigsen, and Kaivola (2004) was the interaction between the redshifted and blueshifted dispersive-wave components and the fundamental solitons generated from the fission of the incident pump pulse. Related theoretical and numerical studies considered the more general way in which a negative dispersion slope could influence soliton propagation dynamics, and a number of novel effects were identified. In particular, Skryabin *et al.* (2003) and Biancalana *et al.* (2004) showed how the transfer of energy from a soliton to a redshifted dispersive wave results in a spectral recoil effect that can stabilize the soliton frequency against the Raman self-frequency shift, even as it continues to lose energy. New wave-mixing phenomena involving solitons, continuous-wave beams, and soliton-soliton interactions have also been the subject of both theoretical and numerical studies (Yulin *et al.*, 2004; Frosz *et al.*, 2005; Skryabin and Yulin, 2005). Comprehensive experimental studies of these effects using cross-correlation FROG have been reported by Efimov *et al.* (2004b, 2005), and the results were found to be in good agreement with GNLSE-based numerical simulations. Interestingly, although motivated by interest in negative GVD slope dynamics, some of the interaction and wave-mixing effects can in fact occur irrespective of the sign of the dispersion slope. The reader is referred to the original references for details.

The critical design criterion leading to multiple dispersion zeros in PCFs or tapered fibers is the reduction of the effective core region diameter; in the experiments above, this diameter was typically $\simeq 1$ μm. However, experiments have also studied nonlinear propagation effects in tapered fibers and tapered PCF structures with transverse dimensions of the order of, or smaller than, an optical wavelength (Foster and Gaeta, 2004; Leon-Saval *et al.*, 2004). Under these conditions, it is not only the GVD characteristics that modify the propagation dynamics, but also the enhanced nonlinearity arising from the very tight confinement. In fact, at the subwavelength level the tradeoff between power localization in the core and cladding regions results in an optimal waveguide dimension that maximizes the nonlinear interaction (Zheltikov, 2003; Foster *et al.*, 2004). With the appropri-

ate choice of waveguide dimensions, however, the threshold for octave-spanning SC generation can be reduced significantly below that required when using standard untapered PCF (Foster and Gaeta, 2004). Accurate modeling of the SC generation process in such structures can still be carried out using a GNLSE approach (Foster, Dudley, *et al.*, 2005), although care must be taken to include the longitudinal dependence of fiber guidance properties along the taper, as well as wavelength-dependent modal attenuation effects (Finazzi *et al.*, 2003; Nguyen *et al.*, 2005). Finally, we note that by exploiting only the initial higher-order soliton effect compression phase of SC generation such subwavelength waveguides have also been successfully used for pulse compression down to the few-cycle regime (Foster, Gaeta, *et al.*, 2005).

B. Supercontinuum generation with multiple pumps

Using a fiber with only one ZDW yet with two different pump wavelengths has been a subject of recent interest. A novel experiment reported by Champert *et al.* (2004) and Couderc *et al.* (2005) used two injected quasi-CW pumps at different wavelengths on either side of the zero-dispersion point. In particular, pulses at 1064 and 532 nm from the fundamental and second harmonic of a passively Q-switched Nd^{3+}:YAG nanosecond laser were injected into different PCFs with ZDWs in the range 790–870 nm. In the absence of the infrared pump, a series of distinct Raman Stokes peaks were observed from 532 to 650 nm, as expected for SC generation with a normal GVD pump (see Fig. 24). The addition of sufficient power in the infrared pump, however, significantly modified the observed spectral broadening and resulted in uniform and symmetrical spectral broadening about the 532 nm pump. In particular, for a peak power of 770 W at 1064 nm, and 300 W at 532 nm, a uniform visible SC from 400 to 700 nm was generated.

Although the particular spectral broadening mechanisms responsible for this effect were not examined quantitatively, the results are consistent with the excitation of a two-color modulation-instability process with two pumps in different regimes of group velocity dispersion (Schadt and Jaskorzynska, 1987; Gouveia-Neto *et al.*, 1988a; Yu *et al.*, 1993). In this case, it would be the XPM between the two pumps that is responsible for phase matching the instability, although the dynamics would be expected to be significantly modified by modulation instability of the infrared pump itself. In particular, it might be expected that solitons generated from the infrared pump modulation instability could modify any components generated in the normal GVD regime through XPM effects as discussed by Genty, Lehtonen, and Ludvigsen (2004). Additional work is required to clarify the detailed interactions between these effects.

In the femtosecond regime, it is not possible to consider the mutual interaction between copropagating pulses in terms of a quasi-CW modulation instability. Nonetheless, the effect of XPM between two copropagating pulses on either side of the ZDW can also lead to significant modification of the spectral broadening processes. In the context of SC generation in PCFs, Genty, Lehtonen, and Ludvigsen (2005) have numerically studied the effect of XPM from a femtosecond soliton pump pulse in the anomalous GVD regime onto a copropagating longer signal pulse in the normal GVD regime. The major result obtained was that XPM from the femtosecond soliton can result in a significant extension of the signal spectrum to both shorter or longer wavelengths depending on the initial delay between the two pulses. Experimental confirmation of these numerical predictions has been provided by Konorov *et al.* (2005) and Schreiber *et al.* (2005).

C. Polarization effects

In order to highlight the essential features of the nonlinear and dispersive interactions that underlie SC generation, we have focused on a scalar treatment and neglected polarization-related effects during propagation. Of course this is a simplified view that neglects a number of both linear and nonlinear polarization-dependent processes. In this section, we present a brief review of the literature dealing with these aspects and point out some possible directions for future investigation. It is not possible, however, to provide a comprehensive description of the polarization dynamics of SC generation, which is still to a great extent unexplored.

The dynamics of light polarization in PCFs is related to the presence (or absence) of birefringence in the fiber structure. Even though progress in manufacturing technologies has led to the fabrication of PCFs with a microstructure lattice of nearly perfect symmetry (Steel *et al.*, 2001; Ritari *et al.*, 2003), the cross section of narrow-core PCFs often exhibits imperfections occurring in the fiber drawing stage. Naturally, intentional birefringence may also be introduced (Ortigosa-Blanch *et al.*, 2000; Hansen *et al.*, 2001).

Injection along an identified principal polarization axis is therefore often necessary to optimize the SC output. This was, in fact, reported in a number of early publications (see, e.g. Apolonski *et al.*, 2002; Coen, Chau, *et al.*, 2002; Ortigosa-Blanch *et al.*, 2002; Price *et al.*, 2002b). Although the precise mechanisms involved were not clearly elucidated at that time, these experiments reported the clear dependence of the generated SC spectrum on the orientation of the input polarization. Indeed, Coen, Chau, *et al.* (2002) even presented numerical modeling of SC generation in birefringent PCFs.

Most early experiments used fibers where the birefringence was accidental and/or of the same magnitude as conventional step-index polarization maintaining fibers (Agrawal, 2001). However, the design flexibility of PCFs allows the production of fibers with birefringence that is orders of magnitude higher than that of standard fibers. This feature of PCFs is particularly interesting in the context of SC generation, because it yields strongly polarization-maintaining behavior that results in all fre-

quency components of the SC generated in a single state of polarization at the fiber output.

This was demonstrated by Lehtonen *et al.* (2003) who injected pulses with an input state of polarization aligned with the principal polarization axis of a highly birefringent PCF. They showed that the pump pulses maintain their linear polarization, and that additional frequency components created in the SC generation process also have a polarization aligned with that of the pump. The experimental SC spectra obtained with each principal axis can be readily interpreted in terms of soliton and dispersive-wave dynamics as in the scalar case, and differences between them are due to the different dispersion characteristics of the two axes [see also Kalashnikov *et al.* (2003)]. Lehtonen *et al.* (2003) also showed that the SC obtained by tuning the polarization of the input pulse at 45° between the principal polarization axes results from a linear superposition of the different SC obtained independently on the two axes with half of the total input power. Indeed, in these highly birefringent fibers, the different group delay associated with each polarization axis results in a relatively short walkoff distance between frequency components generated on each principal axis (on the order of few millimeters for 100 fs pulses). Therefore, these orthogonally polarized components do not interact with each other after this short distance. This finding is supported by additional experiments performed by Proulx *et al.* (2003).

Supercontinuum generation in PCFs with low birefringence has also been investigated. In particular, Zhu and Brown (2004c) analyzed the polarization evolution of the spectral SC content along the fiber length through numerical simulations and revealed complex dynamics. Through the inclusion of random noise and using a procedure similar to that described in Sec. IV.D, they also studied the polarization stability properties of the SC by introducing a spectrally resolved polarization coherence function. Typically, the stability of the polarization state is relatively good for the dispersive wave and the soliton components, whereas it is degraded around the pump wavelength, though improved polarization coherence can be obtained by using shorter pump pulses or fibers with higher birefringence. The same authors confirmed their findings in subsequent experiments (Zhu and Brown, 2004b) and interpreted them as resulting from the noise sensitivity of vectorial modulation instabilities. A related numerical comparison of the polarization dependence on the spectral and temporal SC properties (although not the related coherence properties) for both low- and high-birefringence fibers has also been reported by Tianprateep *et al.* (2005).

Further insight was provided by Lu *et al.* (2004), who carried out experimental and numerical studies on the vectorial dependence of soliton fission itself. This work revealed that, even in an isotropic fiber, multiple solitons generated through the fission of a higher-order soliton have a vectorial character and exhibit different states of elliptical polarization while they emit dispersive waves with complicated polarization features. As the concept of soliton fission plays a central role in the interpretation of PCF-generated SC, we expect this approach to provide a powerful framework for further studies on the polarization dynamics of SC generation. In particular, recent findings on intensity-induced nonlinear birefringence (Fortier *et al.*, 2004) and the behavior of self-frequency-shifted solitons in birefringent PCFs (Kobtsev *et al.*, 2005) could be interpreted in this manner.

As a final point in our discussion of vectorial propagation effects, we note that the high-index contrast in PCFs means that they are strongly guiding, and thus guided mode solutions possess a significant nonzero longitudinal field component (Steel, 2004). Although the effect of such hybrid mode characteristics on nonlinear pulse propagation in PCFs has not yet been considered in detail, it raises the possibility of observing coupled spatiotemporal nonlinear guided wave dynamics at high powers. This is an intriguing subject for further study.

D. Other nonlinear frequency conversion processes

Although white-light SC generation is perhaps the most spectacular manifestation of nonlinear optical propagation effects in PCFs, other frequency-conversion processes have also been a subject of much interest. An important experiment by Sharping *et al.* (2001) reported the use of PCFs in a straightforward four-wave-mixing experiment. A major motivation for this work was quantum optics applications, and subsequent work has since demonstrated soliton squeezing (Fiorentino *et al.*, 2002) and the generation of correlated photon pairs (Fan *et al.*, 2005; Rarity *et al.*, 2005; Vidne and Rosenbluh, 2005). Related research has developed optical parametric amplifiers and oscillators, with results obtained from the CW to the femtosecond regime (Sharping *et al.*, 2002; Lasri *et al.*, 2003; de Matos *et al.*, 2004; Deng *et al.*, 2005; Wong *et al.*, 2005). Work has also been carried out on the use of PCFs in a wide range of telecommunications applications, including thresholding (Lee *et al.*, 2002), wavelength conversion (Lee *et al.*, 2003), and Raman amplification (Yusoff *et al.*, 2002; Varshney *et al.*, 2005).

Another interesting class of nonlinearity reported in experiments involves multimode phase-matched harmonic generation. This has been applied to the case of UV generation (Omenetto *et al.*, 2001; Efimov *et al.*, 2003; Price *et al.*, 2003). A recent development in this area has also reported UV generation in an extended planar waveguide whose fabrication was possible through the application of PCF technologies (Joly *et al.*, 2005).

IX. CONCLUSIONS

A. Choosing a continuum

Supercontinuum generation is a complex process, and any quantitative explanation of the underlying physics must take into account a number of different fiber and pulse parameters. Nonetheless, from an applications perspective, the physics underlying the SC generation process is often less important than knowing how to ef-

ficiently choose a pump source and fiber type in order to generate a SC with particular desired properties. Based on the results and discussions presented, we are now in a position to provide some relatively straightforward practical guidelines to assist experimental design. Discussions of more specific applications have been given by Hansen (2005) and Smirnov *et al.* (2006).

Perhaps the most important consideration relates to the coherence and stability of the desired SC, as this impacts directly on the type of pump source required. For applications such as frequency metrology, telecommunications, pulse compression, and coherent spectroscopy, generating a phase-stable continuum is essential. This implies some kind of femtosecond pulse source. If octave-spanning bandwidths are critical, then nanojoule energy sub-50-fs pulses from a stabilized source are required. With a pump wavelength slightly in the anomalous GVD regime of a highly nonlinear PCF with one ZDW, good results would be expected. Ideally, one would like to use the minimum length of fiber necessary, and a useful guideline is to inject pulses with sufficient peak power so that the required bandwidth is achieved with a fiber length around the characteristic fission length. Because of experimental uncertainties, it is of course advisable to start with a longer length and successively cut back to achieve optimal SC characteristics.

With this configuration, the generated SC will typically possess significant spectral fine structure, although this may not always be an important consideration. For some applications, however, achieving spectral flatness, or strong spectral content in particular wavelength ranges (e.g., toward the blue or red edges of the SC), can be desirable. In this case, careful selection of the PCF type is required, and it may be necessary to exploit more complex dynamical processes such as soliton–dispersive-wave cross-phase modulation or simultaneous blue-shifted and redshifted dispersive-wave generation in a fiber with two ZDWs. Provided stabilized sub-50-fs pulses are used, however, good coherence would still be expected.

Pumping in the normal GVD regime of a PCF will also yield good coherence properties, but at the expense of a reduced bandwidth. An advantage of normal GVD pumping, however, is that the SC spectrum generated will generally be free of fine structure, and this may be a preferred solution in a pulse compression or telecommunications context. Moreover, it may be the only possibility to generate a highly coherent SC in cases where only longer pulses in the 100–200 fs range are available.

For applications in which coherence properties are unimportant, the utility of the SC source resides in its high brightness and broad bandwidth. In this case, any conveniently available high power source in the femtosecond to the CW regime can in principle be combined with an appropriate PCF, with the SC bandwidth generated critically dependent on the proximity of the pump wavelength to the fiber ZDW. Optimal bandwidth and spectral flatness would be expected pumping close to the ZDW.

B. Next steps

The initial surprise associated with SC generation in PCFs has now passed, and extensive research has allowed the physics of the underlying spectral broadening processes to be well understood. Experimentally, SC generation in PCFs is now routine, and research is increasingly focusing on applications rather than the fundamental physics. So, what next?

An immediate answer to this question is found in the topics outlined in Sec. VIII, because research in these areas is at a relatively early stage. The study of vectorial propagation effects is one that we anticipate will undergo significant further development, and a greater number of careful experimental studies would be particularly welcome. It is very easy to list other keywords and phrases that will attract much interest as areas of future study: nonlinear effects in multiple core PCFs, nonlinear propagation in hollow-core photonic band-gap fiber, sonic band gaps, surface modes, microfluidics, and many more.

Another answer to the question involves a more general issue. The photonic crystal fiber has challenged much of the received wisdom of linear guided wave optics, and the study of SC generation has certainly made researchers in nonlinear optics think hard. Currently, envelope equations such as the GNLSE appear to describe satisfactorily the nonlinear propagation effects that have been observed, but perhaps PCF gives experimentalists the chance to search actively for regimes where envelope approaches fail. Understanding the physics under such conditions would represent a significant new challenge in nonlinear guided wave optics, but it would undoubtedly present many opportunities to discover even more surprises. Irrespective of the precise nature of any new developments that might occur, we sincerely hope that they will be as enriching as those that have occurred in the past.

ACKNOWLEDGMENTS

The writing of this review developed from discussions with Philip St. J. Russell and Rick Trebino at the *New Concepts in Photonics and Optical Telecommunications* Summer School held from June 21–25, 2004 in Dijon, France. We are extremely grateful to them for their encouragement, and to Guy Millot from the Université de Bourgogne for his exceptional assistance. Our understanding of the physics and applications of supercontinuum generation has benefited from collaboration and discussion with numerous other colleagues and friends. We hope that they will excuse and forgive us for not being able to acknowledge them all individually. J.M.D. acknowledges financial assistance from the French National Ministry of Education, Research and Technology and the Centre National de la Recherche Scientifique (CNRS). He extends particular thanks to the Institut Universitaire de France, without whose support this review would never have been completed. G.G. acknowledges the Academy of Finland and the Jenny ja Antti

Wihuri foundation for financial support. S.C. thanks the Belgian Fonds National de la Recherche Scientifique (FNRS), the Interuniversity Attraction Pole program of the Belgian government, the New Zealand Foundation for Research, Science & Technology, and The Marsden Fund of The Royal Society of New Zealand.

REFERENCES

Abdullaev, F. Kh., S. A. Darmanyan, S. Bischoff, P. L. Christiansen, and M. P. Sørensen, 1994, "Modulational instability in optical fibers near the zero dispersion point," Opt. Commun. **108**, 60–64.

Abeeluck, A. K., and C. Headley, 2004, "Supercontinuum growth in a highly nonlinear fiber with a low-coherence semiconductor laser diode," Appl. Phys. Lett. **85**, 4863–4865.

Abeeluck, A. K., and C. Headley, 2005, "Continuous-wave pumping in the anomalous- and normal-dispersion regimes of nonlinear fibers for supercontinuum generation," Opt. Lett. **30**, 61–63.

Abeeluck, A. K., C. Headley, and C. G. Jørgensen, 2004, "High-power supercontinuum generation in highly nonlinear, dispersion-shifted fibers by use of a continuous-wave Raman fiber laser," Opt. Lett. **29**, 2163–2165.

Adachi, M., K. Yamane, R. Morita, and M. Yamashita, 2005, "Sub-5-fs pulse compression of laser output using photonic crystal fiber with short zero-dispersion wavelength," Jpn. J. Appl. Phys., Part 2 **44**, L1423–L1425.

Agrawal, G. P., 2001, *Nonlinear Fiber Optics*, 3rd ed. (Academic, San Diego).

Akhmediev, N., and M. Karlsson, 1995, "Cherenkov radiation emitted by solitons in optical fibers," Phys. Rev. A **51**, 2602–2607.

Akimov, D. A., A. A. Ivanov, M. V. Alfimov, S. N. Bagayev, T. A. Birks, W. J. Wadsworth, P. St. J. Russell, A. B. Fedotov, V. S. Pivtsov, A. A. Podshivalov, and A. M. Zheltikov, 2001, "Spectral superbroadening of subnanojoule Cr:forsterite femtosecond laser pulses in a tapered fiber," Pis'ma Zh. Eksp. Teor. Fiz. **74**, 515–519 [JETP Lett. **74**, 460–463 (2001)].

Aközbek, N., M. Scalora, C. M. Bowden, and S. L. Chin, 2001, "White-light continuum generation and filamentation during the propagation of ultra-short laser pulses in air," Opt. Commun. **191**, 353–362.

Alfano, R. R., 2006, Ed., *The Supercontinuum Laser Source* (Springer, New York).

Alfano, R. R., and S. L. Shapiro, 1970a, "Emission in the region 4000 to 7000 Å via four-photon coupling in glass," Phys. Rev. Lett. **24**, 584–587.

Alfano, R. R., and S. L. Shapiro, 1970b, "Observation of self-phase modulation and small-scale filaments in crystals and glasses," Phys. Rev. Lett. **24**, 592–594.

Amans, D., E. Brainis, M. Haelterman, Ph. Emplit, and S. Massar, 2005, "Vector modulation instability induced by vacuum fluctuations in highly birefringent fibers in the anomalous-dispersion regime," Opt. Lett. **30**, 1051–1053.

Ames, J. N., S. Ghosh, R. S. Windeler, A. L. Gaeta, and S. T. Cundiff, 2003, "Excess noise generation during spectral broadening in a microstructured fiber," Appl. Phys. B **77**, 279–284.

Andersen, T. V., K. M. Hilligsøe, C. K. Nielsen, J. Thøgersen, K. P. Hansen, S. R. Keiding, and J. J. Larsen, 2004, "Continuous-wave wavelength conversion in a photonic crystal fiber with two zero-dispersion wavelengths," Opt. Express **12**, 4113–4122.

Apolonski, A., B. Povazay, A. Unterhuber, W. Drexler, W. J. Wadsworth, J. C. Knight, and P. St. J. Russell, 2002, "Spectral shaping of supercontinuum in a cobweb photonic-crystal fiber with sub-20-fs pulses," J. Opt. Soc. Am. B **19**, 2165–2170.

Avdokhin, A. V., S. V. Popov, and J. R. Taylor, 2003, "Continuous-wave, high-power, Raman continuum generation in holey fibers," Opt. Lett. **28**, 1353–1355.

Baldeck, P. L., and R. R. Alfano, 1987, "Intensity effects on the stimulated four photon spectra generated by picosecond pulses in optical fibers," J. Lightwave Technol. **LT-5**, 1712–1715.

Beaud, P., W. Hodel, B. Zysset, and H. P. Weber, 1987, "Ultrashort pulse propagation, pulse breakup, and fundamental soliton formation in a single-mode optical fiber," IEEE J. Quantum Electron. **QE-23**, 1938–1946.

Bellini, M., and T. W. Hänsch, 2000, "Phase-locked white-light continuum pulses: Toward a universal optical frequency-comb synthesizer," Opt. Lett. **25**, 1049–1051.

Benabid, F., J. C. Knight, G. Antonopoulos, and P. St. J. Russell, 2002, "Stimulated Raman scattering in hydrogen-filled hollow-core photonic crystal fiber," Science **298**, 399–402.

Biancalana, F., D. V. Skryabin, and P. St. J. Russell, 2003, "Four-wave mixing instabilities in photonic-crystal and tapered fibers," Phys. Rev. E **68**, 046603.

Biancalana, F., D. V. Skryabin, and A. V. Yulin, 2004, "Theory of the soliton self-frequency shift compensation by the resonant radiation in photonic crystal fibers," Phys. Rev. E **70**, 016615.

Birks, T. A., J. C. Knight, and P. St. J. Russell, 1997, "Endlessly single-mode photonic crystal fiber," Opt. Lett. **22**, 961–963.

Birks, T. A., W. J. Wadsworth, and P. St. J. Russell, 2000, "Supercontinuum generation in tapered fibers," Opt. Lett. **25**, 1415–1417.

Bjarklev, A., J. Broeng, and A. Sanshez Bjarklev, 2003, *Photonic Crystal Fibres* (Kluwer Academic, Boston).

Bloembergen, N., 1973, "The influence of electron plasma formation on superbroadening in light filaments," Opt. Commun. **8**, 285–288.

Bloembergen, N., 2000, "Nonlinear optics: Past, present, and future," IEEE J. Sel. Top. Quantum Electron. **6**, 876–880.

Bloembergen, N., and Y. R. Shen, 1964, "Coupling between vibrations and light waves in Raman laser media," Phys. Rev. Lett. **12**, 504–507.

Blow, K. J., and D. Wood, 1989, "Theoretical description of transient stimulated Raman scattering in optical fibers," IEEE J. Quantum Electron. **25**, 2665–2673.

Bondarenko, N. G., I. V. Eremina, and V. I. Talanov, 1970, "Broadening of spectrum in self-focusing of light in crystals," Pis'ma Zh. Eksp. Teor. Fiz. **12**, 125–128 [JETP Lett. **12**, 85–87 (1970)].

Boyer, G., 1999, "High-power femtosecond-pulse reshaping near the zero-dispersion wavelength of an optical fiber," Opt. Lett. **24**, 945–947.

Boyraz, Ö., J. Kim, M. N. Islam, F. Coppinger, and B. Jalali, 2000, "10 Gb/s multiple wavelength, coherent short pulse source based on spectral carving of supercontinuum generated in fibers," J. Lightwave Technol. **18**, 2167–2175.

Brabec, T., and F. Krausz, 1997, "Nonlinear optical pulse propagation in the single-cycle regime," Phys. Rev. Lett. **78**, 3282–3285.

Brewer, R. G., 1967, "Frequency shifts in self-focused light,"

Phys. Rev. Lett. **19**, 8–10.
Broderick, N. G. R., T. M. Monro, P. J. Bennett, and D. J. Richardson, 1999, "Nonlinearity in holey optical fibers: Measurement and future opportunities," Opt. Lett. **24**, 1395–1397.
Brodeur, A., and S. L. Chin, 1998, "Band-gap dependence of the ultrafast white-light continuum," Phys. Rev. Lett. **80**, 4406–4409.
Cao, Q., X. Gu, E. Zeek, M. Kimmel, R. Trebino, J. M. Dudley, and R. S. Windeler, 2003, "Measurement of the intensity and phase of supercontinuum from an 8-mm-long microstructure fiber," Appl. Phys. B **77**, 239–244.
Cavalcanti, S. B., J. C. Cressoni, H. R. da Cruz, and A. S. Gouveia-Neto, 1991, "Modulation instability in the region of minimum group-velocity dispersion of single-mode optical fibers via an extended nonlinear Schrödinger equation," Phys. Rev. A **43**, 6162–6165.
Champert, P.-A., V. Couderc, P. Leproux, S. Février, V. Tombelaine, L. Labonté, P. Roy, C. Froehly, and P. Nérin, 2004, "White-light supercontinuum generation in normally dispersive optical fiber using original multi-wavelength pumping system," Opt. Express **12**, 4366–4371.
Champert, P.-A., S. V. Popov, M. A. Solodyankin, and J. R. Taylor, 2002a, "Multiwatt average power continua generation in holey fibers pumped by kilowatt peak power seeded ytterbium fiber amplifier," Appl. Phys. Lett. **81**, 2157–2159.
Champert, P.-A., S. V. Popov, and J. R. Taylor, 2002b, "Generation of multiwatt, broadband continua in holey fibers," Opt. Lett. **27**, 122–124.
Chang, G., T. B. Norris, and H. G. Winful, 2003, "Optimization of supercontinuum generation in photonic crystal fibers for pulse compression," Opt. Lett. **28**, 546–548.
Chen, A. Y. H., G. K. L. Wong, S. G. Murdoch, R. Leonhardt, J. D. Harvey, J. C. Knight, W. J. Wadsworth, and P. St. J. Russell, 2005, "Widely tunable optical parametric generation in a photonic crystal fiber," Opt. Lett. **30**, 762–764.
Chen, C.-M., and P. L. Kelley, 2002, "Nonlinear pulse compression in optical fibers: Scaling laws and numerical analysis," J. Opt. Soc. Am. B **19**, 1961–1967.
Chiao, R. Y., E. Garmire, and C. H. Townes, 1964, "Self-trapping of optical beams," Phys. Rev. Lett. **13**, 479–482; **14**, 1056(E) (1965).
Coen, S., A. H. L. Chau, R. Leonhardt, J. D. Harvey, J. C. Knight, W. J. Wadsworth, and P. St. J. Russell, 2001, "White-light supercontinuum generation with 60-ps pump pulses in a photonic crystal fiber," Opt. Lett. **26**, 1356–1358.
Coen, S., A. H. L. Chau, R. Leonhardt, J. D. Harvey, J. C. Knight, W. J. Wadsworth, and P. St. J. Russell, 2002, "Supercontinuum generation by stimulated Raman scattering and parametric four-wave mixing in photonic crystal fibers," J. Opt. Soc. Am. B **19**, 753–764.
Coen, S., D. A. Wardle, and J. D. Harvey, 2002, "Observation of non-phase-matched parametric amplification in resonant nonlinear optics," Phys. Rev. Lett. **89**, 273901.
Cohen, L., 1989, "Time-frequency distributions—A review," Proc. IEEE **77**, 941–981.
Cormack, I. G., D. T. Reid, W. J. Wadsworth, J. C. Knight, and P. St. J. Russell, 2002, "Observation of soliton self-frequency shift in photonic crystal fibre," Electron. Lett. **38**, 167–169.
Corwin, K. L., N. R. Newbury, J. M. Dudley, S. Coen, S. A. Diddams, B. R. Washburn, K. Weber, and R. S. Windeler, 2003a, "Fundamental amplitude noise limitations to supercontinuum spectra generated in a microstructured fiber," Appl. Phys. B **77**, 269–277; **77**, 467–468(E).
Corwin, K. L., N. R. Newbury, J. M. Dudley, S. Coen, S. A. Diddams, K. Weber, and R. S. Windeler, 2003b, "Fundamental noise limitations to supercontinuum generation in microstructure fiber," Phys. Rev. Lett. **90**, 113904.
Couderc, V., P. Leproux, V. Tombelaine, L. Grossard, and A. Barthélémy, 2005, "Raman cascade suppression by using wide band parametric conversion in large normal dispersion regime," Opt. Express **13**, 8584–8590.
Cristiani, I., R. Tediosi, L. Tartara, and V. Degiorgio, 2004, "Dispersive wave generation by solitons in microstructured optical fibers," Opt. Express **12**, 124–135.
de Matos, C. J. S., J. R. Taylor, and K. P. Hansen, 2004, "Continuous-wave, totally fiber integrated optical parametric oscillator using holey fiber," Opt. Lett. **29**, 983–985.
Demircan, A., and U. Bandelow, 2005, "Supercontinuum generation by the modulation instability," Opt. Commun. **244**, 181–185.
Deng, Y., Q. Lin, F. Lu, G. P. Agrawal, and W. H. Knox, 2005, "Broadly tunable femtosecond parametric oscillator using a photonic crystal fiber," Opt. Lett. **30**, 1234–1236.
Dianov, E. M., A. Ya. Karasik, P. V. Mamyshev, A. M. Prokhorov, V. N. Serkin, M. F. Stel'makh, and A. A. Fomichev, 1985, "Stimulated-Raman conversion of multisoliton pulses in quartz optical fibers," Pis'ma Zh. Eksp. Teor. Fiz. **41**, 242–244 [JETP Lett. **41**, 294–297 (1986)].
Dianov, E. M., Z. S. Nikonova, A. M. Prokhorov, and V. N. Serkin, 1986, "Optimal compression of multi-soliton pulses in optical fibers," Pis'ma Zh. Tekh. Fiz. **12**, 756–760 [Sov. Tech. Phys. Lett. **12**, 311–313 (1986)].
Diddams, S. A., D. J. Jones, J. Ye, S. T. Cundiff, J. L. Hall, J. K. Ranka, R. S. Windeler, R. Holzwarth, Th. Udem, and T. W. Hänsch, 2000, "Direct link between microwave and optical frequencies with a 300 THz femtosecond laser comb," Phys. Rev. Lett. **84**, 5102–5105.
Drummond, P. D., and J. F. Corney, 2001, "Quantum noise in optical fibers. I. Stochastic equations," J. Opt. Soc. Am. B **18**, 139–152.
Druon, F., and P. Georges, 2004, "Pulse-compression down to 20 fs using a photonic crystal fiber seeded by a diode-pumped Yb:SYS laser at 1070 nm," Opt. Express **12**, 3383–3396.
Dudley, J. M., L. P. Barry, P. G. Bollond, J. D. Harvey, R. Leonhardt, and P. D. Drummond, 1997, "Direct measurement of pulse distortion near the zero-dispersion wavelength in an optical fiber by frequency-resolved optical gating," Opt. Lett. **22**, 457–459.
Dudley, J. M., and S. Coen, 2002a, "Coherence properties of supercontinuum spectra generated in photonic crystal and tapered optical fibers," Opt. Lett. **27**, 1180–1182.
Dudley, J. M., and S. Coen, 2002b, "Numerical simulations and coherence properties of supercontinuum generation in photonic crystal and tapered optical fibers," IEEE J. Sel. Top. Quantum Electron. **8**, 651–659.
Dudley, J. M., and S. Coen, 2004, "Fundamental limits to few-cycle pulse generation from compression of supercontinuum spectra generated in photonic crystal fiber," Opt. Express **12**, 2423–2428.
Dudley, J. M., X. Gu, L. Xu, M. Kimmel, E. Zeek, P. O'Shea, R. Trebino, S. Coen, and R. S. Windeler, 2002, "Cross-correlation frequency resolved optical gating analysis of broadband continuum generation in photonic crystal fiber: Simulations and experiments," Opt. Express **10**, 1215–1221.
Dudley, J. M., L. Provino, N. Grossard, H. Maillotte, R. S. Windeler, B. J. Eggleton, and S. Coen, 2002, "Supercon-

tinuum generation in air-silica microstructured fibers with nanosecond and femtosecond pulse pumping," J. Opt. Soc. Am. B **19**, 765–771.

Dumais, P., F. Gonthier, S. Lacroix, J. Bures, A. Villeneuve, P. G. J. Wigley, and G. I. Stegeman, 1993, "Enhanced self-phase modulation in tapered fibers," Opt. Lett. **18**, 1996–1998.

Efimov, A., A. J. Taylor, F. G. Omenetto, J. C. Knight, W. J. Wadsworth, and P. St. J. Russell, 2003, "Phase-matched third harmonic generation in microstructured fibers," Opt. Express **11**, 2567–2576.

Efimov, A., A. J. Taylor, F. G. Omenetto, and E. Vanin, 2004a, "Adaptive control of femtosecond soliton self-frequency shift in fibers," Opt. Lett. **29**, 271–273.

Efimov, A., A. J. Taylor, F. G. Omenetto, A. V. Yulin, N. Y. Joly, F. Biancalana, D. V. Skryabin, J. C. Knight, and P. St. J. Russell, 2004b, "Time-spectrally-resolved ultrafast nonlinear dynamics in small-core photonic crystal fibers: Experiment and modelling," Opt. Express **12**, 6498–6507.

Efimov, A., A. V. Yulin, D. V. Skryabin, J. C. Knight, N. Y. Joly, F. G. Omenetto, A. J. Taylor, and P. St. J. Russell, 2005, "Interaction of an optical soliton with a dispersive wave," Phys. Rev. Lett. **95**, 213902.

Elgin, J. N., T. Brabec, and S. M. J. Kelly, 1995, "A perturbative theory of soliton propagation in the presence of third order dispersion," Opt. Commun. **114**, 321–328.

Falk, P., M. H. Frosz, and O. Bang, 2005, "Supercontinuum generation in a photonic crystal fiber with two zero-dispersion wavelengths tapered to normal dispersion at all wavelengths," Opt. Express **13**, 7535–7540.

Fan, J., A. Migdall, and L. J. Wang, 2005, "Efficient generation of correlated photon pairs in a microstructure fiber," Opt. Lett. **30**, 3368–3370.

Fang, X., N. Karasawa, R. Morita, R. S. Windeler, and M. Yamashita, 2003, "Nonlinear propagation of a-few-optical-cycle pulses in a photonic crystal fiber—Experimental and theoretical studies beyond the slowly varying-envelope approximation," IEEE Photonics Technol. Lett. **15**, 233–235.

Fedotov, A. B., A. N. Naumov, A. M. Zheltikov, I. Bugar, D. Chorvat, Jr., D. Chorvat, A. P. Tarasevitch, and D. von der Linde, 2002, "Frequency-tunable supercontinuum generation in photonic-crystal fibers by femtosecond pulses of an optical parametric amplifier," J. Opt. Soc. Am. B **19**, 2156–2164.

Finazzi, V., T. M. Monro, and D. J. Richardson, 2003, "Small-core silica holey fibers: Nonlinearity and confinement loss trade-offs," J. Opt. Soc. Am. B **20**, 1427–1436.

Fiorentino, M., J. E. Sharping, P. Kumar, A. Porzio, and R. S. Windeler, 2002, "Soliton squeezing in microstructure fiber," Opt. Lett. **27**, 649–651.

Fork, R. L., C. V. Shank, C. Hirlimann, R. Yen, and W. J. Tomlinson, 1983, "Femtosecond white-light continuum pulses," Opt. Lett. **8**, 1–3.

Fortier, T. M., S. T. Cundiff, I. T. Lima, Jr., B. S. Marks, C. R. Menyuk, and R. S. Windeler, 2004, "Nonlinear polarization evolution of ultrashort pulses in microstructure fiber," Opt. Lett. **29**, 2548–2550.

Foster, M. A., J. M. Dudley, B. Kibler, Q. Cao, D. Lee, R. Trebino, and A. L. Gaeta, 2005, "Nonlinear pulse propagation and supercontinuum generation in photonic nanowires: Experiment and simulation," Appl. Phys. B **81**, 363–367.

Foster, M. A., and A. L. Gaeta, 2004, "Ultra-low threshold supercontinuum generation in sub-wavelength waveguides," Opt. Express **12**, 3137–3143.

Foster, M. A., A. L. Gaeta, Q. Cao, and R. Trebino, 2005, "Soliton-effect compression of supercontinuum to few-cycle durations in photonic nanowires," Opt. Express **13**, 6848–6855.

Foster, M. A., K. D. Moll, and A. L. Gaeta, 2004, "Optimal waveguide dimensions for nonlinear interactions," Opt. Express **12**, 2880–2887.

François, P. L., 1991, "Nonlinear propagation of ultrashort pulses in optical fibers: Total field formulation in the frequency domain," J. Opt. Soc. Am. B **8**, 276–293.

Friberg, S. R., and K. W. DeLong, 1992, "Breakup of bound higher-order solitons," Opt. Lett. **17**, 979–981.

Frosz, M. H., P. Falk, and O. Bang, 2005, "The role of the second zero-dispersion wavelength in generation of supercontinua and bright-bright soliton-pairs across the zero-dispersion wavelength," Opt. Express **13**, 6181–6192.

Fu, X., L. Qian, S. Wen, and D. Fan, 2004, "Nonlinear chirped pulse propagation and supercontinuum generation in microstructured optical fibre," J. Opt. A, Pure Appl. Opt. **6**, 1012–1016.

Gaeta, A. L., 2000, "Catastrophic collapse of ultrashort pulses," Phys. Rev. Lett. **84**, 3582–3585.

Gaeta, A. L., 2002, "Nonlinear propagation and continuum generation in microstructured optical fibers," Opt. Lett. **27**, 924–926.

Genty, G., M. Lehtonen, and H. Ludvigsen, 2004, "Effect of cross-phase modulation on supercontinuum generated in microstructured fibers with sub-30 fs pulses," Opt. Express **12**, 4614–4624.

Genty, G., M. Lehtonen, and H. Ludvigsen, 2005, "Route to broadband blue-light generation in microstructured fibers," Opt. Lett. **30**, 756–758.

Genty, G., M. Lehtonen, H. Ludvigsen, J. Broeng, and M. Kaivola, 2002, "Spectral broadening of femtosecond pulses into continuum radiation in microstructured fibers," Opt. Express **10**, 1083–1098.

Genty, G., M. Lehtonen, H. Ludvigsen, and M. Kaivola, 2004, "Enhanced bandwidth of supercontinuum generated in microstructured fibers," Opt. Express **12**, 3471–3480.

Genty, G., T. Ritari, and H. Ludvigsen, 2005, "Supercontinuum generation in large mode-area microstructured fibers," Opt. Express **13**, 8625–8633.

Gölles, M., I. M. Uzunov, and F. Lederer, 1997, "Break up of *N*-soliton bound states due to intrapulse Raman scattering and third-order dispersion—An eigenvalue analysis," Phys. Lett. A **231**, 195–200.

Golovchenko, E. A., E. M. Dianov, A. M. Prokhorov, and V. N. Serkin, 1985, "Decay of optical solitons," Pis'ma Zh. Eksp. Teor. Fiz. **42**, 74–77 [JETP Lett. **42**, 87–91 (1985)].

Golovchenko, E. A., P. V. Mamyshev, A. N. Pilipetskii, and E. M. Dianov, 1990, "Mutual influence of the parametric effects and stimulated Raman scattering in optical fibers," IEEE J. Quantum Electron. **26**, 1815–1820.

Golovchenko, E. A., P. V. Mamyshev, A. N. Pilipetskii, and E. M. Dianov, 1991, "Numerical analysis of the Raman spectrum evolution and soliton pulse generation in single-mode fibers," J. Opt. Soc. Am. B **8**, 1626–1632.

González-Herráez, M., S. Martín-López, P. Corredera, M. L. Hernanz, and P. R. Horche, 2003, "Supercontinuum generation using a continuous-wave Raman fiber laser," Opt. Commun. **226**, 323–328.

Gordon, J. P., 1986, "Theory of the soliton self-frequency shift," Opt. Lett. **11**, 662–664.

Gouveia-Neto, A. S., M. E. Faldon, A. S. B. Sombra, P. G. J.

Wigley, and J. R. Taylor, 1988a, "Subpicosecond-pulse generation through cross-phase-modulation-induced modulational instability in optical fibers," Opt. Lett. **13**, 901–903.
Gouveia-Neto, A. S., M. E. Faldon, and J. R. Taylor, 1988b, "Solitons in the region of the minimum group-velocity dispersion of single-mode optical fibers," Opt. Lett. **13**, 770–772.
Gu, X., M. Kimmel, A. P. Shreenath, R. Trebino, J. M. Dudley, S. Coen, and R. S. Windeler, 2003, "Experimental studies of the coherence of microstructure-fiber supercontinuum," Opt. Express **11**, 2697–2703.
Gu, X., L. Xu, M. Kimmel, E. Zeek, P. O'Shea, A. P. Shreenath, R. Trebino, and R. S. Windeler, 2002, "Frequency-resolved optical gating and single-shot spectral measurements reveal fine structure in microstructure-fiber continuum," Opt. Lett. **27**, 1174–1176.
Hansen, K. P., 2005, "Introduction to nonlinear photonic crystal fibers," J. Opt. Fiber. Commun. Rep. **2**, 226–254.
Hansen, T. P., J. Broeng, S. E. B. Libori, E. Knudsen, A. Bjarklev, J. R. Jensen, and H. Simonsen, 2001, "Highly birefringent index-guiding photonic crystal fibers," IEEE Photonics Technol. Lett. **13**, 588–590.
Harbold, J. M., F. Ö. Ilday, F. W. Wise, T. A. Birks, W. J. Wadsworth, and Z. Chen, 2002, "Long-wavelength continuum generation about the second dispersion zero of a tapered fiber," Opt. Lett. **27**, 1558–1560.
Hart, D. L., A. F. Judy, R. Roy, and J. W. Beletic, 1998, "Dynamical evolution of multiple four-wave-mixing processes in an optical fiber," Phys. Rev. E **57**, 4757–4774.
Harvey, J. D., R. Leonhardt, S. Coen, G. K. L. Wong, J. C. Knight, W. J. Wadsworth, and P. St. J. Russell, 2003, "Scalar modulation instability in the normal dispersion regime by use of a photonic crystal fiber," Opt. Lett. **28**, 2225–2227.
Hasegawa, A., and F. Tappert, 1973, "Transmission of stationary nonlinear optical pulses in dispersive dielectric fibers. I. Anomalous dispersion," Appl. Phys. Lett. **23**, 142–144.
Haverkamp, N., and H. R. Telle, 2004, "Complex intensity modulation transfer function for supercontinuum generation in microstructure fibers," Opt. Express **12**, 582–587.
Herrmann, J., U. Griebner, N. Zhavoronkov, A. V. Husakou, D. Nickel, J. C. Knight, W. J. Wadsworth, P. St. J. Russell, and G. Korn, 2002, "Experimental evidence for supercontinuum generation by fission of higher-order solitons in photonic fibers," Phys. Rev. Lett. **88**, 173901.
Hilligsøe, K. M., T. V. Andersen, H. N. Paulsen, C. K. Nielsen, K. Mølmer, S. R. Keiding, R. Kristiansen, K. P. Hansen, and J. J. Larsen, 2004, "Supercontinuum generation in a photonic crystal fiber with two zero dispersion wavelengths," Opt. Express **12**, 1045–1054.
Hilligsøe, K. M., H. N. Paulsen, J. Thøgersen, S. R. Keiding, and J. J. Larsen, 2003, "Initial steps of supercontinuum generation in photonic crystal fibers," J. Opt. Soc. Am. B **20**, 1887–1893.
Hollberg, L., C. W. Oates, E. A. Curtis, E. N. Ivanov, S. A. Diddams, Th. Udem, H. G. Robinson, J. C. Bergquist, R. J. Rafac, W. M. Itano, R. E. Drullinger, and D. J. Wineland, 2001, "Optical frequency standards and measurements," IEEE J. Quantum Electron. **37**, 1502–1513.
Hollenbeck, D., and C. D. Cantrell, 2002, "Multiple-vibrational-mode model for fiber-optic Raman gain spectrum and response function," J. Opt. Soc. Am. B **19**, 2886–2892.
Holzwarth, R., J. Reichert, Th. Udem, and T. W. Hänsch, 2001, "Optical frequency metrology and its contribution to the determination of fundamental constants," in *Atomic Physics 17*, edited by E. Arimondo, P. DeNatale, and M. Inguscio, AIP Conf. Proc. No. 551 (AIP, New York), pp. 58–72.
Hori, T., J. Takayanagi, N. Nishizawa, and T. Goto, 2004, "Flatly broadened, wideband and low noise supercontinuum generation in highly nonlinear hybrid fiber," Opt. Express **12**, 317–324.
Horikis, T. P., and J. N. Elgin, 2001, "Soliton radiation in an optical fiber," J. Opt. Soc. Am. B **18**, 913–918.
Hundertmark, H., D. Kracht, D. Wandt, C. Fallnich, V. V. R. K. Kumar, A. K. George, J. C. Knight, and P. St. J. Russell, 2003, "Supercontinuum generation with 200 pJ laser pulses in an extruded SF6 fiber at 1560 nm," Opt. Express **11**, 3196–3201.
Husakou, A. V., and J. Herrmann, 2001, "Supercontinuum generation of higher-order solitons by fission in photonic crystal fibers," Phys. Rev. Lett. **87**, 203901.
Husakou, A. V., and J. Herrmann, 2002, "Supercontinuum generation, four-wave mixing, and fission of higher-order solitons in photonic-crystal fibers," J. Opt. Soc. Am. B **19**, 2171–2182.
Ilev, I., H. Kumagai, K. Toyoda, and I. Koprinkov, 1996, "Highly efficient wideband continuum generation in a single-mode optical fiber by powerful broadband laser pumping," Appl. Opt. **35**, 2548–2553.
Il'ichev, N. N., V. V. Korobkin, V. A. Korshunov, A. A. Malyutin, T. G. Okroashvili, and P. P. Pashinin, 1972, "Superbroadening of the spectrum of ultrashort pulses in liquids and glasses," Pis'ma Zh. Eksp. Teor. Fiz. **15**, 191–194 [JETP Lett. **15**, 133–135 (1972)].
Iliew, R., and F. Lederer, 2002, "The role of dispersion of nonlinearity in supercontinuum generation with photonic crystal fibers," in *Nonlinear Guided Waves and Their Applications, NLGW'2002*, Stresa, Italy, Trends in Optics and Photonics Series Vol. 80 (The Optical Society of America, Washington, D.C.), paper NLTuD23.
Islam, M. N., G. Sucha, I. Bar-Joseph, M. Wegener, J. P. Gordon, and D. S. Chemla, 1989a, "Broad bandwidths from frequency-shifting solitons in fibers," Opt. Lett. **14**, 370–372.
Islam, M. N., G. Sucha, I. Bar-Joseph, M. Wegener, J. P. Gordon, and D. S. Chemla, 1989b, "Femtosecond distributed soliton spectrum in fibers," J. Opt. Soc. Am. B **6**, 1149–1158.
Ivanov, E. N., L. Hollberg, and S. A. Diddams, 2001, "Experimental study of noise properties of a Ti-sapphire mode-locked laser," in *Proceedings of the 2001 IEEE International Frequency Control Symposium* (IEEE, Piscataway, NJ), pp. 117–121.
Joly, N. Y., T. A. Birks, A. Yulin, J. C. Knight, and P. St. J. Russell, 2005, "Linear and nonlinear guidance in an ultralow loss planar glass membrane," Opt. Lett. **30**, 2469–2471.
Jones, D. J., S. A. Diddams, J. K. Ranka, A. J. Stentz, R. S. Windeler, J. L. Hall, and S. T. Cundiff, 2000, "Carrier-envelope phase control of femtosecond mode-locked lasers and direct optical frequency synthesis," Science **288**, 635–639.
Jones, W. J., and B. P. Stoicheff, 1964, "Inverse Raman spectra: Induced absorption at optical frequencies," Phys. Rev. Lett. **13**, 657–659.
Kaiser, P., and H. W. Astle, 1974, "Low-loss single material fibers made from pure fused silica," Bell Syst. Tech. J. **53**, 1021–1039.
Kalashnikov, V. L., P. Dombi, T. Fuji, W. J. Wadsworth, J. C. Knight, P. St. J. Russell, R. S. Windeler, and A. Apolonski, 2003, "Maximization of supercontinua in photonic crystal fibers by using double pulses and polarization effects," Appl.

Phys. B **77**, 319–324.
Kano, H., and H. Hamaguchi, 2003, "Characterization of a supercontinuum generated from a photonic crystal fiber and its application to coherent Raman spectroscopy," Opt. Lett. **28**, 2360–2362.
Karasawa, N., S. Nakamura, N. Nakagawa, M. Shibata, R. Morita, H. Shigekawa, and M. Yamashita, 2001, "Comparison between theory and experiment of nonlinear propagation for a-few-cycle and ultrabroadband optical pulses in a fused-silica fiber," IEEE J. Quantum Electron. **37**, 398–404.
Karlsson, M., 1998, "Four-wave mixing in fibers with randomly varying zero-dispersion wavelength," J. Opt. Soc. Am. B **15**, 2269–2275.
Kibler, B., C. Billet, J. M. Dudley, R. S. Windeler, and G. Millot, 2004, "Effects of structural irregularities on modulational instability phase matching in photonic crystal fibers," Opt. Lett. **29**, 1903–1905.
Kibler, B., J. M. Dudley, and S. Coen, 2005, "Supercontinuum generation and nonlinear pulse propagation in photonic crystal fiber: Influence of the frequency-dependent effective mode area," Appl. Phys. B **81**, 337–342.
Knight, J. C., 2003, "Photonic crystal fibres," Nature (London) **424**, 847–851.
Knight, J. C., J. Arriaga, T. A. Birks, A. Ortigosa-Blanch, W. J. Wadsworth, and P. St. J. Russell, 2000, "Anomalous dispersion in photonic crystal fiber," IEEE Photonics Technol. Lett. **12**, 807–809.
Knight, J. C., T. A. Birks, P. St. J. Russell, and D. M. Atkin, 1996, "All-silica single-mode optical fiber with photonic crystal cladding," Opt. Lett. **21**, 1547–1549; **22**, 484–485(E) (1997).
Kobtsev, S. M., S. V. Kukarin, N. V. Fateev, and S. V. Smirnov, 2005, "Coherent, polarization and temporal properties of self-frequency shifted solitons generated in polarization-maintaining microstructured fibre," Appl. Phys. B **81**, 265–269.
Kobtsev, S. M., and S. V. Smirnov, 2005, "Modelling of high-power supercontinuum generation in highly nonlinear, dispersion shifted fibers at CW pump," Opt. Express **13**, 6912–6918.
Kodama, Y., and A. Hasegawa, 1987, "Nonlinear pulse propagation in a monomode dielectric guide," IEEE Photonics Technol. Lett. **QE-23**, 510–524.
Kolesik, M., E. M. Wright, and J. V. Moloney, 2004, "Simulation of femtosecond pulse propagation in sub-micron diameter tapered fibers," Appl. Phys. B **79**, 293–300.
Konorov, S. O., D. A. Akimov, A. A. Ivanov, E. E. Serebryannikov, M. V. Alfimov, K. V. Dukel'skii, A. V. Khokhlov, V. S. Shevandin, Yu. N. Kondrat'ev, and A. M. Zheltikov, 2004, "Spectrally and temporally isolated Raman soliton features in microstructure fibers visualized by cross-correlation frequency-resolved optical gating," Appl. Phys. B **79**, 289–292.
Konorov, S. O., D. A. Akimov, A. M. Zheltikov, A. A. Ivanov, M. V. Alfimov, and M. Scalora, 2005, "Tuning the frequency of ultrashort laser pulses by a cross-phase-modulation-induced shift in a photonic crystal fiber," Opt. Lett. **30**, 1548–1550.
Krylov, D., L. Leng, K. Bergman, J. C. Bronski, and J. N. Kutz, 1999, "Observation of the breakup of a prechirped *N*-soliton in an optical fiber," Opt. Lett. **24**, 1191–1193.
Kubota, H., K. R. Tamura, and M. Nakazawa, 1999, "Analyses of coherence-maintained ultrashort optical pulse trains and supercontinuum generation in the presence of soliton-amplified spontaneous-emission interaction," J. Opt. Soc. Am. B **16**, 2223–2232.
Kumar, V. V. R. K., A. K. George, W. H. Reeves, J. C. Knight, P. St. J. Russell, F. G. Omenetto, and A. J. Taylor, 2002, "Extruded soft glass photonic crystal fiber for ultrabroad supercontinuum generation," Opt. Express **10**, 1520–1525.
Kutz, J. N., C. Lyngå, and B. J. Eggleton, 2005, "Enhanced supercontinuum generation through dispersion-management," Opt. Express **13**, 3989–3998.
Lakó, S., J. Seres, P. Apai, J. Balázs, R. S. Windeler, and R. Szipőcs, 2003, "Pulse compression of nanojoule pulses in the visible using microstructure optical fiber and dispersion compensation," Appl. Phys. B **76**, 267–275.
Lasri, J., P. Devgan, R. Tang, J. E. Sharping, and P. Kumar, 2003, "A microstructure-fiber-based 10-GHz synchronized tunable optical parametric oscillator in the 1550-nm regime," IEEE Photonics Technol. Lett. **15**, 1058–1060.
Lee, J. H., W. Belardi, K. Furusawa, P. Petropoulos, Z. Yusoff, T. M. Monro, and D. J. Richardson, 2003, "Four-wave mixing based 10-Gb/s tunable wavelength conversion using a holey fiber with a high SBS threshold," IEEE Photonics Technol. Lett. **15**, 440–442.
Lee, J. H., P. C. Teh, Z. Yusoff, M. Ibsen, W. Belardi, T. M. Monro, and D. J. Richardson, 2002, "A holey fiber-based nonlinear thresholding device for optical CDMA receiver performance enhancement," IEEE Photonics Technol. Lett. **14**, 876–878.
Lehtonen, M., G. Genty, H. Ludvigsen, and M. Kaivola, 2003, "Supercontinuum generation in a highly birefringent microstructured fiber," Appl. Phys. Lett. **82**, 2197–2199.
Leon-Saval, S. G., T. A. Birks, W. J. Wadsworth, P. St. J. Russell, and M. W. Mason, 2004, "Supercontinuum generation in submicron fibre waveguides," Opt. Express **12**, 2864–2869.
Lin, C., and R. H. Stolen, 1976, "New nanosecond continuum for excited-state spectroscopy," Appl. Phys. Lett. **28**, 216–218.
Linden, S., H. Giessen, and J. Kuhl, 1998, "XFROG—A new method for amplitude and phase characterization of weak ultrashort pulses," Phys. Status Solidi B **206**, 119–124.
Liu, X., C. Xu, W. H. Knox, J. K. Chandalia, B. J. Eggleton, S. G. Kosinski, and R. S. Windeler, 2001, "Soliton self-frequency shift in a short tapered air-silica microstructure fiber," Opt. Lett. **26**, 358–360.
Lu, F., Y. Deng, and W. H. Knox, 2005, "Generation of broadband femtosecond visible pulses in dispersion-micromanaged holey fibers," Opt. Lett. **30**, 1566–1568.
Lu, F., and W. H. Knox, 2004, "Generation of a broadband continuum with high spectral coherence in tapered single-mode optical fibers," Opt. Express **12**, 347–353.
Lu, F., and W. H. Knox, 2005, "Low noise wavelength conversion of femtosecond pulses with dispersion micro-managed holey fibers," Opt. Express **13**, 8172–8178.
Lu, F., Q. Lin, W. H. Knox, and G. P. Agrawal, 2004, "Vector soliton fission," Phys. Rev. Lett. **93**, 183901.
Mamyshev, P. V., and S. V. Chernikov, 1990, "Ultrashort-pulse propagation in optical fibers," Opt. Lett. **15**, 1076–1078.
Mamyshev, P. V., P. G. J. Wigley, J. Wilson, G. I. Stegeman, V. A. Semenov, E. M. Dianov, and S. I. Miroshnichenko, 1993, "Adiabatic compression of Schrödinger solitons due to the combined perturbations of higher-order dispersion and delayed nonlinear response," Phys. Rev. Lett. **71**, 73–76.
Manassah, J. T., R. R. Alfano, and M. Mustafa, 1985, "Spectral distribution of an ultrafast supercontinuum laser source," Phys. Lett. **107A**, 305–309.
Manassah, J. T., P. P. Ho, A. Katz, and R. R. Alfano, 1984,

"Ultrafast supercontinuum laser source," Photonics Spectra **18**, 53–59.

Marks, D. L., A. L. Oldenburg, J. J. Reynolds, and S. A. Boppart, 2002, "Study of an ultrahigh-numerical-aperture fiber continuum generation source for optical coherence tomography," Opt. Lett. **27**, 2010–2012.

Matera, F., A. Mecozzi, M. Romagnoli, and M. Settembre, 1993, "Sideband instability induced by periodic power variation in long-distance fiber links," Opt. Lett. **18**, 1499–1501.

McConnell, G., and E. Riis, 2004, "Ultra-short pulse compression using photonic crystal fibre," Appl. Phys. B **78**, 557–563.

Milam, D., 1998, "Review and assessment of measured values of the nonlinear refractive-index coefficient of fused silica," Appl. Opt. **37**, 546–550.

Mitschke, F. M., and L. F. Mollenauer, 1986, "Discovery of the soliton self-frequency shift," Opt. Lett. **11**, 659–661.

Mogilevtsev, D., T. A. Birks, and P. St. J. Russell, 1998, "Group-velocity dispersion in photonic crystal fibers," Opt. Lett. **23**, 1662–1664.

Mollenauer, L. F., R. H. Stolen, and J. P. Gordon, 1980, "Experimental observation of picosecond pulse narrowing and solitons in optical fibers," Phys. Rev. Lett. **45**, 1095–1098.

Mollenauer, L. F., R. H. Stolen, J. P. Gordon, and W. J. Tomlinson, 1983, "Extreme picosecond pulse narrowing by means of soliton effect in single-mode optical fibers," Opt. Lett. **8**, 289–291.

Morioka, T., S. Kawanishi, K. Mori, and M. Saruwatari, 1994, "Nearly penalty-free, <4 ps supercontinuum Gbit/s pulse generation over 1535–1560 nm," Electron. Lett. **30**, 790–791.

Morioka, T., K. Mori, and M. Saruwatari, 1993, "More than 100-wavelength-channel picosecond optical pulse generation from single laser source using supercontinuum in optical fibres," Electron. Lett. **29**, 862–864.

Mussot, A., E. Lantz, H. Maillotte, T. Sylvestre, C. Finot, and S. Pitois, 2004, "Spectral broadening of a partially coherent CW laser beam in single-mode optical fibers," Opt. Express **12**, 2838–2843.

Nakazawa, M., K. Suzuki, H. Kubota, and H. A. Haus, 1989, "High-order solitons and the modulational instability," Phys. Rev. A **39**, 5768–5776.

Nakazawa, M., K. R. Tamura, H. Kubota, and E. Yoshida, 1998, "Coherence degradation in the process of supercontinuum generation in an optical fiber," Opt. Fiber Technol. **4**, 215–223.

Newbury, N. R., B. R. Washburn, K. L. Corwin, and R. S. Windeler, 2003, "Noise amplification during supercontinuum generation in microstructure fiber," Opt. Lett. **28**, 944–946.

Nguyen, H. C., B. T. Kuhlmey, M. J. Steel, C. L. Smith, E. C. Mägi, R. C. McPhedran, and B. J. Eggleton, 2005, "Leakage of the fundamental mode in photonic crystal fiber tapers," Opt. Lett. **30**, 1123–1125.

Nicholson, J. W., A. K. Abeeluck, C. Headley, M. F. Yan, and C. G. Jørgensen, 2003, "Pulsed and continuous-wave supercontinuum generation in highly nonlinear, dispersion-shifted fibers," Appl. Phys. B **77**, 211–218.

Nicholson, J. W., P. S. Westbrook, K. S. Feder, and A. D. Yablon, 2004a, "Supercontinuum generation in ultraviolet-irradiated fibers," Opt. Lett. **29**, 2363–2365.

Nicholson, J. W., A. D. Yablon, P. S. Westbrook, K. S. Feder, and M. F. Yan, 2004b, "High power, single mode, all-fiber source of femtosecond pulses at 1550 nm and its use in supercontinuum generation," Opt. Express **12**, 3025–3034.

Nicholson, J. W., and M. F. Yan, 2004, "Cross-coherence measurements of supercontinua generated in highly-nonlinear, dispersion shifted fiber at 1550 nm," Opt. Express **12**, 679–688.

Nikolov, N. I., T. Sørensen, O. Bang, and A. Bjarklev, 2003, "Improving efficiency of supercontinuum generation in photonic crystal fibers by direct degenerate four-wave mixing," J. Opt. Soc. Am. B **20**, 2329–2337.

Nowak, G. A., J. Kim, and M. N. Islam, 1999, "Stable supercontinuum generation in short lengths of conventional dispersion-shifted fiber," Appl. Opt. **38**, 7364–7369.

Omenetto, F. G., A. J. Taylor, M. D. Moores, J. Arriaga, J. C. Knight, W. J. Wadsworth, and P. St. J. Russell, 2001, "Simultaneous generation of spectrally distinct third harmonics in a photonic crystal fiber," Opt. Lett. **26**, 1158–1160.

Ortigosa-Blanch, A., J. C. Knight, and P. St. J. Russell, 2002, "Pulse breaking and supercontinuum generation with 200-fs pump pulses in photonic crystal fibers," J. Opt. Soc. Am. B **19**, 2567–2572.

Ortigosa-Blanch, A., J. C. Knight, W. J. Wadsworth, J. Arriaga, B. J. Mangan, T. A. Birks, and P. St. J. Russell, 2000, "Highly birefringent photonic crystal fibers," Opt. Lett. **25**, 1325–1327.

Ouzounov, D. G., F. R. Ahmad, D. Müller, N. Venkataraman, M. T. Gallagher, M. G. Thomas, J. Silcox, K. W. Koch, and A. L. Gaeta, 2003, "Generation of megawatt optical solitons in hollow-core photonic band-gap fibers," Science **301**, 1702–1704.

Pitois, S., and G. Millot, 2003, "Experimental observation of a new modulational instability spectral window induced by fourth-order dispersion in a normally dispersive single-mode optical fiber," Opt. Commun. **226**, 415–422.

Price, J. H. V., W. Belardi, T. M. Monro, A. Malinowski, A. Piper, and D. J. Richardson, 2002a, "Soliton transmission and supercontinuum generation in holey fiber, using a diode pumped ytterbium fiber source," Opt. Express **10**, 382–387.

Price, J. H. V., K. Furusawa, T. M. Monro, L. Lefort, and D. J. Richardson, 2002b, "Tunable, femtosecond pulse source operating in the range 1.06–1.33 μm based on an Yb^{3+}-doped holey fiber amplifier," J. Opt. Soc. Am. B **19**, 1286–1294.

Price, J. H. V., T. M. Monro, K. Furusawa, W. Belardi, J. C. Baggett, S. Coyle, C. Netti, J. J. Baumberg, R. Paschotta, and D. J. Richardson, 2003, "UV generation in a pure-silica holey fiber," Appl. Phys. B **77**, 291–298.

Proulx, A., J.-M. Menard, N. Hô, J. M. Laniel, and R. Vallée, 2003, "Intensity and polarization dependences of the supercontinuum generation in birefringent and highly nonlinear microstructured fibers," Opt. Express **11**, 3338–3345.

Provino, L., J. M. Dudley, H. Maillotte, N. Grossard, R. S. Windeler, and B. J. Eggleton, 2001, "Compact broadband continuum source based on microchip laser pumped microstructured fibre," Electron. Lett. **37**, 558–560.

Ranka, J. K., R. S. Windeler, and A. J. Stentz, 2000a, "Visible continuum generation in air-silica microstructure optical fibers with anomalous dispersion at 800 nm," Opt. Lett. **25**, 25–27.

Ranka, J. K., R. S. Windeler, and A. J. Stentz, 2000b, "Optical properties of high-delta air-silica microstructure optical fibers," Opt. Lett. **25**, 796–798.

Rarity, J. G., J. Fulconis, J. Duligall, W. J. Wadsworth, and P. St. J. Russell, 2005, "Photonic crystal fiber source of correlated photon pairs," Opt. Express **13**, 534–544.

Reeves, W. H., D. V. Skryabin, F. Biancalana, J. C. Knight, P. St. J. Russell, F. G. Omenetto, A. Efimov, and A. J. Taylor, 2003, "Transformation and control of ultra-short pulses in

dispersion-engineered photonic crystal fibres," Nature (London) **424**, 511–515.
Ritari, T., T. Niemi, H. Ludvigsen, M. Wegmuller, N. Gisin, J. R. Folkenberg, and A. Petterson, 2003, "Polarization-mode dispersion of large mode-area photonic crystal fibers," Opt. Commun. **226**, 233–239.
Roberts, P. J., B. J. Mangan, H. Sabert, F. Couny, T. A. Birks, J. C. Knight, and P. St. J. Russell, 2005, "Control of dispersion in photonic crystal fibers," J. Opt. Fiber. Commun. Rep. **2**, 435–461.
Rothenberg, J. E., 1992, "Space-time focusing: Breakdown of the slowly varying envelope approximation in the self-focusing of femtosecond pulses," Opt. Lett. **17**, 1340–1342.
Rulkov, A. B., M. Y. Vyatkin, S. V. Popov, J. R. Taylor, and V. P. Gapontsev, 2005, "High brightness picosecond all-fiber generation in 525–1800 nm range with picosecond Yb pumping," Opt. Express **13**, 377–381.
Russell, P. St. J., 1991, personal papers, cited in Russell (2003).
Russell, P. St. J., 2003, "Photonic crystal fibers," Science **299**, 358–362.
Sakamaki, K., M. Nakao, M. Naganuma, and M. Izutsu, 2004, "Soliton induced supercontinuum generation in photonic crystal fiber," IEEE J. Sel. Top. Quantum Electron. **10**, 876–884.
Satsuma, J., and N. Yajima, 1974, "Initial value problems of one-dimensional self-modulation of nonlinear waves in dispersive media," Prog. Theor. Phys. (Japan) Suppl. **55**, 284–306.
Schadt, D., and B. Jaskorzynska, 1987, "Generation of short pulses from CW light by influence of crossphase modulation (CPM) in optical fibers," Electron. Lett. **23**, 1090–1091.
Schenkel, B., R. Paschotta, and U. Keller, 2005, "Pulse compression with supercontinuum generation in microstructure fibers," J. Opt. Soc. Am. B **22**, 687–693.
Schreiber, T., T. V. Andersen, D. Schimpf, J. Limpert, and A. Tünnermann, 2005, "Supercontinuum generation by femtosecond single and dual wavelength pumping in photonic crystal fibers with two zero dispersion wavelengths," Opt. Express **13**, 9556–9569.
Schreiber, T., J. Limpert, H. Zellmer, A. Tünnermann, and K. P. Hansen, 2003, "High average power supercontinuum generation in photonic crystal fibers," Opt. Commun. **228**, 71–78.
Schütz, J., W. Hodel, and H. P. Weber, 1993, "Nonlinear pulse distortion at the zero dispersion wavelength of an optical fibre," Opt. Commun. **95**, 357–365.
Seefeldt, M., A. Heuer, and R. Menzel, 2003, "Compact white-light source with an average output power of 2.4 W and 900 nm spectral bandwidth," Opt. Commun. **216**, 199–202.
Sharping, J. E., M. Fiorentino, A. Coker, P. Kumar, and R. S. Windeler, 2001, "Four-wave mixing in microstructure fiber," Opt. Lett. **26**, 1048–1050.
Sharping, J. E., M. Fiorentino, P. Kumar, and R. S. Windeler, 2002, "Optical parametric oscillator based on four-wave mixing in microstructure fiber," Opt. Lett. **27**, 1675–1677.
Shen, Y. R., and N. Bloembergen, 1965, "Theory of stimulated Brillouin and Raman scattering," Phys. Rev. **137**, A1787–A1805.
Shimizu, F., 1967, "Frequency broadening in liquids by a short light pulse," Phys. Rev. Lett. **19**, 1097–1100.
Shirakawa, A., J. Ota, M. Musha, K. Nakagawa, K. Ueda, J. R. Folkenberg, and J. Broeng, 2005, "Large-mode-area erbium-ytterbium-doped photonic-crystal fiber amplifier for high-energy femtosecond pulses at 1.55 μm," Opt. Express **13**, 1221–1227.
Silberberg, Y., 1990, "Solitons and two-photon absorption," Opt. Lett. **15**, 1005–1007.
Sinkin, O. V., R. Holzlöhner, J. Zweck, and C. R. Menyuk, 2003, "Optimization of the split-step Fourier method in modeling optical-fiber communications systems," J. Lightwave Technol. **21**, 61–68.
Skryabin, D. V., F. Luan, J. C. Knight, and P. St. J. Russell, 2003, "Soliton self-frequency shift cancellation in photonic crystal fibers," Science **301**, 1705–1708.
Skryabin, D. V., and A. V. Yulin, 2005, "Theory of generation of new frequencies by mixing of solitons and dispersive waves in optical fibers," Phys. Rev. E **72**, 016619.
Smirnov, S. V., J. D. Ania-Castanon, T. J. Ellingham, S. M. Kobtsev, S. V. Kukarin, and S. K. Turitsyn, 2006, "Optical spectral broadening and supercontinuum generation in telecom applications," Opt. Fiber Technol. **12**, 122–147.
Smith, R. G., 1972, "Optical power handling capacity of low loss optical fibers as determined by stimulated Raman and Brillouin scattering," Appl. Opt. **11**, 2489–2494.
Snyder, A. W., and J. D. Love, 2000, *Optical Waveguide Theory* (Kluwer Academic, Dordrecht).
Steel, M. J., 2004, "Reflection symmetry and mode transversality in microstructured fibers," Opt. Express **12**, 1497–1509.
Steel, M. J., T. P. White, C. M. de Sterke, R. C. McPhedran, and L. C. Botten, 2001, "Symmetry and degeneracy in microstructured optical fibers," Opt. Lett. **26**, 488–490.
Stoicheff, B. P., 1963, "Characteristics of stimulated Raman radiation generated by coherent light," Phys. Lett. **7**, 186–188.
Stolen, R. H., 1975, "Phase-matched-stimulated four-photon mixing in silica-fiber waveguides," IEEE J. Quantum Electron. **QE-11**, 100–103.
Stolen, R. H., and J. E. Bjorkholm, 1982, "Parametric amplification and frequency conversion in optical fibers," IEEE J. Quantum Electron. **QE-18**, 1062–1072.
Stolen, R. H., J. P. Gordon, W. J. Tomlinson, and H. A. Haus, 1989, "Raman response function of silica-core fibers," J. Opt. Soc. Am. B **6**, 1159–1166.
Stolen, R. H., C. Lee, and R. K. Jain, 1984, "Development of the stimulated Raman spectrum in single-mode silica fibers," J. Opt. Soc. Am. B **1**, 652–657.
Stolen, R. H., L. F. Mollenauer, and W. J. Tomlinson, 1983, "Observation of pulse restoration at the soliton period in optical fibers," Opt. Lett. **8**, 186–188.
Tai, K., A. Hasegawa, and N. Bekki, 1988, "Fission of optical solitons induced by stimulated Raman effect," Opt. Lett. **13**, 392–394; **13**, 937(E) (1988).
Tamura, K. R., H. Kubota, and M. Nakazawa, 2000, "Fundamentals of stable continuum generation at high repetition rates," IEEE J. Quantum Electron. **36**, 773–779.
Tartara, L., I. Cristiani, and V. Degiorgio, 2003, "Blue light and infrared continuum generation by soliton fission in a microstructured fiber," Appl. Phys. B **77**, 307–311.
Thomann, I., A. Bartels, K. L. Corwin, N. R. Newbury, L. Hollberg, S. A. Diddams, J. W. Nicholson, and M. F. Yan, 2003, "420-MHz Cr:forsterite femtosecond ring laser and continuum generation in the 1–2-μm range," Opt. Lett. **28**, 1368–1370.
Tianprateep, M., J. Tada, and F. Kannari, 2005, "Influence of polarization and pulse shape of femtosecond initial laser pulses on spectral broadening in microstructure fibers," Opt. Rev. **12**, 179–189.
Town, G. E., T. Funaba, T. Ryan, and K. Lyytikainen, 2003,

"Optical supercontinuum generation from nanosecond pump pulses in an irregularly microstructured air-silica optical fiber," Appl. Phys. B **77**, 235–238.

Travers, J. C., R. E. Kennedy, S. V. Popov, J. R. Taylor, H. Sabert, and B. J. Mangan, 2005, "Extended continuous-wave supercontinuum generation in a low-water-loss holey fiber," Opt. Lett. **30**, 1938–1940.

Travers, J. C., S. V. Popov, and J. R. Taylor, 2005, "Extended blue supercontinuum generation in cascaded holey fibers," Opt. Lett. **30**, 3132–3134.

Treacy, E. B., 1971, "Measurement and interpretation of dynamic spectrograms of picosecond light pulses," J. Appl. Phys. **42**, 3848–3858.

Trebino, R., 2002, *Frequency-resolved Optical Gating: The Measurement of Ultrashort Laser Pulses* (Kluwer Academic, Dordrecht).

Türke, D., S. Pricking, J. Teipel, and H. Giessen, 2005, "Coherence properties of white light continuum generation in tapered fibers in the fs and ps regime," in *Lasers and Electro-Optics Society (LEOS) Summer Topical Meeting on Optical Frequency & Time Measurement and Generation* (IEEE/LEOS Piscataway, NJ), paper WB1.2.

Türke, D., W. Wohlleben, J. Teipel, M. Motzkus, B. Kibler, J. M. Dudley, and H. Giessen, 2006, "Chirp-controlled soliton fission in tapered optical fibers," Appl. Phys. B **83**, 37–42.

Tyrrell, J. C. A., P. Kinsler, and G. H. C. New, 2005, "Pseudospectral spatial-domain: A new method for nonlinear pulse propagation in the few-cycle regime with arbitrary dispersion," J. Mod. Opt. **52**, 973–986.

Udem, Th., R. Holzwarth, and T. W. Hänsch, 2002, "Optical frequency metrology," Nature (London) **416**, 233–237.

Udem, Th., J. Reichert, R. Holzwarth, S. A. Diddams, D. J. Jones, J. Ye, S. T. Cundiff, T. W. Hänsch, and J. L. Hall, 2000, "A new type of frequency chain and its application to fundamental frequency metrology," in *The Hydrogen Atom: Precision Physics of Simple Atomic Systems*, edited by S. G. Karshenboim, F. S. Pavone, G. F. Bassani, M. Inguscio, and T. W. Hänsch, Lecture Notes in Physics Vol. 570 (Springer, Berlin), pp. 125–144.

Udem, Th., J. Reichert, R. Holzwarth, and T. W. Hänsch, 1999, "Accurate measurement of large optical frequency differences with a mode-locked laser," Opt. Lett. **24**, 881–883.

Udem, Th., J. Reichert, R. Holzwarth, M. Niering, M. Weitz, and T. W. Hänsch, 2000, "Measuring the frequency of light with mode-locked lasers," in *Frequency Measurement and Control: Advanced Techniques and Future Trends*, edited by A. N. Luiten, Topics in Applied Physics Vol. 79 (Springer, Berlin), pp. 275–294.

Vanholsbeeck, F., Ph. Emplit, and S. Coen, 2003, "Complete experimental characterization of the influence of parametric four-wave mixing on stimulated Raman gain," Opt. Lett. **28**, 1960–1962.

Vanholsbeeck, F., S. Martín-López, M. González-Herráez, and S. Coen, 2005, "The role of pump incoherence in continuous-wave supercontinuum generation," Opt. Express **13**, 6615–6625.

Van Simaeys, G., Ph. Emplit, and M. Haelterman, 2002, "Experimental study of the reversible behavior of modulational instability in optical fibers," J. Opt. Soc. Am. B **19**, 477–486.

Varshney, S. K., T. Fujisawa, K. Saitoh, and M. Koshiba, 2005, "Novel design of inherently gain-flattened discrete highly nonlinear photonic crystal fiber Raman amplifier and dispersion compensation using a single pump in C-band," Opt. Express **13**, 9516–9526.

Vidne, Y., and M. Rosenbluh, 2005, "Spatial modes in a PCF fiber generated continuum," Opt. Express **13**, 9721–9728.

von der Linde, D., 1986, "Characterization of the noise in continuously operating mode-locked lasers," Appl. Phys. B **39**, 201–217.

Wadsworth, W. J., N. Y. Joly, J. C. Knight, T. A. Birks, F. Biancalana, and P. St. J. Russell, 2004, "Supercontinuum and four-wave mixing with Q-switched pulses in endlessly single-mode photonic crystal fibres," Opt. Express **12**, 299–309.

Wadsworth, W. J., J. C. Knight, A. Ortigosa-Blanch, J. Arriaga, E. Silvestre, and P. St. J. Russell, 2000, "Soliton effects in photonic crystal fibres at 850 nm," Electron. Lett. **36**, 53–55.

Wadsworth, W. J., A. Ortigosa-Blanch, J. C. Knight, T. A. Birks, T.-P. M. Man, and P. St. J. Russell, 2002, "Supercontinuum generation in photonic crystal fibers and optical fiber tapers: A novel light source," J. Opt. Soc. Am. B **19**, 2148–2155.

Wai, P. K. A., C. R. Menyuk, Y. C. Lee, and H. H. Chen, 1986, "Nonlinear pulse propagation in the neighborhood of the zero-dispersion wavelength of monomode optical fibers," Opt. Lett. **11**, 464–466.

Washburn, B. R., and N. R. Newbury, 2004, "Phase, timing, and amplitude noise on supercontinua generated in microstructure fiber," Opt. Express **12**, 2166–2175.

Washburn, B. R., S. E. Ralph, P. A. Lacourt, J. M. Dudley, W. T. Rhodes, R. S. Windeler, and S. Coen, 2001, "Tunable near-infrared femtosecond soliton generation in photonic crystal fibres," Electron. Lett. **37**, 1510–1512.

Washburn, B. R., S. E. Ralph, and R. S. Windeler, 2002, "Ultrashort pulse propagation in air-silica microstructure fiber," Opt. Express **10**, 575–580.

Werncke, W., A. Lau, M. Pfeiffer, K. Lenz, H.-J. Weigmann, and C. D. Thuy, 1972, "An anomalous frequency broadening in water," Opt. Commun. **4**, 413–415.

Wong, G. K. L., A. Y. H. Chen, S. G. Murdoch, R. Leonhardt, J. D. Harvey, N. Y. Joly, J. C. Knight, W. J. Wadsworth, and P. St. J. Russell, 2005, "Continuous-wave tunable optical parametric generation in a photonic-crystal fiber," J. Opt. Soc. Am. B **22**, 2505–2511.

Xu, L., X. Gu, M. Kimmel, P. O'Shea, R. Trebino, and A. Galvanauskas, 2001, "Ultra-broadband IR continuum generation and its phase measurement using cross-correlation FROG," in *Conference on Lasers and Electro-Optics*, Baltimore, Trends in Optics and Photonics Series Vol. 56 (The Optical Society of America, Washington, D.C.), pp. 198–200, paper CTuN1.

Xu, S., D. H. Reitze, and R. S. Windeler, 2004, "Controlling nonlinear processes in microstructured fibers using shaped pulses," Opt. Express **12**, 4731–4741.

Yamamoto, T., H. Kubota, S. Kawanishi, M. Tanaka, and S. Yamaguchi, 2003, "Supercontinuum generation at 1.55 μm in a dispersion-flattened polarization-maintaining photonic crystal fiber," Opt. Express **11**, 1537–1540.

Yanovsky, V. P., and F. W. Wise, 1994, "Nonlinear propagation of high-power, sub-100-fs pulses near the zero-dispersion wavelength of an optical fiber," Opt. Lett. **19**, 1547–1549.

Yu, M., C. J. McKinstrie, and G. P. Agrawal, 1993, "Instability due to cross-phase modulation in normal-dispersion regime," Phys. Rev. E **48**, 2178–2186.

Yulin, A. V., D. V. Skryabin, and P. St. J. Russell, 2004, "Four-wave mixing of linear waves and solitons in fibers with higher-order dispersion," Opt. Lett. **29**, 2411–2413.

Yusoff, Z., J. H. Lee, W. Belardi, T. M. Monro, P. C. Teh, and D. J. Richardson, 2002, "Raman effects in a highly nonlinear holey fiber: Amplification and modulation," Opt. Lett. **27**, 424–426.

Zakharov, V. E., and A. B. Shabat, 1971, "Exact theory of two-dimensional self-focusing and one-dimensional self-modulation of waves in nonlinear media," Zh. Eksp. Teor. Fiz. **61**, 118–134 [Sov. Phys. JETP **34**, 62–69 (1971)].

Zeylikovich, I., V. Kartazaev, and R. R. Alfano, 2005, "Spectral, temporal, and coherence properties of supercontinuum generation in microstructure fiber," J. Opt. Soc. Am. B **22**, 1453–1460.

Zheltikov, A. M., 2003, "The physical limit for the waveguide enhancement of nonlinear-optical processes," Opt. Spektrosk. **95**, 440–446 [Opt. Spectrosc. **95**, 410–415 (2003)].

Zheltikov, A. M., 2004, "Nonlinear optics of microstructure fibers," Usp. Fiz. Nauk **147**, 73–105 [Phys. Usp. **47**, 69–98 (2004)].

Zhu, Z., and T. G. Brown, 2004a, "Effect of frequency chirping on supercontinuum generation in photonic crystal fibers," Opt. Express **12**, 689–694.

Zhu, Z., and T. G. Brown, 2004b, "Experimental studies of polarization properties of supercontinua generated in a birefringent photonic crystal fiber," Opt. Express **12**, 791–796.

Zhu, Z., and T. G. Brown, 2004c, "Polarization properties of supercontinuum spectra generated in birefringent photonic crystal fibers," J. Opt. Soc. Am. B **21**, 249–257.

Zolla, F., G. Renversez, A. Nicolet, B. T. Kuhlmey, S. Guenneau, and D. Felbacq, 2005, *Foundations of Photonic Crystal Fibres* (Imperial College, London).

See EPAPS Document No. E-RMPHAT-78-006603 for animations corresponding to the figures. For more information on EPAPS see http://www.aip.org/pubservs/epaps.html.